Assessment of the X-LES Method and a Decomposed Turbulence Model by application to Turbulent Channel Flow

by

M. Henger

to obtain the degree of Master of Science
at the Delft University of Technology,
to be defended publicly on Monday July 20, 2020 at 14:00 PM

Student number:	4091221	
Project duration:	June 1, 2019 – June 30, 2020	
Thesis committee:	Prof. dr. S. Hickel,	TU Delft, supervisor
	Dr. ir. J. C. Kok,	NLR, supervisor
	Prof. dr. D. A. von Terzi,	TU Delft
	Dr. S. J. Hulshoff,	TU Delft

An electronic version of this thesis is available at http://repository.tudelft.nl/.

TU Delft

Abstract

Reynolds-Averaged Navier-Stokes (RANS) turbulence models are in widespread use in the commercial application of Computational Fluid Dynamics (CFD), but lack the capability to accurately compute unsteady flows and aeroacoustics due to its implied averaging of turbulent effects. In order to compute these kinds of flows, Large Eddy Simulation (LES) may be applied. However, this comes with a large computational cost. Hybrid RANS/LES aims to combine the turbulence-resolving aspects of LES, while attempting to approach the computational efficiency of RANS by applying a RANS turbulence model near walls.

The X-LES turbulence model developed at NLR has been successfully applied to massively separated flows. A future application of the method is to obtain aeroacoustic predictions of turbulent noise near sharp edges and wakes. In anticipation of this goal, this work aims to assess the accuracy of the X-LES model when it resolves part of the near-wall turbulent spectrum of Turbulent Channel Flow (TCF).

Multiple TCF simulations have been performed at a variety of friction Reynolds numbers Re_τ. It was found that the presence of resolved turbulent stress in the RANS-domain is not detrimental to the velocity profile in this domain, as it still conforms to the laws governing the viscous sublayer and the log-layer. The presence of so-called superstreaks causes a flow system where streamwise ribbons of high eddy viscosity, originating from within the RANS-domain, are transported away from the wall into the LES-domain. Here they contribute to the lack of development of turbulent stress, leading to an undesirable increase in velocity in the log-layer known as the Log-Layer Mismatch (LLM). Applying stochastic forcing led to a reduction in the LLM and broke up the large streamwise regions of eddy viscosity. It remains unclear in which proportion the disappearance of the high eddy-viscosity regions, and the stochastic forcing itself, contributed to the reduction in LLM.

An attempt has been made in formulating a consistent hybrid RANS/LES framework in which the effects of turbulence on the mean and fluctuating flow are governed by separate turbulence models throughout the entire domain. The initial results are presented in this report, which may be used to further develop the model in the future.

Preface

Performing my MSc thesis at NLR has been a humbling experience in which I was able to learn a lot by practically applying everything I learned during my studies on an existing fluid solver under excellent supervision.

I wouldn't be myself if I wouldn't at least mention in passing that I'm grateful to all of the people behind the open-source software that I was able to use.

But of course, this work wouldn't be possible without the help of several people. First of all I would like to thank all my colleagues at the AVFP department at NLR. I learned a lot from all of you, and had a lot of fun in and around the office. My gratitude also goes out to Dominic von Terzi and Steven Hulshoff for their willingness to be on the thesis committee.

I would like to thank Stefan Hickel for his supervision and comments. I would also like to thank Johan Kok for his supervision at NLR: for the helpful hints, reminding me every now and then to focus on matters of importance, and for his patience answering my questions at appropriate times, and at times close to the lunch breaks.

I would like to mention my family for their support during all of my studies. Thanks to Frank, friend and roommate, for his understanding while I was working on my thesis for significant portions of the day during the past couple of months.

Finally I would like to thank Marijne for her love, understanding and patience.

M. Henger
Delft, June 2020

Contents

List of Tables

List of Figures

List of Abbreviations

CFD	Computational Fluid Dynamics
CFL	Courant Friedrichs-Lewy
CLES	Constrained Large Eddy Simulation
DDES	Delayed Detached Eddy Simulation
DES	Detached Eddy Simulation
DNS	Direct Numerical Simulation
HIT	Homogeneous Isotropic Turbulence
HPF	High-Pass Filtered
IDDES	Improved Delayed Detached Eddy Simulation
LES	Large Eddy Simulation
LLM	Log-Layer Mismatch
NLR	Nederlands Luchtvaart en Ruimtevaartcentrum
RANS	Reynolds-Averaged Navier-Stokes
SA	Spalart-Allmaras
SBS	Stochastic BackScatter
SGS	SubGrid Scale
TCF	Turbulent Channel Flow
WMLES	Wall-Modeled Large Eddy Simulation
WRLES	Wall-Resolved Large Eddy Simulation
X-LES	eXtra-Large Eddy Simulation
ZDES	Zonal Detached Eddy Simulation

List of Symbols

Roman Symbols

A	Area
b	Smoothing coefficient
B	Constant in log-law
c_p	Specific heat at constant pressure
C	Generic constant
C_1	Filter width factor
C_D	Cross-diffusion (of the ω-equation)
C_I	Stochastic forcing intensity coefficient
C_s	Smagorinsky coefficient
C_s	Spatial correlation coefficient
C_t	Temporal correlation coefficient
CFL	Courant Friedrichs-Lewy number
d	Spatial correlation term
d	Wall distance
D	Damping factor
$\mathcal{D}$	Diffusion term (of a turbulence modeling equation)
e	Internal energy
E	Total energy
E	Turbulent kinetic energy spectrum
f	Generic force or function
f_b	Blending function
f_w	Law of the wall function
f_o	Objective function
$\mathcal{F}$	Fourier transformation function
g	Growth rate of cell size
G	Filter kernel
H	Transfer function
I	Identity operator
k	Turbulent kinetic energy
L	Turbulent lengthscale
$\mathcal{L}$	Flow-characterizing lengthscale
M	Grid size in grid-generated turbulence experiment
N	Generic count/length
$\mathcal{N}$	Random variable with normal distribution
p	Pressure
$\mathcal{P}$	Production term (of a turbulence modeling equation)
Pr	Prandtl number
q	Heat flux
q	Quantile
$\underline{r}$	Relative position vector
R	Specific gas constant
Re	Reynolds number
Re_b	Bulk Reynolds number
Re_τ	Friction Reynolds number
s	Time (when the symbol has to be distinct from t)
S	Rate of strain

$\widehat{S}$	Traceless rate of strain
t	Time
T	Temperature
T	Span of time
u	Velocity in x-direction
u	Generic velocity component (clarified by subscript)
$\underline{u}$	Velocity vector
$\mathcal{U}$	Velocity scale
u_τ	Friction velocity
v	Velocity in y-direction
V	Uncorrelated random field
w	Velocity in z-direction
W	Spatially correlated random field
x	Position along x-axis
x	Generic position component (clarified by subscript)
$\underline{x}$	Position vector
y	Position along y-axis
z	Position along z-axis

Greek Symbols

α	Thermal conductivity
α	Model constant (in production term of turbulence modeling equations)
α	Generic blending factor
α	Time constant
β	Model constant (in dissipation term of turbulence modeling equations)
δ	Channel half-height
δ_{ij}	Kronecker delta
Δ_t	Timestep
Δ	Cell size
Δ	Filter width
ϵ	Dissipation
κ	Wavenumber
κ	von Kármán constant
λ	Wavelength
λ	Bulk viscosity
μ	Dynamic viscosity
ν	Kinematic viscosity
ν_t	Eddy viscosity
ξ	Spatially and temporally correlated random field
ρ	Density
σ	Model constant (in diffusion term of turbulence modeling equations)
τ_{ij}	Subfilter stress (i.e. Reynolds stress or subgrid scale stress)
τ	Temporal correlation term
τ_w	Wall friction
ϕ	Generic quantity to define functions and operators
Φ_I	Non-dimensional universal function for the inner-layer wall
Ψ	Compensated Kolmogorov spectrum function
ω	Specific turbulent dissipation
$\underline{\omega}$	Vorticity vector

ω	Frequency

Subscripts

0	Reference quantity
c	Correction term
c	At cut-off frequency
exp	Experimentally measured quantity
i	Generic index
j	Generic index
k	Generic index
k	Related to turbulent kinetic energy
l	Generic index
L	Based on LES formulation
L	Laminar quantity
m	Generic index
M	Model quantity
r	Resolved quantity
R	Based on RANS formulation
R	Pertaining to a refined wavenumber space
sim	Quantity derived from a simulation
t	Turbulent quantity
T	Pertaining to time
w	Evaluated at a wall
x	Measured along x-axis
y	Measured along y-axis
z	Measured along z-axis
α	Generic index
β	Generic index
γ	Generic index
κ	Measured in wavenumber space
ω	Related to specific turbulent dissipation

Superscripts

c	Correction term
HPF	High-pass filtered quantity
L	Based on LES formulation
M	Model quantity
r	Resolved component
R	Based on RANS formulation
$+$	Non-dimensionalized in viscous units, or: wall-units

Operators

$\langle\cdot\rangle$	Reynolds averaging
$\cdot'$	Reynolds fluctuation
$\{\cdot\}$	Favre averaging
$\cdot''$	Favre fluctuation

$\bar{\cdot}$ Spatial filtering
$\cdot^{>}$ Resolved (after spatial filtering) fluctuation
$\cdot^{<}$ Unresolved (after spatial filtering) fluctuation
$\widetilde{\cdot}$ Favre filtering
$\cdot^{\gg}$ Resolved (after Favre filtering) fluctuation
$\cdot^{\ll}$ Unresolved (after Favre filtering) fluctuation
$\underline{\cdot}$ Vector quantity
$\widehat{\cdot}$ Fourier transformed

1 Introduction

Reynolds-averaged Navier-Stokes (RANS) modeling has been the workhorse of computational fluid dynamics for the past couple of decades [1]. RANS models all turbulence and computes the mean flow variables explicitly for a particular configuration. An alternative method is Large Eddy Simulation (LES), which resolves a portion of the turbulent spectrum. LES facilitates a more accurate simulation of unsteady flows and aeroacoustics, but its inherent computational cost prohibits its use in computing large geometries embedded in high Reynolds number flows.

The computational cost of LES is mainly incurred when turbulence has to be resolved at small timescales and lengthscales. For the mentioned geometries this implies that the cost is incurred near walls [2]. A solution to this predicament is to augment the LES formulation with additional modeling in boundary layers to remove this cost. Hybrid RANS/LES is one such model, where a portion of the boundary layer is modeled using a RANS formulation and the outer layer with an LES formulation [3].

Results obtained with turbulence-resolving hybrid methods depend on the position of the interface between the RANS-domain and LES-domain. If the interface lies at the edge of the boundary layer then hybrid methods should be capable of simulating large-scale unsteadiness such as massively separated flows. As the interface is placed closer to the solid surface then these hybrid methods should ideally allow for increasingly accurate predictions of separated flows, and better resolve the turbulence residing in the boundary layer.

Many hybrid methods exhibit an anomolous result called the log-layer mismatch when placing the interface inside the boundary layer [4]: the velocity profile approaches the interface on opposite sides with approximately the same slope but a different intercept. This phenomenon is associated with incorrectly computed wall friction values [5].

This thesis was executed at the Royal Netherlands Aerospace Center (NLR), where an in-house CFD solver called `ensolv` has been developed. It is a structured multi-block solver supporting a variety of fluid and turbulence models. Its variant of hybrid RANS/LES is called eXtra-Large Eddy Simulation (X-LES) and has been previously applied to massively separated flows where the entire boundary layer is modeled using a k-ω RANS formulation and the outer flow using a k-equation SGS formulation [6]. The method is additionally capable of performing stochastic forcing of the flow to expedite the transition to turbulence using a stochastic backscatter model [7]. In addition the subgrid scale model may be optionally formulated in terms of the fluctuating rate of strain tensor by applying high-pass filtering to the velocity gradients.

A future application of the method is to determine the levels of aeroacoustic noise originating from sharp edges and wakes, such as the noise generated at the trailing edge of airfoils. To obtain accurate noise predictions the solution has to contain resolved turbulence in the upstream boundary layer, which requires moving the RANS/LES interface closer to the walls.

The goal of this thesis is perform an assessment of the performance of the X-LES method when it resolves turbulence within the boundary layer. Turbulent Channel Flow (TCF) driven by a constant body force on a periodic domain will be used as the main test case for the assessment. This work aims to answer the following questions:

- To which degree does the X-LES method reproduce the mean velocity profile and turbulent velocity (co)variances as obtained from RANS and DNS simulations at its default tuned parameters?
- How are these results influenced when the stochastic backscatter model is applied?
- How are these results influenced when the high-pass filtered SGS formulation is employed?
- How are these results influenced when the RANS/LES interface is moved closer to or further away from the wall.

The expected appearance of the log-layer mismatch will be given special attention. Several models that attempt to remove this error have been investigated, and a formulation based on those models will be proposed and briefly analyzed.

The basics of modeling fluids, and the manner in which turbulence is modeled, is described in chapter 2. This chapter also provides the theoretical background for the particular types of flows that have been used to gauge the accuracy of X-LES. Chapter 3 will investigate several types of hybrid RANS/LES models that are relevant to this work and the issues they commonly face. The analysis of the X-LES method is detailed in chapter 4. A particular kind of formulating hybrid RANS/LES models, heavily based on work by other authors, has been investigated in chapter 5. A model based on this formulation is discussed in chapter 6. Finally, the conclusions and recommendations based on the performed work will be given in chapter 7 and 8.

2 Governing Equations

This chapter will introduce the fundamentals of fluid mechanics with modeled turbulence in order to support the analyses and statements in this work. Most of the information is taken from common reference material on the study of aerodynamics and turbulence modeling [8, 9, 10].

The governing equations for fluids are discussed in section 2.1. Simulations may be performed in which these governing equations are solved directly, but due to their enormous computational cost these equations are usually rewritten such that the terms governing turbulence may be modeled. Such transformations and the associated modeling assumptions are given in section 2.2. Finally, the particular flows this work is concerned with allow for some theoretical results, which are given in section 2.3, and used to motivate later analyses and findings.

2.1 Modeling Fluids

Any fluid that is considered a continuum may be modeled by the continuity, momentum (or: Navier-Stokes) and energy equations. These equations ensure the conservation of mass, momentum and energy, respectively. These form a closed system of equations when combined with equations for the transport properties and the equation of state. Using Einstein notation, they are written as [8]:

$$\frac{\partial \rho}{\partial t} + \frac{\partial \rho u_i}{\partial x_i} = 0, \tag{1}$$

$$\frac{\partial \rho u_j}{\partial t} + \frac{\partial \rho u_i u_j}{\partial x_i} = -\frac{\partial p}{\partial x_j} + \frac{\partial t_{ij}}{\partial x_i}, \tag{2}$$

$$\frac{\partial \rho E}{\partial t} + \frac{\partial \rho u_i E}{\partial x_i} = -\frac{\partial u_i p}{\partial x_i} + \frac{\partial t_{ij} u_j}{\partial x_i} - \frac{\partial q_i}{\partial x_i}, \tag{3}$$

$$p = \rho R T \ . \tag{4}$$

Here ρ is density, u_i are the velocity components, p denotes pressure, $E = e + u_i u_i/2$ is the total energy, T denotes temperature and $\underline{q}$ represents a heat flux. Any body forces or sources of heat have been left out.

The molecular viscous stresses t_{ij} are given by:

$$t_{ij} = \mu \left(\frac{\partial u_i}{\partial x_j} + \frac{\partial u_j}{\partial x_i} \right) - \delta_{ij} \lambda \frac{\partial u_k}{\partial x_k} = 2\mu S_{ij} - \delta_{ij} \lambda \frac{\partial u_k}{\partial x_k} = 2\mu \widehat{S}_{ij} \ . \tag{5}$$

Here μ is the dynamic viscosity and λ the bulk viscosity. Applying Stokes' hypothesis one may redefine the bulk viscosity as $\lambda = 2\mu/3$. S_{ij} is known as the rate of strain tensor, and when it incorporates the term containing the velocity divergence it is known as the traceless rate of strain tensor $\widehat{S}_{ij}$. For isothermal flows the viscosity μ may be considered a constant. In compressible flows the dependence of the dynamic viscosity μ on temperature T is taken into account using Sutherland's law:

$$\mu = \mu_0 \left(\frac{T}{T_0} \right)^{3/2} \left(\frac{T_0 + S}{T + S} \right), \tag{6}$$

where μ_0, T_0 and S are constants depending on the type of modeled fluid. The heat flux may be modeled by Fourier's law of heat conduction:

$$-q_i = \alpha \frac{\partial T}{\partial x_i} = \frac{c_p \mu}{Pr_L} \frac{\partial T}{\partial x_i}, \tag{7}$$

where α is the thermal conductivity, c_p is the specific heat coefficient at constant pressure and Pr_L is the laminar Prandtl number, defined as $Pr_L = \mu c_p / \alpha$. The emphasis on it being laminar will become clear

in section 2.2.3, where a turbulent term will be modeled using a turbulent Prandtl number.

Assuming incompressibility and negligible changes in temperature allows simplifications to these governing equations. Although this work often simply assumes constant density, incompressibility may be formally defined as constant density along streamlines. Applying this assumption to eq. (1) produces the incompressible continuity equation:

$$\rho \frac{\partial u_i}{\partial x_i} = 0 \implies \frac{\partial u_i}{\partial x_i} = 0 \ . \tag{8}$$

Due to this result incompressible flows are also called divergence-free flows. Applying the incompressible assumption to eq. (2), applying eq. (8) where possible, and noting that under negligible temperature variations the viscosity μ is constant, the incompressible momentum equations become:

$$\frac{\partial u_j}{\partial t} + u_i \frac{\partial u_j}{\partial x_i} = -\frac{1}{\rho}\frac{\partial p}{\partial x_j} + \nu \frac{\partial^2 u_j}{\partial x_i \partial x_i} \ . \tag{9}$$

By taking the divergence of eq. (9), a direct equation for the pressure may be obtained:

$$-\frac{1}{\rho}\frac{\partial^2 p}{\partial x_j \partial x_j} = \frac{\partial u_i}{\partial x_j}\frac{\partial u_j}{\partial x_i} \ . \tag{10}$$

As the pressure may now be directly computed from the velocity field, the energy equation becomes decoupled from the governing equations for incompressible flow.

2.2 Modeling Turbulence

The presented equations in section 2.1 may be used directly to perform Computational Fluid-Dynamic (CFD) simulations. As will be motivated in section 2.3, using these equations as-is will require a very fine spatiotemporal discretisation to ensure that correct results are obtained. These kinds of fully resolved simulations are called Direct Numerical Simulations (DNS).

For practical engineering flows the computational requirements are simply too demanding, hence certain filtering operations are applied to the governing equations. The result is a set of equations in which the terms which incur the computational demand are isolated, and may subsequently be modeled in order to remove this cost. There are two main approaches to filtering. The first is temporal filtering, or Reynolds averaging. This operation produces the Reynolds-averaged Navier-Stokes (RANS) equations and is presented in section 2.2.1. The second approach is decribed in section 2.2.2 and involves spatial averaging to produce the Large-Eddy Simulation (LES) formulation. The discussion of these filters is concluded by an approach to modeling the isolated terms in section 2.2.3.

2.2.1 Reynolds and Favre Averaging

The effects of turbulence are elucidated if one applies temporal filtering to eq. (1) through eq. (3) or their incompressible variants. The operator performing the filtering operation $\langle \cdot \rangle$ is defined for a generic quantity ϕ as [10]:

$$\langle \phi \rangle = \frac{1}{T}\int_0^T \phi\,(t)\,\mathrm{d}t, \quad \text{or} \quad \langle \phi \rangle = \frac{1}{N_T}\sum_i^{N_T} \phi\,(t_i)\,, \quad \phi' = \phi - \langle \phi \rangle \ . \tag{11}$$

The integral-based definition would compute the true mean as $T \to \infty$. The two formulations become equivalent if their averaging span is of comparable magnitude, and the sampling frequency of the sum-based definition is large enough to produce a comparable mean (i.e. a Riemann sum where $\Delta_t \to 0$).

The sum-based definition is known as ensemble averaging and commonly referred to as Reynolds averaging for historical reasons. This definition ensures that repeated application of the Reynolds averaging

operation results in the same value, i.e. that $\langle\langle\phi\rangle\rangle = \langle\phi\rangle$. The term ϕ' is the fluctuation of the quantity ϕ. If the averaging span does not change throughout the domain and is so large that a true average is obtained, then it may be assumed that the filter commutes with spatial and temporal derivatives, i.e. $\langle\partial\phi/\partial t\rangle = \partial\langle\phi\rangle/\partial t$ and $\langle\partial\phi/\partial x\rangle = \partial\langle\phi\rangle/\partial x$.

Applying Reynolds averaging to the Navier-Stokes equations yields the Reynolds-Averaged Navier Stokes (RANS) equations. Formally an average does not change with time (i.e. $\partial\langle\phi\rangle/\partial t = 0$), so all the time derivatives should vanish. A formulation known as unsteady RANS assumes that the averaging span is much larger than the turbulent timescales, but smaller than the non-turbulent timescales, such that the mean is allowed to vary. With this assumption Reynolds averaging the incompressible continuity and momentum equations produces:

$$\frac{\partial\langle u_i\rangle}{\partial x_i} = 0 \implies \frac{\partial u_i}{\partial x_i} - \frac{\partial\langle u_i\rangle}{\partial x_i} = \frac{\partial u_i'}{\partial x_i} = 0, \tag{12}$$

$$\frac{\partial\langle u_j\rangle}{\partial t} + \frac{\partial\langle u_i\rangle\langle u_j\rangle}{\partial x_i} = -\frac{1}{\rho}\frac{\partial\langle p\rangle}{\partial x_j} + \frac{\partial 2\nu\langle S_{ij}\rangle}{\partial x_i} - \frac{\partial\langle u_i'u_j'\rangle}{\partial x_i}, \quad \text{since :} \quad \langle u_iu_j\rangle - \langle u_i\rangle\langle u_j\rangle = \langle u_i'u_j'\rangle \ . \tag{13}$$

Equation 12 is the Reynolds-averaged continuity equation and shows that both the mean velocity as the fluctuating velocity are divergence free, such that $\langle\widehat{S}_{ij}\rangle = \langle S_{ij}\rangle$. In eq. (13) $\langle u_i'u_j'\rangle$ represents the effect the unresolved velocity correlations have on the evolution of the mean flow $\langle u_j\rangle$. As a RANS simulation will implicitly solve for the mean flow $\langle u_i\rangle$, the fluctuations u_i' are unknown, so the term $\langle u_i'u_j'\rangle$ will have to be modeled. Due to the similarity of this term with the viscous stress these models are called Reynolds stress models.

For compressible flows the energy equation has to be explicitly averaged as well. When compressible flows are averaged then Favre averaging is used to prevent a large number of density-fluctuation terms to appear in the equations. Favre averaging is defined in terms of Reynolds averaging as:

$$\{\phi\} = \frac{\langle\rho\phi\rangle}{\langle\rho\rangle}, \quad \phi'' \equiv \phi - \{\phi\} \ . \tag{14}$$

Using this definition the Reynolds-averaged momentum and energy equations are formulated as:

$$\frac{\partial}{\partial t}\left[\langle\rho\rangle\{u_j\}\right] + \frac{\partial}{\partial x_i}\left[\langle\rho\rangle\{u_i\}\{u_j\}\right] = -\frac{\partial\langle p\rangle}{\partial x_j} + \frac{\partial\langle t_{ij}\rangle}{\partial x_i} - \frac{\partial\langle\rho u_i''u_j''\rangle}{\partial x_i}, \tag{15}$$

$$\begin{aligned}\frac{\partial}{\partial t}\left[\langle\rho\rangle E_R + \langle\rho\frac{1}{2}u_i''u_i''\rangle\right] + \frac{\partial}{\partial x_j}\left[\langle\rho\rangle\{u_j\}E_R + \{u_j\}\langle\rho\frac{1}{2}u_i''u_i''\rangle\right] = -\frac{\partial}{\partial x_j}\left[\{u_j\}\langle p\rangle\right] + \\ + \frac{\partial}{\partial x_j}\left[\frac{\mu c_p}{Pr_L}\frac{\partial\langle T\rangle}{\partial x_j} - \langle\rho h''u_j''\rangle\right] + \frac{\partial}{\partial x_j}\left[\langle u_j''t_{ij}\rangle - \langle\rho u_j''u_i''u_i''\rangle\right] + \frac{\partial}{\partial x_j}\left[\{u_i\}\left(\langle t_{ij}\rangle - \langle\rho u_i''u_j''\rangle\right)\right],\end{aligned} \tag{16}$$

where $E_R = \{e\} + \{u_i\}\{u_i\}/2$. The averaged energy equation in eq. (16) contains several new unclosed terms: $\langle\rho u_i''u_i''\rangle/2$ is the turbulent kinetic energy (or: half the trace of the Reynolds stress), $\langle\rho h''u_j''\rangle$ is the turbulent heat flux, and $\langle u_j''t_{ij}\rangle$ and $\langle\rho u_j''u_i''u_i''\rangle$ are the molecular diffusion and the turbulent transport of turbulent kinetic energy.

Note that formally the viscous stress should be averaged as well. With its definition in eq. (5), this would imply an extra correlation between fluctuations in molecular viscosity μ (due to variations in temperature T), and the traceless rate of strain tensor $\widehat{S}_{ij}$. In practice this is neglected, such that $\langle t_{ij}\rangle \approx 2\mu\langle\widehat{S}_{ij}\rangle$, where $\mu = \mu\left(\langle T\rangle\right)$.

2.2.2 Spatial and Favre Filtering

Spatial filtering is defined as the spatial convolution of a variable $\phi(\underline{x}, t)$ with a filter kernel $G(\underline{x}, \underline{r})$, again giving rise to a filtered quantity $\overline{\phi}$ and the corresponding fluctuation $\phi^< = \phi - \overline{\phi}$. That is [9]:

$$\overline{\phi} = \int \phi(\underline{x} + \underline{r})\, G(\underline{x}, \underline{r})\, \mathrm{d}\underline{r}, \quad \text{where} \quad \int G(\underline{x}, \underline{r})\, \mathrm{d}\underline{r} = 1 \;\forall\; \underline{x}\;. \tag{17}$$

The notation for the spatially filtered fluctuation $\phi^<$ is different from commonly used notation to disambiguate it from other kind of fluctuating quantities. It represents the subfilter fluctuating component of ϕ. Although a large variety of filters are possible [9], in practice the spatial filter kernel G may be assumed to be non-zero in a limited region around $\underline{x}$. This region approximately corresponds to the so-called filter width, which is generally defined in terms of the discretized domain's grid size. If the grid does not change with time then the spatial filter commutes with the temporal derivative (i.e. $\overline{\partial\phi/\partial t} = \partial\overline{\phi}/\partial t$), but it does not generally commute with the spatial derivative:

$$\frac{\partial\overline{\phi}}{\partial x} = \frac{\partial}{\partial x}\left[\int \phi G \mathrm{d}\underline{r}\right] = \int \frac{\partial\phi}{\partial x} G \mathrm{d}\underline{r} + \int \phi \frac{\partial G}{\partial x}\mathrm{d}\underline{r} = \overline{\frac{\partial\phi}{\partial x}} + \int \phi\frac{\partial G}{\partial x}\mathrm{d}\underline{r} \implies \overline{\frac{\partial\phi}{\partial x}} = \frac{\partial\overline{\phi}}{\partial x} - \int \phi\frac{\partial G}{\partial x}\mathrm{d}\underline{r}\;. \tag{18}$$

Hence spatially averaging the governing equations for fluids will formally result in a large variety of terms depending on the spatial derivative. In practice these are often neglected, leading to the so-called commutation error. Neglecting this error, then spatially filtering the incompressible continuity and Navier-Stokes equations result in

$$\frac{\partial\overline{u_i}}{\partial x_i} = 0 \implies \frac{\partial u_i}{\partial x_i} - \frac{\partial\overline{u_i}}{\partial x_i} = \frac{\partial u_i^<}{\partial x_i} = 0, \tag{19}$$

$$\frac{\partial\overline{u_j}}{\partial t} + \frac{\partial\overline{u_i}\;\overline{u_j}}{\partial x_i} = -\frac{1}{\rho}\frac{\partial\overline{p}}{\partial x_j} + \frac{\partial 2\nu\overline{S_{ij}}}{\partial x_i} - \frac{\partial}{\partial x_i}\left(\overline{u_i u_j} - \overline{u_i}\;\overline{u_j}\right)\;. \tag{20}$$

Like the Reynolds-averaged equation in eq. (13), because a simulation will solve only for the filtered variables $\bar{\cdot}$, the correlations $\overline{u_i u_j}$ are unknown. When applying spatial filtering the turbulent stress term $\overline{u_i}\;\overline{u_j} - \overline{u_i u_j}$ is called the SubGrid Scale (SGS) stress. Formally the turbulent term may not be simplified. The turbulent stress obtained by Reynolds averaging represents the effect of all fluctuations on the mean flow. But when applying spatial then filtering part of the turbulence is resolved, so there are non-zero interactions between the filtered quantities and subfilter quantities (e.g. $\overline{u_i u_j^<} \neq 0$). These represent the so-called forward scatter and backscatter effects. On top of that repeated application of spatial filtering does not produce the same quantity (i.e. $\overline{\overline{\phi}} \neq \overline{\phi}$), such that a filtering a subfilter quantity does not eliminate it (i.e. $\overline{\phi^<} \neq 0$). Simulations where the governing equations are spatially filtered are called Large Eddy Simulations (LES), which already indicates that only the larger types of eddies are resolved.

For compressible flows Favre filtering is used, which is defined as:

$$\widetilde{\phi} = \frac{\overline{\rho\phi}}{\overline{\rho}}, \quad \phi^{\ll} = \phi - \widetilde{\phi}\;. \tag{21}$$

Applying spatial averaging to the governing equations for compressible flow, again neglecting the commutation error, the momentum and energy equations amount to:

$$\frac{\partial\overline{\rho}\widetilde{u_j}}{\partial t} + \frac{\partial\overline{\rho}\widetilde{u_i}\widetilde{u_j}}{\partial x_i} = -\frac{\partial\overline{p}}{\partial x_j} + \frac{\partial}{\partial x_i}\left[\overline{t}_{ij} - \overline{\rho}\left(\widetilde{u_i u_j} - \widetilde{u_i}\widetilde{u_j}\right)\right], \tag{22}$$

$$\frac{\partial}{\partial t}\left[\overline{\rho}\left(E_L+\frac{1}{2}\left(\widetilde{u_iu_i}-\widetilde{u}_i\widetilde{u}_i\right)\right)\right]+\frac{\partial}{\partial x_j}\left[\overline{\rho}\widetilde{u}_j\left(E_L+\frac{1}{2}\left(\widetilde{u_iu_i}-\widetilde{u}_i\widetilde{u}_i\right)\right)+\overline{p}\right]=$$
$$=\frac{\partial}{\partial x_j}\left[\frac{\mu c_p}{Pr_L}\frac{\partial\overline{T}}{\partial x_j}-\overline{\rho}\left(\widetilde{hu_j}-\widetilde{h}\widetilde{u}_j\right)\right]+\frac{\partial}{\partial x_j}\left[\left(\overline{u_jt_{ij}}-\overline{u_j}\;\overline{t}_{ij}\right)-\right.$$
$$\left.-\overline{\rho}\left(2\widetilde{u}_j\widetilde{u}_i\widetilde{u}_i+\widetilde{u_ju_iu_i}-2\widetilde{u}_i\widetilde{u_iu_j}-\widetilde{u}_j\widetilde{u_iu_i}\right)\right]+\frac{\partial}{\partial x_j}\left[\overline{u_j}\;\overline{t}_{ij}-\overline{\rho}\widetilde{u}_i\left(\widetilde{u_iu_j}-\widetilde{u}_i\widetilde{u}_j\right)\right], \quad (23)$$

where $E_L = \widetilde{e} + \widetilde{u}_i\widetilde{u}_i/2$. The compressible filtered momentum and energy equations feature a lot of similar terms as the corresponding Reynolds-averaged equations, with roughly the same interpretation. They differ in that these turbulent terms do not contain solely subfilter correlations but also contain interactions between the subfilter and the filtered components of a quantity.

2.2.3 Modeling the Unclosed Terms

Any turbulent flow will exhibit chaotic motion of the fluid particles. Looking at this chaotic motion in a fully developed turbulent flow with the human eye one may be able to identify whorling motion. The whorls (or: eddies) seem to exhibit a fractal nature: existing at a wide range of scales where, apart from the smallest of scales, each eddy seems to be composed of a variety of smaller eddies.

The various unclosed terms in eq. (13) through eq. (23) represent the statistics of the subfilter portions of these turbulent motions and require appropriate models. The point of departure is modeling the turbulent stress term. This work will only consider a class of models called eddy viscosity models. These invoke the Boussinesq hypothesis and assume the turbulent stress is proportional to the mean rate of strain. The coefficient of proportionality is called the eddy viscosity ν_t, as the term is similar in form to the molecular viscosity. From dimensional grounds this term should be a combination of a velocity scale $\mathcal{U}$ and a lengthscale $\mathcal{L}$. At the same time, half the trace of the turbulent stress term should equal the turbulent kinetic energy k. The combination of these two requirements leads to

$$-\langle\rho u_i''u_j''\rangle=\tau_{ij}=2\langle\rho\rangle\mathcal{U}\mathcal{L}\widehat{S}_{ij}-\frac{2}{3}\langle\rho\rangle k\delta_{ij}=2\langle\rho\rangle\sqrt{k}\mathcal{L}\widehat{S}_{ij}-\frac{2}{3}\langle\rho\rangle k\delta_{ij},\quad\text{where}\quad\nu_t=\rho\sqrt{k}\mathcal{L}\;. \quad (24)$$

The second form of this equation uses the square root of the turbulent kinetic energy $k = \langle\rho u_i''u_i''\rangle/2\langle\rho\rangle$ as the velocity scale. An equation for the turbulent kinetic energy k may be formed from the Navier-Stokes equations by computing $\langle u_i'\partial\left(\rho u_j\right)/\partial t + u_j'\partial\left(\rho u_i\right)/\partial t\rangle$. This results in [10]:

$$\frac{\partial\langle\rho\rangle k}{\partial t}+\frac{\partial\langle\rho\rangle\left\{u_i\right\}k}{\partial x_i}=\underbrace{\tau_{ij}\frac{\partial\left\{u_i\right\}}{\partial x_j}}_{\mathcal{P}_k}-\underbrace{\langle t_{ij}\frac{\partial u_i'}{\partial x_j}\rangle}_{\epsilon_k}+\frac{\partial}{\partial x_j}\left[\langle u_i''t_{ij}\rangle-\langle\rho u_j''\frac{1}{2}u_i''u_i''\rangle-\langle p'u_j''\rangle\right]-$$
$$\langle u_i''\rangle\frac{\partial\langle p\rangle}{\partial x_i}+\langle p'\frac{\partial u_i''}{\partial x_i}\rangle\;. \quad (25)$$

Where the pressure term in the momentum equations caused the appearance of the pressure diffusion $\langle p'u_j''\rangle$, pressure work $\langle u_i''\rangle\partial\langle p\rangle/\partial x_i$, and pressure dilation $\langle p'\partial u_i''/\partial x_i\rangle$ terms. The term $\langle t_{ij}\partial u_i'/\partial x_j\rangle$ may be identified as the dissipation rate of turbulent kinetic energy ϵ_k.

At this point the responsibility of modeling $\mathcal{U}$ has been delegated to modeling the turbulent kinetic energy k. The dissipation rate, with units of energy per second, may again be modeled on terms of dimensional grounds, i.e. $\epsilon_k \propto \rho\mathcal{U}^3/\mathcal{L}$. By reusing the velocity scale $\mathcal{U} = \sqrt{k}$ the formulation becomes $\epsilon_k \propto \rho k^{3/2}/\mathcal{L}$. By neglecting all of the pressure terms and modeling the molecular diffusion and turbulent transport of

k by a gradient diffusion hypothesis (i.e. the term $\mathcal{D}_k$), eq. (26) becomes the model equation for the turbulent kinetic energy:

$$\frac{\partial\langle\rho\rangle k}{\partial t}+\frac{\partial\langle\rho\rangle\left\{u_i\right\}k}{\partial x_i}=\underbrace{\langle\rho\rangle\sqrt{k}\mathcal{L}\widehat{S}_{ij}\widehat{S}_{ij}-\frac{2}{3}\langle\rho\rangle k\frac{\partial\left\{u_i\right\}}{\partial x_i}}_{\mathcal{P}_k}-\underbrace{\beta_k\langle\rho\rangle\frac{k^{3/2}}{\mathcal{L}}}_{\epsilon_k}+\underbrace{\frac{\partial}{\partial x_i}\left[\langle\rho\rangle\left(\nu+\sigma_k\nu_t\right)\frac{\partial k}{\partial x_i}\right]}_{\mathcal{D}_k}, \tag{26}$$

where the production term has been expanded by substituting the model for the turbulent stress τ_{ij} defined in eq. (24). Although these equations have been derived using Reynolds averaging, similar equations may be derived using a spatial filter and applying the same assumptions.

To complete the construction of turbulence modeling equations by dimensional analysis two main approaches are considered. The first approach is to model the specific turbulent dissipation $\omega\equiv\mathcal{U}/\mathcal{L}$, such that $\nu_t=k/\omega$ and $\epsilon_k\propto k\omega$. The governing equation for ω may be related to the enstrophy equation, but is historically formulated partly on dimensional grounds and partly on empirical grounds as [11]:

$$\frac{\partial\langle\rho\rangle\omega}{\partial t}+\frac{\partial\langle\rho\rangle\left\{u_i\right\}\omega}{\partial x_i}=\alpha_\omega\frac{\omega}{k}\tau_{ij}\frac{\partial u_i}{\partial x_j}+C_D-\beta_\omega\rho\omega^2+\frac{\partial}{\partial x_i}\left[\rho\left(\nu+\sigma_\omega\nu_t\right)\frac{\partial\omega}{\partial x_i}\right], \tag{27}$$

where one may optionally include the cross-diffusion term C_D as defined in eq. (28) in order to reduce the dependency of the specific turbulent dissipation ω on its freestream value:

$$C_D=\sigma_d\frac{\langle\rho\rangle}{\omega}\max\left[0,\frac{\partial k}{\partial x_i}\frac{\partial\omega}{\partial x_i}\right]\ . \tag{28}$$

The combination of these two modeling equations is known as the k-ω turbulence model. This model is generally (tuned to be) very dissipative and prevents the appearance of any resolved turbulence. Hence the entire turbulent spectrum will be modeled by the k-ω equations. This corresponds to the underlying assumption of Reynolds averaging: modeling the effects of the complete turbulent spectrum on the mean flow. As such the k-ω model finds its application as a RANS turbulence model.

The model coefficients for the classical Wilcox k-ω model, the Wilcox model with cross diffusion, and the turbulent/non-turbulent (TNT) k-ω model (the one used in this thesis) are given in tab. (1) [10, 12].

Table 1: Model coefficients for the Wilcox, Wilcox with cross-diffusion, and TNT variants of the k-ω RANS turbulence model

Coefficient	Wilcox	Wilcox with C_D	TNT
β_k	0.09	0.09	0.09
σ_k	0.5	1.0	0.67
α_ω	0.55	0.50	0.55
β_ω	0.075	0.075	0.075
σ_d	0.0	0.3	0.5
σ_ω	0.5	0.6	0.5

The second approach is to model the lengthscale $\mathcal{L}$ by relating it to the local grid size in a simulation as $\mathcal{L}=C_1\Delta$, where Δ is a measure of the grid size and C_1 a model constant. This approach is usually taken for SGS models where some portion of the turbulence is resolved. In this case eq. (26) may be used directly to model the turbulent kinetic energy k.

The Smagorinsky model is a classical turbulence model that further assumes that the production $\mathcal{P}_k$ and dissipation ϵ_k of turbulent kinetic energy k are balanced. For incompressible flows the governing algebraic equation for k is given by [9]:

$$\mathcal{P}_k=\epsilon_k\implies k=\mathcal{L}^2\frac{1}{\beta_k}\widehat{S}_{ij}\widehat{S}_{ij}\implies\nu_t=\rho\sqrt{k}\mathcal{L}=\rho C_s\Delta^2\sqrt{\widehat{S}_{ij}\widehat{S}_{ij}},\quad\text{where}\quad C_s=\frac{C_1^2}{\beta_k}\ . \tag{29}$$

The Smagorinsky SGS model tends to require very fine grids in simulations with walls. If the grids are too coarse then the production and dissipation of SGS turbulent kinetic energy are not accurately modeled, leading to incorrect results. In order to ameliorate this issue one may apply a form of van Driest damping: reducing the lengthscale near the wall, effectively reducing the eddy viscosity, without explicitly refinining the grid near the wall.

In this particular derivation the Smagorinsky constant C_s is written in terms of a model constant of the k-equation. Ordinarily a derivation would arrive at the second form for ν_t in eq. (29) by only introducing the model constant C_1 and omitting β_k.

By modeling the turbulent stress using a k-equation, its turbulent transport and molecular diffusion by a diffusion term, and neglecting the pressure-based correlations, all unclosed terms are accounted for except for the turbulent heat flux term. Like the turbulent stress term it is modeled analogously to the molecular heat flux as:

$$\langle \rho h'' u_j'' \rangle = -\frac{\mu_t c_p}{Pr_t} \frac{\partial \langle T \rangle}{\partial x_j}, \tag{30}$$

where the turbulent Prandtl number may be fixed at a constant value [10].

2.3 Considered Flows

Simulations of two types of flows have been performed to investigate hybrid RANS/LES models and the performance of the `ensolv` program: decaying Homogeneous Isotropic Turbulence (HIT) and Turbulent Channel Flow (TCF). HIT provides a simple test case to ensure that the modeled turbulent stress produces the correct distribution of turbulent energy over the resolved lengthscales, while TCF simulations may be used to assert that the modeling results in solutions that adhere to several universal laws describing the behaviour of flows near walls. This section will present some distilled background information on these two classical CFD test cases. For a more satisfactory and more detailed exposition of these subjects one may consult various reference materials [9, 10, 11].

2.3.1 Homogeneous Isotropic Turbulence

Turbulent flow may be informally described as the chaotic motion of a collection of eddies, each of them having a characterizing lengthscale l, velocity scale u and timescale τ. From dimensional analysis of the equations of flow one finds that the velocity scale $u(l)$ and the timescale $\tau(l)$ decrease with decreasing lengthscale l. When the momentum equation is decomposed into its Fourier components, one finds that the magnitude with which dissipation acts on these components scales with the wavenumber $\kappa = 2\pi/l$ squared, hence that most of the dissipation takes place at the smallest of scales.

Combining these two observations allows one to approximately subdivide the full range of lengthscales into three particular subscales: the energy-containing scale, the inertial equilibrium scale and the dissipation scale. The somewhat arbitrary demarcation between the former and latter pair of scales is denoted l_{EI} and l_{DI} (or: κ_{EI} and κ_{DI}). Energy is transferred from the energy-containing scales through the equilibrium range down to the dissipation range, where it is finally dissipated by molecular viscosity. Hence at any given point in time the transfer of energy is roughly equal along all scales down to the dissipation range, and necessarily the rate of transfer must match the rate of dissipation [9].

The governing parameters in the dissipation range are then the rate of dissipation ϵ and viscosity ν. From which one may form the Kolmogorov lengthscale η, velocity scale u_η, and timescale τ_η as:

$$\eta = \left(\frac{\nu^3}{\epsilon}\right)^{1/4}, \quad u_\eta = (\epsilon\nu)^{1/4}, \quad \tau_\eta = \left(\frac{\nu}{\epsilon}\right)^{1/2}. \tag{31}$$

If indeed most of the dissipation occurs at the smallest scales, then due to the constant transfer, the dissipation may be dimensionally approximated at the largest scales as $\epsilon = u_0^3/l_0$ (the subscript 0 indicating the largest scales). Substituting this expression into eq. (31) and forming ratios of scale produces:

$$\frac{\eta}{l_0} = Re^{-3/4}, \quad \frac{u_\eta}{u_0} = Re^{-1/4}, \quad \frac{\tau_\eta}{\tau_0} = \frac{\tau_\eta u_0}{l_0} = Re^{-1/2}, \tag{32}$$

which provides a motivation for the ealier mentioned computational cost of DNS. To a first order approximation: if all turbulent effects have to be captured accurately without any turbulence modeling then the spatial and temporal discretization needs to be on the order of η and τ_η, leading to an expected scaling of computational cost of:

$$\left(\frac{l_0}{\eta}\right)^3 \left(\frac{\tau_0}{\tau_\eta}\right) = \left(Re^{3/4}\right)^3 Re^{1/2} = Re^{11/4} \ . \tag{33}$$

One may expect the velocity statistics in the dissipation range to be fully governed by the dissipation ϵ and the viscosity ν, an observation known as Kolmogorov's first similarity hypothesis. While in the inertial equilibrium range one may expect the flow to depend solely on the dissipation ϵ as governing parameter (as it equals the rate of transfer in that subscale, and the viscosity should not play a large role), known as Kolmogorov's second similarity hypothesis.

Applying a Fourier transformation to the velocity field $\underline{u}\left(\underline{x}, t\right)$ allows one to define the turbulent kinetic energy spectrum $E\left(\underline{\kappa}, t\right) = \langle \hat{u}_i^* \left(\underline{\kappa}, t\right) \hat{u}_i \left(\underline{\kappa}, t\right) \rangle / 2$. The kinetic energy spectrum E may be related to the turbulent kinetic energy k through Parseval's theorem as:

$$k\left(t\right) = \frac{1}{2} \int_{\underline{x}} \langle u_i \left(\underline{x}, t\right) u_i \left(\underline{x}, t\right) \rangle \mathrm{d}\underline{x} = \frac{1}{2} \int_{\underline{\kappa}} \langle \hat{u}_i^* \left(\underline{\kappa}, t\right) \hat{u}_i \left(\underline{\kappa}, t\right) \rangle \mathrm{d}\underline{\kappa} = \int_{\underline{\kappa}} E\left(\underline{\kappa}, t\right) \mathrm{d}\underline{\kappa} \ . \tag{34}$$

From the two aforementioned similarity hypotheses and dimensional analysis (ignoring the dimension of time), one may expect the turbulent kinetic energy spectrum to be described by:

$$E\left(\kappa\right) = \epsilon^{2/3} \kappa^{-5/3} \Psi\left(\kappa\eta\right) \implies E\left(\kappa\right) = C\epsilon^{2/3}\kappa^{-5/3} \text{ if } \kappa\eta \ll 1, \tag{35}$$

where Ψ is the compensated Kolmogorov spectrum function. The latter form is known as the Kolmogorov $-5/3$ spectrum and has been extensively confirmed experimentally [9]. It describes how turbulent kinetic energy is distributed over the wavenumbers (or: lengthscales), which may be used in the practical context of creating turbulence-resolving (e.g. LES-like) turbulence models or testing turbulence-resolving solvers by providing a validation case.

2.3.2 Turbulent Channel Flow

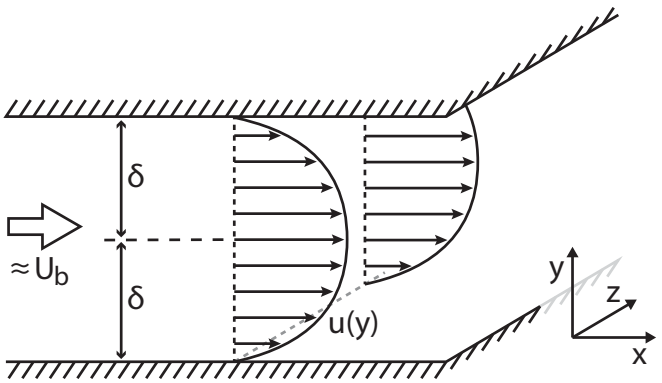

Figure 1: Sketch of the physical dimensions, definitions of the axes, and mean flow direction of TCF

Turbulent Channel Flow (TCF) is the flow between two parallel walls, as depicted in fig. (1), with the mean flow moving parallel to the walls. The channel is defined to have a half-height δ. The x axis is defined to be aligned with the mean flow, and the y and the z-axes are aligned with the wall-normal and the spanwise axis. Turbulence will manifest itself if the Reynolds number is large enough. In this analysis the flow is expected to be steady and the turbulence expected to be fully developed: the mean flow and the turbulence statistics are constant along the homogeneous x and z-axes. By the additional assumption of incompressibility the continuity equation reduces to $\partial\langle v\rangle/\partial y = 0$, hence $\langle v\rangle = 0$ due to the no-slip walls. The Reynolds-averaged equations for the $\langle u\rangle$ and $\langle v\rangle$ velocity components reduce to [9]:

$$\frac{1}{\rho}\frac{\partial\langle p\rangle}{\partial x} = \frac{\partial}{\partial y}\left[\nu\frac{\partial\langle u\rangle}{\partial y} - \langle u'v'\rangle\right], \quad \frac{1}{\rho}\frac{\partial\langle p\rangle}{\partial y} = \frac{\partial\langle v'v'\rangle}{\partial y} \ . \tag{36}$$

By the assumption of fully developed flow the v-momentum equation may be integrated to:

$$\frac{1}{\rho}\langle p\rangle\,(x,y) = p_w\,(x) + \tau_{22}\,(y) \implies \frac{1}{\rho}\frac{\partial\langle p\rangle}{\partial x} = \frac{\partial p_w}{\partial x}, \tag{37}$$

where $p_w\,(x)$ (incorporating the reference pressure) arose by evaluating the integrated expression at the wall. As the streamwise pressure gradient $\partial\langle p\rangle/\partial x$ only depends on the x-coordinate the terms in the u-momentum equation must evaluate to a constant. Integrating and evaluating the resulting equation at the wall clarifies that the streamwise pressure gradient equals the shear stress at the wall:

$$\nu\frac{\partial\langle u\rangle}{\partial y} = u_\tau^2\left(1-\frac{y}{\delta}\right) + \langle u'v'\rangle \implies \frac{\partial\langle u^+\rangle}{\partial\,(y/\delta)} = Re_\tau\left(1-\frac{y}{\delta} + \langle u'^+v'^+\rangle\right), \tag{38}$$

where the second form of the equation uses the non-dimensionalization introduced in eq. (39).

Close to the walls one may apply additional assumptions. Given the importance of shear and viscosity, non-dimensionalization is performed in terms of a friction velocity u_τ. This provides distances in terms of wall-units y^+ and an appropriate friction Reynolds number Re_τ, all defined as:

$$u_\tau = \sqrt{\frac{\tau_w}{\rho}} = \sqrt{\nu\left.\frac{\partial\langle u\rangle}{\partial y}\right|_w}, \quad Re_\tau = \frac{u_\tau\delta}{\nu}, \quad y^+ = \frac{u_\tau y}{\nu} = Re_\tau\frac{y}{\delta} \ . \tag{39}$$

There are several roads to arriving at the universal law of the wall: the practical approach of applying boundary-layer approximations and invoking a mixing length hypothesis, or by dimensional analysis. Taking the approach of dimensional analysis: a governing equation for the mean velocity gradient is formulated using a non-dimensional function Φ, its non-dimensional arguments (formed from ρ, ν, δ, and τ_w) being a lengthscale ratio y/δ and a viscous lengthscale ratio $y/\delta_\nu = y^+$ [9], as:

$$\frac{\partial\langle u^+\rangle}{\partial y^+} = \frac{1}{y^+}\Phi\left(\frac{y}{\delta}, y^+\right) \ . \tag{40}$$

Two limits of this equation are considered. For the former one assumes the viscous scale dominates near the wall, thereby obtaining an expression for the inner layer:

$$\lim_{y/\delta\to 0}\frac{\partial\langle u^+\rangle}{\partial y^+} = \frac{1}{y^+}\Phi_I\left(y^+\right) \implies \langle u^+\rangle = \int_0^{y^+}\frac{1}{y'}\Phi_I\left(y'\right)\mathrm{d}y' = f_w\left(y^+\right), \tag{41}$$

where Φ_I is the near-wall variant of Φ, and f_w embodies the law of the wall. Due to the no-slip condition $f_w\,(0) = 0$, and due to the chosen non-dimensionalization:

$$\left.\frac{\partial\langle u^+\rangle}{\partial y^+}\right|_{y^+=0} = \left.\frac{\partial f_w}{\partial y^+}\right|_{y^+=0} = 1 \ . \tag{42}$$

Hence, very close to the wall, in the so-called viscous sublayer, one may expect $u^+ \approx y^+$. Moving away from the wall, but remaining in the inner layer, viscosity becomes negligable. Hence Φ_I loses its

dependency on y^+ and approaches a constant $1/\kappa$, $\kappa \approx 0.41$ being the von Kármán constant. The integral in eq. (41) may then be evaluated to:

$$\langle u^+ \rangle = \int_0^{y^+} \frac{1}{\kappa y'} \mathrm{d}y' = \frac{1}{\kappa} \log\left(y^+\right) + B, \tag{43}$$

which is known as the log-law, the region in which it applies is known as the log-layer. The intermediate region between the viscous sublayer and the log-layer is called the buffer layer.

The other limit of Φ is obtained when moving even further away from the wall: the viscous stresses remain negligible, but the lengthscale ratio y/δ becomes of importance again. The equation for this outer layer is often written in terms of the velocity defect law:

$$\langle u^+ \big|_{y=\delta} \rangle - \langle u^+ \rangle = F_D\left(\frac{y}{\delta}\right) = \int_{y/\delta}^{1} \frac{1}{y'} \Phi_O\left(y'\right) \mathrm{d}y', \quad \text{where} \quad \lim_{y^+ \to \infty} \Phi\left(\frac{y}{\delta}, y^+\right) = \Phi_O\left(\frac{y}{\delta}\right) \ . \tag{44}$$

The velocity defect law F_D is a non-universal function, and the region where the inner and outer layer overlap is aptly referred to as the overlap region. All of the aforementioned regions change in relative size with varying Reynolds numbers. A stylistic representation of the aforementioned wall regions is shown in fig. (2).

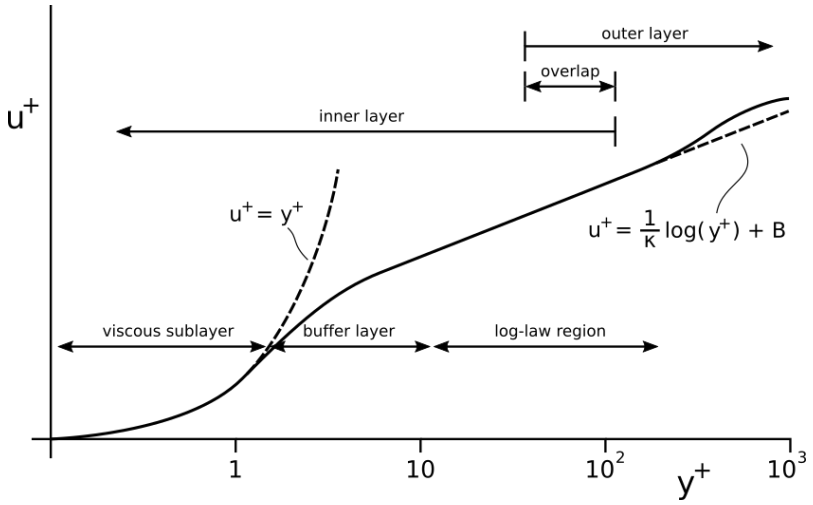

Figure 2: Stylistic depiction of a near-wall region with annotations for the various characteristic regions.

As the viscous sublayer and the log-law region are governed by roughly universal laws (at a high enough Reynolds number, and noting there is always some discussion regarding the exact value of the von Kármán constant κ [1]), the performance of turbulence models may be measured in part by how well they produce the expected near-wall velocity profile.

3 Blended RANS/LES Models

In industrial CFD applications the RANS formulation has been applied successfully with a variety of turbulence models [1]. Due to the modeling of all turbulent scales the computational cost on modern computers is relatively low, allowing the simulation of entire aircraft. The implicit downside of a RANS model lies in its averaging: the models cannot handle unsteadiness, massive separation or aeroacoustic simulations well.

LES would allow for all of these flow phenomena to be captured more accurately, but this comes at a high computational cost. Because actual turbulence is resolved, and because most of these models (excluding Very-Large Eddy Simulation) require a high resolved-to-unresolved turbulence ratio, these models feature very fine spatial and temporal discretizations [9]. An estimation of the total computational cost of a Wall-Resolved LES (WRLES) is $Re^{0.6}$ for the outer layer and amounts to $Re^{2.4}$ if the boundary layer is resolved [2]. Hence the cost of a WRLES approaches the scaling ordinarily associated with DNS.

This computational cost was recognized early and led to the development of a large number of wall-modeling techniques to reduce the excessive computational cost near walls [2]. Among these ideas are methods that use a type of RANS turbulence modeling near walls, and (gradually) switch to a SGS model away from them. These types of models are called hybrid RANS/LES models, belonging to the larger category of Wall-Modeling LES (WMLES).

A rough classification of these models will be given in section 3.1, along with several examples of hybrid formulations and their inherent issues. After this introductory tour of hybrid models, the issues they generally suffer from will be discussed in more detail in section 3.2.

3.1 Types of Blended RANS/LES Models

The inspiration for blended RANS/LES methods is the similarity between the equations produced by Reynolds-averaging and those produced by spatial filtering, as shown in eq. (13) and eq. (20). Most solvers do not apply these filters explicitly, but solve implicitly for the filtered quantities. Hence as one blends between a Reynolds stress-like to a SGS-like turbulence model one may expect the solution for the flow quantities to blend between Reynolds-averaged and spatially filtered quantities. In generic terms, such a blended turbulence model τ_{ij}^M may be formulated as [3]:

$$\tau_{ij}^M = f_R \tau_{ij}^R + f_L \tau_{ij}^L \tag{45}$$

Where f_R blends the RANS turbulence model τ_{ij}^R and f_L blends the SGS model τ_{ij}^L. This formulation may be used to arrive at a rough classification in order to simplify further discussions [3]: a damped RANS model is formulated by setting $f_L = 0$ and $f_R \in [0, 1]$, while a blended turbulence model varies both f_L and f_R. For a blended turbulence model the most common formulation is $f_L = f$ and $f_R = 1 - f$. In case f varies smoothly then the model has a soft interface and in case f is a step function then the model has a hard interface.

In case the blending functions are prescribed and do not depend on the flow then the model is called zonal. Conversely, if the blending automatically adjusts to the local flow conditions and/or the grid then it is called a non-zonal method. In the remainder of this document subdomains where $f_R \to 1$ and $f_L \to 0$ are called RANS-domains, and subdomains where $f_R \to 0$ and $f_L \to 1$ will be called LES-domains. Additionally, non-hybrid simulations using a RANS model or a SGS model will be called pure RANS and pure LES simulations.

A wide variety of hybrid RANS/LES have been formulated. This chapter will only discuss the ones that are relevant to this work, either because their line of thought has been adopted, or because they are historically relevant to the presented results.

3.1.1 Detached Eddy Simulation

Detached Eddy Simulation (DES) is an early non-zonal hybrid RANS/LES model whose formulation is motivated by the fact that although near-wall resolved turbulence requires very refined grids for accurate simulations, the turbulence in regions of massively separated flow may be accurately computed using cell sizes much larger than the Kolmogorov scales [13]. Ordinary RANS models cannot deal with unsteadiness in separated regions, so replacing it with a SGS formulation should allow for more accurate simulations of these flows, and potentially allows the quantification of unsteady loads and/or aerodynamically generated noise. To achieve such a formulation DES switches from a near-wall Spalart-Allmaras (SA) model to a Smagorinsky-like SGS model in the outer flow based on the lengthscales involved in each of the models.

If the production and dissipation term in the SA equation are in balance, then $\nu_t \propto |S|\, d^2$, where d is the wall distance. In a Smagorinsky SGS model the balance between production and dissipation is assumed, and the eddy viscosity scales as $\nu_t \propto |S|\, \Delta^2$, where Δ is the filter width. The principle behind DES is to replace the lengthscale d in the SA model with a term $\tilde{d}$ that is defined as:

$$\tilde{d} = \min\left[d, C_{\mathrm{DES}}\Delta\right], \quad \text{where} \quad \Delta = \max\left[\Delta_x, \Delta_y, \Delta_z\right] \ . \tag{46}$$

Then near walls $d < C_{\mathrm{DES}}\Delta$, causing DES to employ a normal SA turbulence model, while a certain distance away from the wall $C_{\mathrm{DES}}\Delta < d$, causing the formulation to use a Smagorinsky-like model. Because the SA turbulence model governs the eddy viscosity to molecular viscosity ratio $\nu_t/\nu = \tilde{\nu}$, there are no discontinuities in the eddy viscosity field or in the terms constituting the SA-equation.

Although the original author has stated that the intention of DES was to model the entire boundary layer using the RANS formulation, it has seen many applications in which the switch between formulations ocurred inside the boundary layer [5]. This resulted in a variety of issues (discussed in section 3.2). To prevent some of these a boundary-layer shielding function is included in the Delayed DES (DDES) method to prevent an undesirable switch between RANS and LES formulation [14]. Improved Delayed DES (IDDES) redefines the filter width Δ to include the wall distance, such that it exhibits a sharp near-wall variation (accompanied by a similarly sharp variation in eddy viscosity ν_t) [15]. IDDES defines two types of lengthscales: one is essentially the DDES formulation and called the DDES branch, the other one is empirically formulated in order to make the DES-like formulation work more satisfactory with a near-wall interface, therefore called the WMLES branch. These two branches are then blended together with an empirical function such that the method is allowed to work well with a near-wall interface.

3.1.2 Constrained Large Eddy Simulation

The problems encountered with hybrid methods introduced in section 3.2 pertain both to incorrect mean quantities (such as an incorrect near-wall velocity profile), as to incorrect turbulent statistics (such as the resolved turbulent stress). An incorrect sum of resolved and modeled stresses leads to an incorrect mean flow solution. The Constrained LES (CLES) formulation aims to correct for the errors in the mean flow by constraining the mean turbulent stress to the stresses predicted by a RANS formulation [16].

To arrive at the constraining term the spatially filtered Navier-Stokes equations are Reynolds averaged. Comparing the resulting equation to the RANS formulation produces the following identity:

$$\underbrace{\langle \widetilde{u_i}\widetilde{u_j}\rangle - \langle \widetilde{u_i}\rangle\langle \widetilde{u_j}\rangle}_{\tau_{ij}^r} + \underbrace{\langle \widetilde{u_i u_j} - \widetilde{u_i}\widetilde{u_j}\rangle}_{\langle \tau_{ij}^L\rangle} = \underbrace{\langle u_i u_j\rangle - \langle u_i\rangle\langle u_j\rangle}_{\tau_{ij}^R} \implies \langle \tau_{ij}^L\rangle = \tau_{ij}^R - \tau_{ij}^r, \tag{47}$$

where τ_{ij}^r are the resolved stresses, τ_{ij}^L the SGS stresses and τ_{ij}^R the total Reynolds stresses. The equation provides a formulation for a constrained model's stress τ_{ij}^M by decomposing the SGS stress into its mean $\langle \tau_{ij}^L\rangle$ and its fluctuating part $(\tau_{ij}^L)' = \tau_{ij}^L - \langle \tau_{ij}^L\rangle$. By subsequently replacing the mean with the expression in eq. (47) the constrained model is formulated as:

$$\tau_{ij}^M = \tau_{ij}^R - \tau_{ij}^r + \tau_{ij}^L - \langle \tau_{ij}^L \rangle \ . \tag{48}$$

A similar kind of constraining term may be derived for the modeled turbulent heat flux [17]. Both the incompressible as the compressible formulation produce favourable results on a wide variety of flows.

3.1.3 Isotropic/Anisotropic Decomposition

The two-velocity method is based on the decomposition of the turbulent stress into an isotropic part and an anisotropic part, as shown in eq. (49) [18]. This type of decomposition inspired many hybrid models and can therefore be seen in earlier hybridization attempts as well [19].

$$\tau_{ij}^M = 2\nu_a \langle S_{ij} \rangle + 2\nu_i \left(S_{ij} - \langle S_{ij} \rangle \right) \ . \tag{49}$$

The two-velocity method used a RANS model to govern ν_a as $(1 - f_b)\nu_R$ and a SGS model to govern ν_i as $f_b \nu_L$. The empirical blending function f_b is based on the models' lengthscales and formulated as:

$$f_b = \tanh \left[\left(C_l \frac{L_t}{\Delta} \right)^n \right], \tag{50}$$

where C_l and n are empirical factors, L_t the turbulent lengthscale as predicted by the RANS model and Δ the filter width. The model may be described as a hybrid RANS/LES method where a RANS model blends with a high-pass filtered SGS model. The model has some success in reproducing the expected velocity profiles in channel flow, but there is still a reasonable dependence on the chosen blending function.

The dual-grid method builds upon the two-velocity method described above and the dual-mesh method [20]. The blending function from the two-velocity method is redefined to be dependent on the SGS lengthscale $C_1\Delta$ instead of just the filter width Δ, and introduces a CLES corrective term (as defined in eq. (48)) [21]. The corrective term is subject to a second blending function such that it is activated near the walls and disabled away from it.

The dual-grid method borrows the idea of using two simultaneously running simulations on separate grids from the dual-mesh framework. One simulation is governed solely by a RANS formulation on a wall-refined grid that expands rapidly away from the wall. The other grid uses the hybrid formulation on a grid that has roughly isotropic grid cells and is rather underresolved near the walls. The two simulations are coupled through so-called drift terms.

3.1.4 Model Split Method

The model split method is introduced with the reasoning that any LES model does not simultaneously predict both the full Reynolds stresses and the SGS stress at the same time [22]. Hence the model stress τ_{ij}^M is decomposed into a subgrid Reynolds stress term $\tau_{ij}^{\mathrm{SGRS}}$ and a subgrid energy transfer term $\tau_{ij}^{\mathrm{SGET}}$. Given that a hybrid simulation contains resolved turbulence, the average turbulent stress is $\tau_{ij}^{\mathrm{SGRS}} \approx \langle u_i' u_j' \rangle - \langle u_i^> u_j^> \rangle$, where u_i' is the Reynolds fluctuation, and $u_i^>$ is the resolved portion of the fluctuations.

The model split method then approximates this mean component as $\tau_{ij}^{\mathrm{SGRS}} \approx \alpha \tau_{ij}^R$, where τ_{ij}^R would be governed by a RANS turbulence model. The parameter α is formulated in terms of the resolved turbulent kinetic energy k_r and the total turbulent kinetic energy k_{tot} as $\alpha = 1 - k_r/k_{\mathrm{tot}}$. The SGET term may take any form, but the author states that a high-pass filtered variant is chosen such that $\langle \tau_{ij}^{\mathrm{SGET}} \rangle = 0$. This produces the following formulation:

$$\tau_{ij}^M = \tau_{ij}^{\mathrm{SGRS}} + \tau_{ij}^{\mathrm{SGET}} \approx \tau_{ij}^R - \langle u_i^> u_j^> \rangle + \tau_{ij}^{\mathrm{SGET}} \approx \alpha \tau_{ij}^R + \tau_{ij}^{\mathrm{SGET}}, \quad \text{where} \quad \alpha = 1 - \frac{k_r}{k_{\mathrm{tot}}} \ . \tag{51}$$

Although implied, but not explicitly stated in the paper introducing the model split method: if the implementation of the SGET term is written in terms of a SGS model τ_{ij}^L as $\tau_{ij}^{\text{SGET}} = \tau_{ij}^L - \langle \tau_{ij}^L \rangle$, then the CLES model is obtained once more.

3.2 Problems Encountered in Blended RANS/LES Models

Blended RANS/LES models suffer from a variety of issues. These are to some degree also present in other hybrid and wall-modeling approaches. The interpretation of these issues is somewhat simplified by considering a hypothetical hard interface method. Fig. (3) is a stylistic depiction of phenomena present in hybrid RANS/LES simulations.

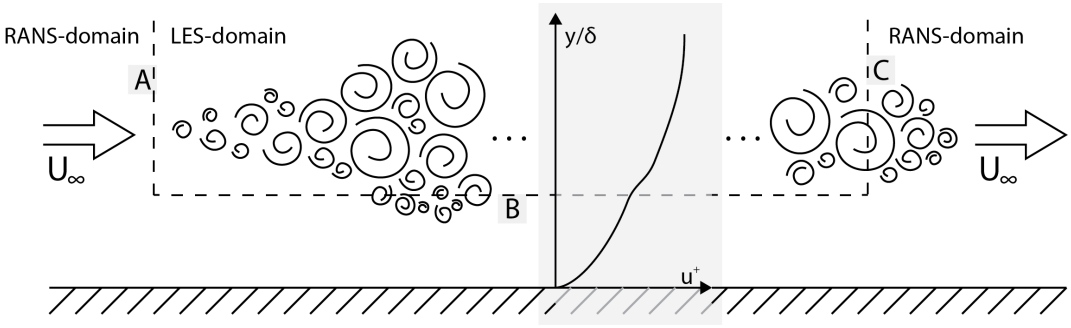

Figure 3: Graphical depiction of the issues present in hybrid RANS/LES simulations

With the flow moving from left to right. The flow is initially modeled using a RANS formulation, followed by an LES-domain large enough to attain fully developed turbulence. Finally the turbulent flow moves into a RANS domain again, where the resolved turbulence is dissipated. In the middle there is a flow-parallel interface near a wall where turbulence is resolved at some distance above the interface, and dissipated at some distance below the interface. Near this interface the turbulence is underdeveloped in the LES-domain, and undesirable in the RANS-domain. This is spatially correlated with a "jump" in velocity profile, known as the Log-Layer Mismatch (LLM).

The RANS-inflow issue is discussed in section 3.2.1, while the issues due to the flow-parallel interface in a boundary layer are discussed in section 3.2.2 through section 3.2.4. The RANS-outflow issue will not be discussed in this work. Finally, within the RANS-domain there are large streak-like structures commonly referred to as superstreaks, these will be discussed in section 3.2.5.

3.2.1 Grey Area

In the region marked A in fig. (3) flow moves from a RANS-domain into an LES-domain. If the flow is turbulent according to the RANS turbulence model, then ideally this modeled turbulence should manifest itself as resolved turbulence and the appropriate amount of SGS modeled stress the moment it passes the interface.

Due to the ad-hoc coupling of the velocity field and the turbulence modeling the actual situation is that the modeled turbulent kinetic energy k is quickly dissipated in the LES-domain (if modeled by an equation at all, otherwise there will simply be a discontinuity), and turbulence must still develop. This lack of resolved turbulence is called the grey area problem.

Focusing solely on this lack of resolved turbulence, two types of solutions have been proposed in literature. One is to reduce the dissipation close to the interface such that turbulence may develop more quickly [23]. One such example, which may be applied in a Smagorinsky-like SGS model for highly anisotropic grid cells, is to sensitize the filter width Δ to the direction of the vorticity vector, which is defined for grid cells with vertices $\underline{r}_n$ as:

$$\Delta = \Delta_\omega = \alpha \frac{1}{\sqrt{3}} \max_{n,m} \left| \frac{\underline{\omega}}{|\underline{\omega}|} \times (\underline{r}_n - \underline{r}_m) \right| . \tag{52}$$

In the simple case of the vorticity vector being aligned with the largest axis of a hexahedral cell, the filter width will be defined by the other two smaller axes. As an example: for a quasi-2D simulation of a planar shear layer with grid cells elongated in the spanwise direction, the filter width will be dependent on the other two (smaller) axes during the initial large-scale instabilities.

Another approach is to force the transition to turbulence through some kind of forcing. A large number of industrially applicable methods have been proposed. Some of these will be mentioned here in passing, but without delving in too much detail. The Stochastic Eddy Method defines a certain box surrounding the RANS/LES domain [24]. A fixed number of control points $\underline{x}_i$ are introduced at the inflow plane, convected with the flow inside the box, and are removed upon reaching the outflow plane. These control points govern a forcing field that has a certain level of spatial correlation. The Stochastic BackScatter (SBS) method convects a random field with the flow that applies random forcing to the momentum equation. This method is explained in more detail in section section 4.2. Alternatively, the Zonal DES (ZDES) method may introduce cylindrical surface-attached obstacles in the flow using immersed boundary conditions. These generate streamwise vortices which are broken down some distance downstream using a forcing method [25].

3.2.2 Double Accounting of Stress

If a flow containing resolved turbulence enters a RANS-domain, either by the mean flow directly entering a RANS-domain (region C in fig. (3)) or by turbulent motions across an interface parallel to the mean flow (region B in fig. (3)), then two issues present themselves. Firstly there is a combination of resolved stress and modeled stress in the RANS-domain, while the RANS turbulence model is supposed to be modeling all turbulent stress without the presence of this resolved portion. This double-accounting of stress is an issue if the resolved turbulence is not dissipated fast enough. Secondly, the resolved turbulence interferes with the RANS modeling equations and might cause the modeled eddy viscosity ν_t to deviate from the predictions of a simulation without resolved turbulence.

Haering et al. [22] mention that hybrid models should aim towards transferring resolved turbulent kinetic energy to modeled turbulent kinetic energy as soon as possible when it enters the RANS-domain, but shows that reasonable results may be obtained without doing this actively. Section 4.5.3 investigates the influence the turbulent fluctuations have on the total stress and a k-ω turbulence model for the X-LES formulation.

3.2.3 Modeled Stress Depletion and Grid Induced Separation

As explained in the introduction of this chapter hybrid RANS/LES models are formulated to facilitate the use of coarse near-wall grids to reduce the computational cost associated with a WRLES. Whenever a switch to LES model occurs too deep in the boundary layer then the filter width is likely too large to allow turbulence to develop. In this case only the SGS stress model is governing the turbulent stress. The resulting diminished turbulent stress is known as modeled stress depletion. In severe cases this leads to early separation of the flow, in that case one speaks of grid induced separation [4].

As mentioned in section 3.1.1, the DDES and IDDES method circumvent this issue by preventing the switch inside the boundary layer in the first place. Another approach is taken in the ZDES method, in which the burden of correct modeling is transferred from turbulence modeler to the CFD user [26]. In this method subdomains are marked by the CFD user to indicate the expected turbulent phenomena.

3.2.4 Log-Layer Mismatch

The original DES model was formulated such that the entire boundary layer would be modeled using a RANS formulations. However, upon application of the method with the interface closer to the wall many authors find a jump in the velocity profile known as the LLM, as depicted graphically in the graph and region B in fig. (3). These problems present themselves in other kinds of WMLES simulations as well [27].

If such a RANS/LES switch occurs inside the boundary-layer, then the mean flow is generally parallel to the interface. This implies that the turbulent velocity field passes through the interface in a chaotic fashion. Here all of the aformentioned problems present themselves: if the turbulent flow field moves into the RANS-domain then it will interfere with the RANS turbulence modeling and is dissipated rapidly due to the high eddy viscosity. Due to the high damping near the interface there is a general lack of resolved turbulence within the LES domain.

Apart from preventing the switch to LES through a shielding function, as in DDES, several solutions have been proposed to reduce the LLM. IDDES artificially augments the eddy viscosity within the LES-domain to make up for the lack of resolved stress, but this has the downside of further delaying the development of turbulence. Some authors have also attempted to use precomputed RANS solutions to augment the eddy viscosity to desirable levels [28].

Introducing stochastic forcing to the flow near the interface is quite effective at reducing the LLM. An early attempt applied forcing with a white-noise spectrum, both with a prescribed forcing intensity profile and with a controller aiming for a prescribed resolved-to-unresolved turbulent kinetic energy ratio [29, 30]. In some cases the LLM was completely removed, but required rather large amount of forcing. A reason for the large amount of forcing may be that it induces small-scale fluctuations in the flow. This is somewhat advantageous, as it prevents interference with the well-developed large-scale structures [22]. On the other hand these small-scale fluctuations are also the ones that are most quickly dissipated. A study investigating the effect of forcing scales on the LLM found that the most effective forcing scales (measured by the reduction in LLM, not by how physically correct the forcing is, as emphasized by the author) have wavelengths λ on the order of $3\Delta < \lambda < \delta$, where Δ and δ are the cell size and channel half-height, respectively [31].

Several other fundamental approaches have been considered as well. Some noteworthy ones have attempted to interpret the RANS modeling as a SGS model with an extremely large filter width applied along the flow's homogeneous directions [32]. This would allow recasting problems near the hybrid RANS/LES interface as LES commutation error problems. This resulted in a smaller LLM, but also spread out over a larger region.

3.2.5 Superstreaks

An anomolous result in hybrid RANS/LES simulations of TCF is the presence of so-called superstreaks. These superstreaks are very long streamwise elongated structures that have a lower or higher velocity than the average in a wall-parallel plane. Visualising the flow in wall-parallel surfaces shows alternatingly large and small streamwise velocities along the spanwise direction. These superstreaks start in the boundary layer, very close to the wall in the RANS-domain, but extend towards the center of the channel, past the RANS/LES interface, to inside the LES domain.

Most of the studies on DES-like methods report these superstreaks, independent of the grid discretization, employed turbulence models, location of the interface or matching conditions [31]. In a peculiar test case where the role of RANS and SGS models is reversed the superstreaks are present as well [33]. It appears that stochastically forcing the flow (with the original intent of reducing the LLM) manages to reduce the size of the superstreaks [30], although if the forcing is applied away from the interface then the LLM may be removed as well while keeping the superstreaks somewhat intact [31]. It is still somewhat unclear why these structures are present at all and whether they are closely coupled to other anomolous results

or a completely separate issue. To some degree it has at least been ascertained that the superstreaks do not cause the decorrelation of the $\langle u^{>} v^{>} \rangle$ turbulent stress.

4 Analysis of the X-LES method

The eXtra-Large Eddy Simulation (X-LES) method is a hybrid RANS/LES method with optionally applied stochastic forcing and high-pass filtering of the SGS model. This method will be investigated in detail in this chapter. The formulation of the method is given in section 4.1. Its particular formulation of stochastically forcing the flow is shortly described in section 4.2. The HIT and TCF simulations that have been performed are described in section 4.3. The former type of simulation has been used to retune the stochastic model, as detailed in section 4.4, whereas the latter type of flow is used in section 4.5 to ascertain the accuracy of the method.

4.1 X-LES Turbulence Modeling Equations

The X-LES method is a hybrid RANS/LES method applying a RANS formulation near walls [6]. Within these RANS-domains a k-ω turbulence model is used, which includes a cross-diffusion term C_D in the dissipation equation. The LES-domains are governed by a k-equation SGS model. The definition of these turbulence modeling equations is given in eq. (53) and eq. (54) where, due to the ambiguity of employed filtering, indications of Reynolds averaging or spatial filtering are omitted. Both models use the same k-field, and a modification is made to the dissipation equation to ensure that the switching between RANS and SGS formulation occurs simultaneously in both turbulence modeling equations.

$$\frac{\partial \rho k}{\partial t} + \frac{\partial \rho u_i k}{\partial x_i} = \mathcal{P}_k - \epsilon_k + \frac{\partial}{\partial x_i}\left[\rho\left(\nu + \sigma_k \nu_t\right)\frac{\partial k}{\partial x_i}\right], \tag{53}$$

$$\frac{\partial \rho \omega}{\partial t} + \frac{\partial \rho u_i \omega}{\partial x_i} = \mathcal{P}_\omega - \epsilon_\omega + \sigma_d \frac{\rho}{\omega}\max\left[0, \frac{\partial k}{\partial x_i}\frac{\partial \omega}{\partial x_i}\right] + \frac{\partial}{\partial x_i}\left[\rho\left(\nu + \sigma_\omega \nu_t\right)\frac{\partial \omega}{\partial x_i}\right], \tag{54}$$

where the production and dissipation terms for the k and ω-equation are written as:

$$\mathcal{P}_k = \rho\sqrt{k} L S_{ij}^M S_{ij}^M - \frac{2}{3}\rho k \frac{\partial u_k}{\partial x_k}, \quad \epsilon_k = \beta_k \rho \frac{k^{3/2}}{L}, \quad \mathcal{P}_\omega = \alpha_\omega \rho S_{ij}^M S_{ij}^M - \frac{2}{3}\alpha_\omega \rho \omega \frac{\partial u_k}{\partial x_k}, \quad \epsilon_\omega = \beta_\omega \rho \omega^2 \ . \tag{55}$$

The lengthscale L is then defined in DES-fashion as the minimum of the RANS and LES lengthscales:

$$L = \min\left[L_{\mathrm{RANS}}, L_{\mathrm{LES}}\right] = \min\left[\frac{\sqrt{k}}{\omega}, C_1 \Delta\right], \quad \text{where} \quad \Delta = \max\left[\Delta_x, \Delta_y, \Delta_z\right] \ . \tag{56}$$

As a result, the eddy viscosity ν_t is then implicitly defined as:

$$\nu_t = \sqrt{k} L = \begin{cases} \frac{k}{\omega} & \text{if } \frac{\sqrt{k}}{\omega} < C_1 \Delta \\ C_1 \Delta \sqrt{k} & \text{otherwise} \end{cases} \ . \tag{57}$$

Furthermore, the X-LES method has two options that can be enabled in the solver. The first is the introduction of stochastic forcing through a SBS model added as a forcing term in momentum equations (with corresponding removal from the production term in the k-equation), and the second is to High-Pass Filter (HPF) the rate of strain tensor in the SGS stress and k-prodution term within the LES-domain. Due to the optional filtering the rate of strain term is denoted S_{ij}^M. When it is applied the HPF modeled turbulent stress is governed by:

$$\tau_{ij}^{\mathrm{HPF}} = 2 C_1 \Delta \sqrt{k}\left(\widehat{S}_{ij} - \langle \widehat{S}_{ij} \rangle\right) - \frac{2}{3}\overline{\rho} k \delta_{ij} \ . \tag{58}$$

From experience with the method at NLR the non-zonal application of the method results in switching between both formulations in a small near-wall region. However, when applied to TCF spurious switching between the RANS and LES formulations ocurred in the center of the channel. Hence the method is mainly applied in a zonal manner within this thesis.

4.2 Stochastic Backscatter Model

The SBS model is capable of stochastically forcing the flow [7]. It has its theoretical grounding in attempting to model backscatter from the unresolved scales, and a practical grounding in accelerating the transition to turbulence. The model has been successfully applied to shear layers in order to reduce the grey area. A basic description of the full method will be repeated here in condensed format for completeness sake, albeit with different symbols for the various coefficients.

The point of departure is a completely uncorrelated random field $\mathrm{d}V_j = \mathcal{N}(0, \mathrm{d}\underline{x}\ \mathrm{d}t)$. This random field is transformed into a spatially correlated random field $\mathrm{d}W_j$ by solving the following equation:

$$\left[\mathrm{d}\underline{x}\prod_i\left(I - b^2\frac{\partial^2}{\partial x_i^2}\right)\right]\mathrm{d}W_j = 8b^{3/2}\mathrm{d}V_j\ . \tag{59}$$

Here W_j is the spatially correlated random field associated with the uncorrelated random field V_j. I represents the identity operator and b is a parameter that ensures the desired level of spatial correlation.

To attain a desired level of temporal correlation, and to ensure that the correlated random field ξ satisfies continuity, a Langevin-type equation is solved:

$$\rho\xi_j\mathrm{d}t + \tau\left(\frac{\partial\rho\xi_j}{\partial t} + \frac{\partial\rho u_i\xi_j}{\partial x_i}\right)\mathrm{d}t = \sqrt{2\tau}\rho\mathrm{d}W_j, \tag{60}$$

where ξ_j is a spatially and temporally correlated random field. The parameter τ ensures the desired level of temporal correlation. The stochastic forcing is added to the momentum equation as a forcing function $\underline{f}$ and defined as:

$$\underline{f} = \nabla\times\left(C_I k\underline{\xi}\right), \tag{61}$$

where k is the modeled turbulent kinetic energy and C_I is the forcing intensity coefficient. By modeling the forcing as the curl of a random field the forcing is divergence-free, ensuring that it does not induce any acoustic noise. This also ensures that the power spectrum scales as κ^4, κ being the wavenumber of the forcing, which corresponds to the scaling of backscatter.

This method of construction ensures that the field $\underline{\xi}$ is spatially and temporally correlated as:

$$\langle\xi_i(\underline{x},t),\xi_j(\underline{y},s)\rangle = \delta_{ij}e^{-d^2/2}e^{-|t-s|/\tau},\quad \text{where}\quad d^2 = \frac{\left|\underline{x}-\underline{y}\right|^2}{C_s\Delta^2},\ \tau = \frac{C_t\Delta}{\sqrt{k}}, \tag{62}$$

C_s is the spatial correlation coefficient, C_t is the temporal correlation coefficient and Δ is the grid size as defined in eq. (56). All of the model coefficients were tuned to an intensity of $C_I = 1.0$, spatial correlation of $C_s = 0.1$ and a temporal correlation of $C_t = 0.05$ from earlier work on shear layers and round jets.

4.3 Setup of Simulations

Both HIT as TCF simulations have been performed in order to gauge the effectiveness of the X-LES method. The goal of the HIT simulations was firstly to check how the parameters in the SBS model affected the energy addition/removal across the turbulent kinetic energy spectrum, and secondly to retune its governing parameters such that higher forcing intensities were achieved. The TCF simulations were performed to see how well the X-LES method could reproduce the velocity profiles of RANS and DNS, and to see how well the turbulent statistics match DNS when the RANS/LES interface is placed inside the boundary layer. Setting up these simulations is discussed in section 4.3.1 and section 4.3.2 for HIT and TCF, respectively.

4.3.1 Homogenous Isotropic Turbulence

The simulation setup for HIT is derived from earlier work by Rozema as a PhD student employed at NLR [34]. The flow field is initialized and non-dimensionalized based on experimental results of grid-generated turbulence [35].

Within the experiment $M = 5.08\ cm$ is the grid size used to generate the turbulence. The freestream velocity is $U_0 = 10\ m/s$ and the streamwise RMS fluctuating velocity $\sqrt{u_1^2}$ at the first measurement station is 22.2 cm/s. The experiment measured the 3D turbulent kinetic energy spectrum $E_{\exp}(\kappa_i)$ at three stations, indicated as the locations where $U_0 t/M$ equals 42, 98 and 171.

The simulation domain is a periodic box measuring $11M$ along each axis, with $N = 64$ cells per axis. The velocity is non-dimensionalized using the square root of the energy scale at the initial measurement station, i.e. $u_r = \sqrt{3/2 \cdot 22.2^2} = 27.19 cm/s$, leading to a Reynolds number of $Re = 10129.2$. The Courant Friedrichs-Lewy number is set at $CFL = 1/8 = \Delta_t u_r / \Delta_x$ (which, from experience at NLR, causes the errors due to implicit Runge-Kutta 2$^{\text{nd}}$ order time integration to match those of the spatial discretization), hence the non-dimensional timestep $\tilde{\Delta}_t = \Delta_t u_r / L$ is given as CFL/N.

The initial velocity field for the simulation is generated in Fourier space. At each point in Fourier space the three velocity components represent three degrees of freedom. The first degree of freedom is used to ensure the correct initial energy spectrum is obtained. To this end the experimental spectrum is interpolated in log-log space to produce a continuous experimental spectrum $E_{\exp}(\kappa)$. This represents the energy integrated over a shell in wavenumber of space with radius $|\underline{\kappa}|$. The kinetic energy $E(\underline{\kappa})$ may be computed from the Fourier transformed velocity field $\hat{\underline{u}}(\underline{\kappa})$ as $E(\underline{\kappa}) = \hat{\underline{u}}(\underline{\kappa}) \cdot \hat{\underline{u}}^*(\underline{\kappa})/2 = |\hat{u}(\underline{\kappa})|$. Hence assuming that the transformed velocity magnitude is the same everywhere within a shell of radius $|\underline{\kappa}|$ in wavenumber space, then:

$$|\hat{\underline{u}}| = \frac{1}{\Delta_x^3} \sqrt{\frac{2 E_{\exp}(\underline{\kappa}) \Delta_\kappa^3}{4\pi |\underline{\kappa}|^2}}, \tag{63}$$

where $\Delta_\kappa = 2\pi/\mathcal{L}$ transforms the energy at a singular point into an approximation of the integrated energy in a cube of size Δ_κ^3. The division by the grid size Δ_x^3 ensures that performing an inverse discrete Fourier transform produces the correct velocities.

The second degree of freedom is used to ensure that the generated velocity field is divergence free. On an orthogonal grid the finite volume formulation for the first order derivative is equivalent to a second order finite difference. Denoting the wavenumber indices as $\underline{k} = [k, l, m]^T$ and the grid indices as $\underline{\alpha} = [\alpha, \beta, \gamma]^T$, the derivative of a single velocity component $\partial u/\partial x$ may be written as:

$$\frac{\partial u}{\partial x} \approx \frac{1}{2\Delta_x} \left(u_{\alpha+1,\beta,\gamma} - u_{\alpha-1,\beta,\gamma} \right) = \frac{1}{2\Delta_x N^3} \sum_{k,l,m} \hat{u}_{k,l,m} \exp\left(\frac{2\pi i \underline{k} \cdot \underline{\alpha}}{N} \right) 2i \sin\left(\frac{2\pi k}{N} \right) . \tag{64}$$

Assuming similar grid spacing in all directions ($\Delta_x = \Delta_y = \Delta_z$) then the divergence free requirement may be formulated in discretized fashion as:

$$\sum_j \left. \frac{\partial u_j}{\partial x_j} \right|_{\underline{\alpha}} = \frac{2i}{2\Delta_x N^3} \sum_{k,l,m} \exp\left(\frac{2\pi i \underline{k} \cdot \underline{\alpha}}{N} \right) \left(\hat{u}_{\underline{k}} \sin\left(\frac{2\pi k}{N} \right) + \hat{v}_{\underline{k}} \sin\left(\frac{2\pi l}{N} \right) + \hat{w}_{\underline{k}} \sin\left(\frac{2\pi m}{N} \right) \right) . \tag{65}$$

If this condition must be true for all possible values of $\underline{u}$ at all $\underline{x}_{\underline{\alpha}}$, then this condition may be written as:

$$\hat{\underline{u}}_{\underline{k}} \cdot \begin{bmatrix} \sin(2\pi k/N) \\ \sin(2\pi l/N) \\ \sin(2\pi m/N) \end{bmatrix} = 0 \quad \forall\ \underline{k} . \tag{66}$$

The remaining degree of freedom, the direction of the velocity $\underline{\hat{u}}$ in the plane described by eq. (66), is randomized. After setting the mean components of the velocity field to 0, the Fourier components $\underline{\hat{u}}_{\underline{k}}$ are mirrored in a plane in Fourier space to ensure that performing the discrete inverse Fourier transform produces real values for $\underline{u}_{\underline{\alpha}}$ in physical space.

The density ρ is set to its freestream value everywhere in the domain. The HIT simulations are performed using a k-equation LES model (the SGS branch of the hybrid formulation), whose turbulent kinetic energy k is inititalized assuming a balance between production and dissipation. From eq. (53) and eq. (55), using $C_1\Delta$ as the lengthscale, this means the SGS turbulent kinetic energy k may be computed as:

$$k = \frac{1}{\beta_k} \left(C_1 \Delta\right)^2 \widehat{S}_{ij} \widehat{S}_{ij} \ . \tag{67}$$

Since incompressibility is assumed the pressure p, therefore the total energy, may be computed from the velocity field.

When a simulation adhering the described setup is finished, the turbulent kinetic energy spectrum $\hat{E}_{\text{sim}}$ is obtained from the velocity field $\underline{u}$. The maximum wavenumber at which integration over a sphere can be accurately performed in a box with length L along each axis is $\kappa_{\max} = 2\pi N/2L$. This expression accounts for the Nyquist criterion and the largest sphere that fits inside the periodic box.

The range $\kappa \in [0, \kappa_{\max}]$ is subdivided into N_B bins. The velocity field is Fourier transformed into $\underline{\hat{u}}_{\underline{k}}$, after which the energy may be computed as $\hat{E}_{\underline{k}} = \underline{\hat{u}}_{\underline{k}} \cdot \underline{\hat{u}}^*_{\underline{k}}/2$. Then the energy in a cell in wavenumber space of size Δ_k^3 may be written as $\hat{E}_{\underline{k}} \Delta_k^3$. This energy is equally subdivided over N_R^3 subcells using a spatial refinement factor of N_R along each axis. Then each subcell has an associated wavenumber $\underline{\kappa}_R$ and energy $\hat{E}_{\underline{k}_R} = \hat{E}_{\underline{k}} \Delta_k^3 / N_R^3$. These energies are added to the bin whose bounds contain the refined wavenumber $|\underline{\kappa}_R|$. After this binning operating is performed for all $\underline{\hat{u}}_{\underline{k}}$ then the bins represent the discretized 3D turbulent kinetic energy spectrum $\hat{E}_{\text{sim}}$.

4.3.2 Turbulent Channel Flow

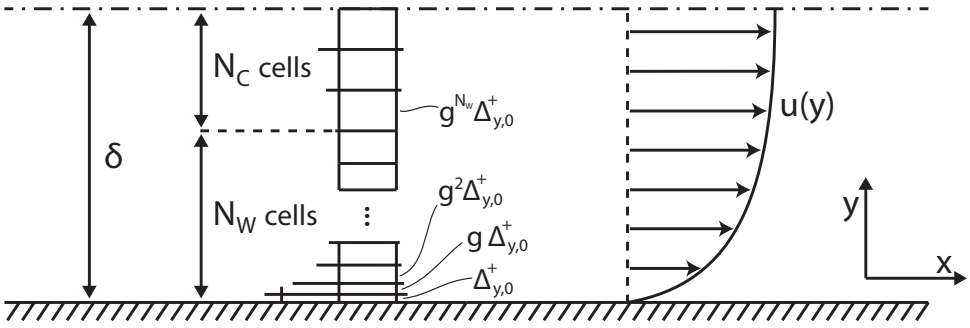

Figure 4: Sketch of the dimensions of half the channel and definitions of grid sizes used to perform simulations.

The TCF simulations are all non-dimensionalized using the channel half-height δ and the bulk Reynold number $Re_b = U_b \delta/\nu$, the bulk velocity U_b being the geometric mean streamwise velocity through the domain. The x, y and z-axes are aligned with the mean flow, wall-normal and spanwise directions. The non-dimensionalized domain measures $[2\pi, 2, \pi]$, has no-slip boundary conditions applied to the bounding y-planes, and periodic boundary conditions applied to the x- and z-planes.

The simulations are performed at various different friction Reynolds numbers Re_τ. Since a large variety of simulations are performed in a zonal manner, which requires placing the RANS/LES interface

at a specific wall-normal coordinate, the generation of grids is automated. The cell size is equispaced in the streamwise and spanwise directions. In the wall-normal direction the region from the wall up to the center of the channel subdivided into a wall-region and a core-region. In the wall-region there is a user-defined initial cell size $\Delta^+_{y,0} < 1$, which grows exponentially with a growth rate g up until the core region, where the remaining cells are equisized. For completeness sake, this is achieved by solving the following equation iteratively for g:

$$\sum_i \Delta^+_{y,i} = Re_\tau = \sum_{i=0}^{N_w} \Delta^+_{y,0} g^i + (N_y - N_w)\, \Delta_{y,0} g^{N_w}, \tag{68}$$

where N_y is the number of cells in half the channel, N_w is the number of cells in the wall-region, $N_c = N_y - N_w$ the number of cells in the core-region, and g is the growth rate. The growth rate is always kept under 1.15 for all simulations.

Because of friction in the channel, the flow will ordinarily slow down. Hence a body force $\underline{f}$ is applied to counteract the friction. Applying a control volume analysis to the incompressible Reynolds-averaged momentum equations, and omitting the terms that disappear at the boundaries due to the periodic boundary conditions, results in the following expression for the u-momentum equation:

$$\frac{1}{\rho}\int_\Omega \frac{\partial \langle p \rangle}{\partial x} \mathrm{d}\Omega - 2A_w \delta f_x = 2\nu A_w \left.\frac{\partial \langle u \rangle}{\partial y}\right|_w . \tag{69}$$

Matching the body force f_x to the wall friction $\tau_w = \sqrt{\nu\, \partial u/\partial y|_w}$ provides the following expression:

$$f_x = \frac{\rho u_\tau^2}{\delta} \implies f_x \frac{\delta}{\rho_\infty u_b^2} = \frac{\rho}{\rho_\infty}\left(\frac{Re_\tau}{Re_b}\right)^2, \tag{70}$$

where the latter form expresses the body force in non-dimensional terms. A streamwise pressure gradient would ordinarily drive the flow, but is now replaced by a body force.

Turbulent and mean flow statistics are collected using a running time-average sampling at the end of each full Runge-Kutta timestep. Simulations using the X-LES method that were started from an initial RANS solution, without SBS model or applied HPF, showed that the turbulent statistics converged to steady values at $TU_b/\delta \approx 240$. From this point onwards statistics are measured over a timespan of $\Delta_T U_b/\delta \approx 300$. The application of the SBS model and/or the HPF SGS formulation showed a more rapid development of turbulence, but even in those cases all statistical results presented in this work use the aforementioned timespan.

4.4 Retuning the Stochastic Backscatter Model

As mentioned in section 4.2, the SBS model has four tunable parameters: the forcing intensity C_I, the spatial and temporal correlation coefficients C_s and C_t, and the X-LES constant C_1. The X-LES constant C_1 also controls the turbulent lengthscale, hence the amount of dissipation.

An initial investigation into the influence of these parameters was performed in a series of HIT simulations where $C_I = 2.0$. The turbulent kinetic energy spectra produced by these simulations are shown in fig. (5). Each of the three sets of lines in each subfigure represent the spectrum at a specific point in time corresponding to experimental measurement stations, as detailed in section 4.3.1.

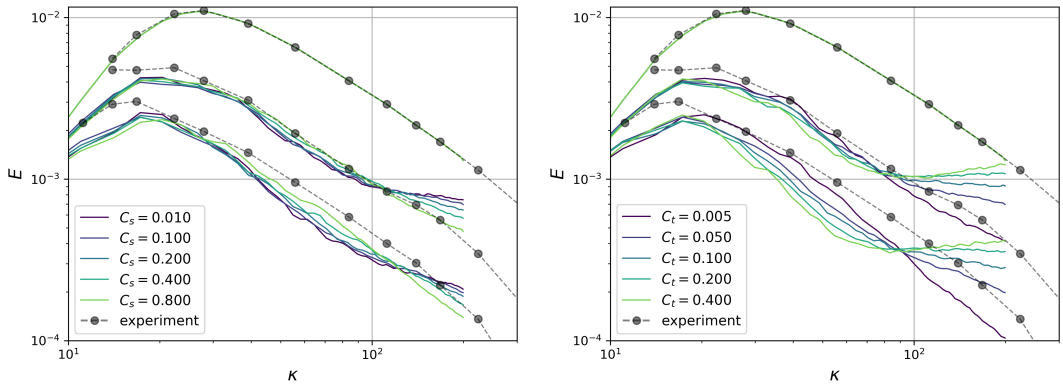

(a) Variation in spatial correlation C_s (b) Variation in temporal correlation C_t

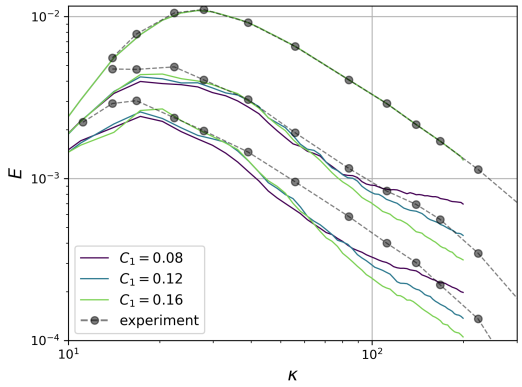

(c) Variation in filter width ratio C_1

Figure 5: Turbulent kinetic energy spectra from a HIT simulation using the SBS model configured to the defaults $C_I = 2.0$, $C_1 = 0.08$, $C_s = 0.1$ and $C_t = 0.05$. In each subfigure one of these parameters is varied.

As can be seen, an increase in spatial correlation reduces the energy buildup at the smaller turbulent scales, while an increase in temporal correlation increases the energy buildup at the smaller turbulent scales. Increasing the filter width ratio has the expected effect of increasing dissipation at the smallest scales. Furthermore, although this has not been quantified, an increase in spatial correlation coefficient likely results in forcing ocurring at smaller wavenumbers κ.

The results presented in fig. (5) may be explained through a simple model formulated as following:

$$\frac{\partial \underline{u}}{\partial t} = \underline{f} = \nabla\times\left(C_I k \underline{\xi}\right) \implies \underline{u} = C_I k \int_0^{t'} \nabla\times\underline{\xi}\,\mathrm{d}t \implies |\underline{u}|^2 = C_I^2 k^2 \int \nabla\times\underline{\xi}\left(\underline{x},t\right)\mathrm{d}t \cdot \int \nabla\times\underline{\xi}\left(\underline{x},s\right)\mathrm{d}t\,. \quad (71)$$

The time derivative may be interpreted as the substantial derivative, and k is assumed constant. Focusing on a single component u_z^2 and combining the two integrals above, we obtain:

$$u_z^2 = C_I^2 k^2 \int_0^t \int_0^t \langle \frac{\partial \xi_y\left(\underline{x},t'\right)}{\partial x}\frac{\partial \xi_y\left(\underline{x},s'\right)}{\partial x} + \frac{\partial \xi_x\left(\underline{t},t'\right)}{\partial y}\frac{\partial \xi_x\left(\underline{x},s'\right)}{\partial y}\rangle \mathrm{d}t'\mathrm{d}s', \quad (72)$$

which results from the fact that $\langle \xi_i\left(\underline{x},t\right)\xi_j\left(\underline{y},s\right)\rangle = 0$ if $i \neq j$. Approximating these terms with finite differences and denoting the grid size used to approximate the derivatives as Δ_x (where $\Delta_x \to 0$ will be applied later) and the filter width as Δ_f, then the first term in eq. (72) may be evaluated using the expected correlations of ξ_i (given in eq. (62)) as:

$$\langle \frac{\partial \xi_y\left(\underline{x},t'\right)}{\partial x}\frac{\partial \xi_y\left(\underline{x},s'\right)}{\partial x}\rangle \approx \frac{1}{2\Delta_x^2}\exp\left(-\frac{|t'-s'|}{\tau}\right)\left[1 - 1\exp\left(-\frac{2\Delta_x^2}{C_s\Delta_f^2}\right)\right]\,. \quad (73)$$

Assuming an isotropic grid ($\Delta_x = \Delta_y = \Delta_z$), then the second term in eq. (72) will produce a similar result, likewise for the u_x^2 and u_y^2 components. The time-dependent integral term in eq. (72) is solved as:

$$\int_0^t \int_0^t \exp\left(-\frac{|t'-s'|}{\tau}\right) \mathrm{d}s'\mathrm{d}t' = 2\tau\left[t + \tau\left(e^{-t/\tau} - 1\right)\right] \ . \tag{74}$$

By combining the spatial and temporal components the energy addition per unit time may be written as:

$$\lim_{t\to\infty} \frac{\partial\,|\underline{u}|^2}{\partial t} = 6C_I^2 k^2 \tau \frac{1}{\Delta_x^2}\left[1 - \exp\left(-\frac{2\Delta_x^2}{C_s\Delta_f^2}\right)\right] \equiv \frac{\mathrm{d}E_{\mathrm{SBS}}}{\mathrm{d}t} \ . \tag{75}$$

In this last equation one can see that the spatial and temporal correlations have a separate effect on the flow. Although this arises in this case due to the simplified model formulation, this may also be understood from the formulation of the SBS model: eq. (59) ensures spatial correlation and produces a smoothed random field. Through eq. (60) this field is convected with the flow and imbued with a certain temporal correlation. The larger the spatial gradients (i.e. the smaller the spatial correlation), the larger the forcing term according to eq. (61). While a larger temporal correlation causes a packet of flow to be accelerated in the same direction for a longer time (i.e. a larger correlation between the forcing and the velocity field), causing a larger addition of energy to the flow.

Two limits of the equation will be considered. Firstly one may take the limit as $\Delta_x \to 0$, corresponding to computing the actual derivative. Secondly the grid size Δ_x is set equal to the filter width Δ_f, as will be the case for an isotropic grid where the filter width is formulated in DES-fashion as $\Delta_f = \max\left[\Delta_x, \Delta_y, \Delta_z\right]$ and the derivative being evaluated numerically. This results in the following two formulations:

$$\lim_{\Delta_x\to 0} \frac{\mathrm{d}E_{\mathrm{SBS}}}{\mathrm{d}t} = 12\frac{C_I^2 C_t}{C_s} k^{3/2}\frac{1}{\Delta_f}, \quad \left.\frac{\mathrm{d}E_{\mathrm{SBS}}}{\mathrm{d}t}\right|_{\Delta_x=\Delta_f} = 6C_I^2 C_t k^{3/2}\frac{1}{\Delta_f}\left[1 - \exp\left(-\frac{2}{C_s}\right)\right] \ . \tag{76}$$

As $C_s \to 0$ the continuous case provides an infinite energy increase as a continuous random field has arbitrarily large derivatives. In the discrete case the solution becomes bounded by the grid size on which the derivatives are evaluated. Similar results may be obtained for the temporal contribution to the energy addition if approximated with finite differences.

Although the model explains the general trends shown in fig. (5), it was found to be too simplistic to be used to determine appropriate combinations of parameters. Quite simply because variations in k, coupling to the turbulence model equations, pressure variations, turbulent interactions, and the dissipative effects of (eddy) viscosity are neglected.

Initial tests showed that using the SBS model in the X-LES formulation caused turbulence in TCF simulations to develop more rapidly, but it did not significantly alter the LLM. As other authors found a significant reduction in the LLM when applying different variants of stochastic forcing, the SBS model was returned to a higher forcing intensity in an optimization. The intensity C_I was fixed at 1.5 and the other parameters were determined by minimizing the objective function in eq. (77). The penalty term P was required to ensure that the optimization routine would not get stuck in local minima where there was still a large amount of energy buildup. C_P tunes the amount to which it factors into the objective function and was determined empirically.

$$f_o = (1+P)\int_{\kappa_l}^{\kappa_h} \left(\log E_{\mathrm{sim}} - \log E_{\mathrm{exp}}\right)^2 \mathrm{d}\left(\log\kappa\right),$$
$$\text{where} \quad P = C_P \int_{k_l}^{k_h} \left[\frac{\mathrm{d}\left(\log E_{\mathrm{sim}}\right)}{\mathrm{d}\left(\log\kappa_{\mathrm{sim}}\right)} - \frac{\mathrm{d}\left(\log E_{\mathrm{exp}}\right)}{\mathrm{d}\left(\log\kappa_{\mathrm{exp}}\right)}\right]^2 \mathrm{d}\left(\log\kappa\right) \ . \tag{77}$$

The tuned parameters are $C_I = 1.5$, $C_s = 0.463$, $C_t = 0.231$ and $C_1 = 0.12$. The ratio of correlation coefficients $C_s/C_t = 2.0$ exists solely due to performing manually initiated line searches as the full-parameter optimization proved difficult due to the noisy objective function space. The resulting spectrum is shown in fig. (6).

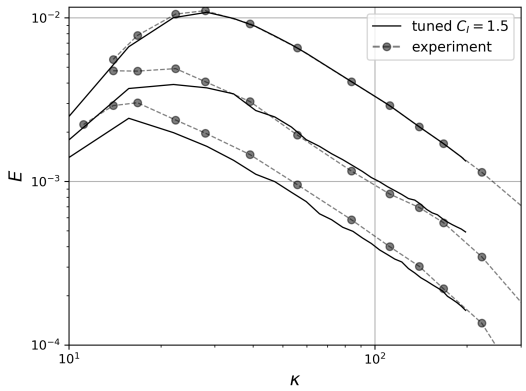

Figure 6: Turbulent kinetic energy spectrum of a HIT simulation with the SBS model tuned to $C_I = 1.5$, $C_s = 0.463$, $C_t = 0.231$, $C_1 = 0.12$.

The optimization results are by no means optimal. The final set of parameters not only changes the forcing intensity, but also the length and timescales over which the forcing is applied. It is assumed that the total forcing intensity, taking the changes in scale into account, must have been increased as the X-LES constant C_1 (dictating the amount of dissipation) is set to 1.5 times its originally tuned value while there is no significant buildup of energy at the final measurement station.

4.5 Turbulent Channel Flow Simulations

This section will detail the results the X-LES method produces when applied to TCF, and will compare them to pure RANS and DNS simulations. A generic introduction displaying the produced velocity profiles and relevant velocity statistics will be given in section 4.5.1. Extra attention is given to the issues that arise due to the zonal application of the method and the HPF in section 4.5.2. The interference with the turbulence modeling equations is investigated in section 4.5.3, alongside a qualitative investgation into the superstreaks. Finally the results obtained with the retuned SBS model are displayed in section 4.5.4.

4.5.1 Velocity Profile and Reynolds Stresses

Without the SBS model or the HPF enabled, the default parameters of the X-LES model produce velocity profiles as shown in fig. (7). In order to compare cases at different Reynolds numbers, results are plotted with y/δ on the x-axis. The setup of the respective grids is shown in tab. (4), with which the grid may be reproduced using the method outlined in section 4.3.2. The results are compared to a RANS-only simulation produced by `ensolv`, and to reference DNS data [36]. Due to presence of the superstreaks the x and z-axes are not necessarily statistically homogeneous directions. So it is worth stating that all graphs containing profiles along the channel height are produced by averaging the relevant quantities along wall-parallel surfaces (i.e. even variances and covariances are averaged, disregarding differences in the means from which these statistics were produced).

Table 2: Grid properties and Reynolds numbers for the TCF run without SBS model

$Re_{\tau,\text{set}}$	x^+	z^+	y^+_{wall}	y^+_{core}	N_y	N_c	$Re_{\tau,\text{XLES}}$	$Re_{\tau,\text{RANS}}$	$Re_{b,\text{XLES}}$	$Re_{b,\text{RANS}}$	$Re_{b,\text{DNS}}$
1000	200	100	0.62	104.0	96	0	1040.0	1003.5	21160	19780	20000
5200	255	128	0.69	511.9	128	0	5183.2	5218.5	130700	124600	125000

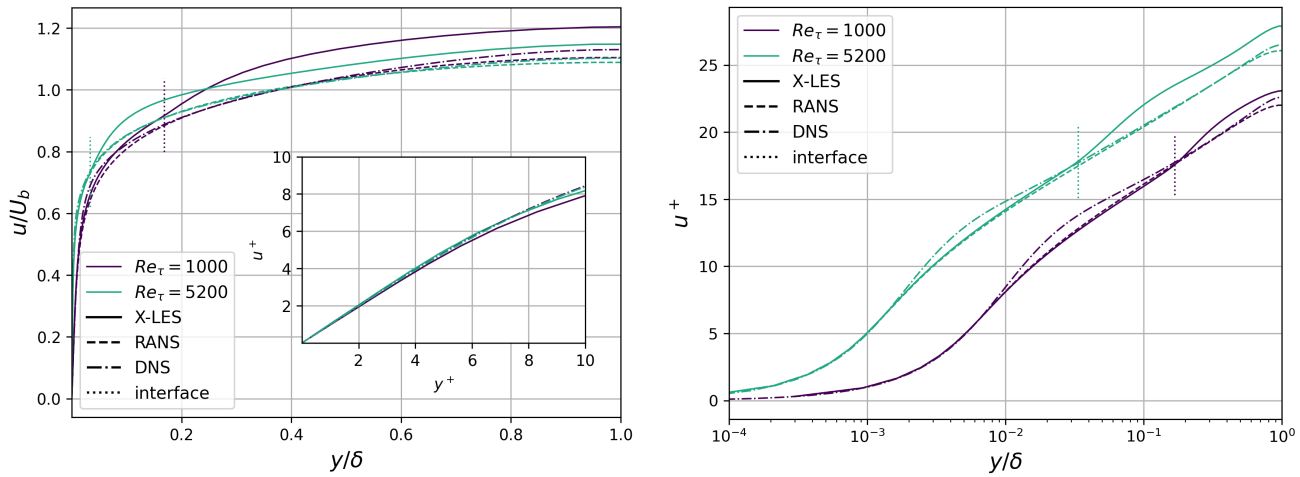

Figure 7: Velocity profile in u^+ of X-LES, RANS and DNS at $Re_\tau = 1000$ and $Re_\tau = 5200$

All of the formulations have the expected $u^+ \approx y^+$ behaviour in the viscous sublayer. Within the log-layer both RANS and X-LES solutions deviate from the DNS velocity profile. Although incorrect, this will not be further investigated as the X-LES formulation desirably behaves like a pure RANS formulation within the log-layer. The velocities within the log-layer are slightly lower than the RANS prediction. Both the $Re_\tau = 1000$ and $Re_\tau = 5200$ cases clearly exhibit the LLM. The deviation from the RANS velocity profile starts in the last cell within the RANS region (consistently so along a wide range of investigated friction Reynolds numbers Re_τ, whereas for other hybrid RANS/LES models the LLM might occur deeper within the RANS-domain) and recovers to the desired velocity gradient at some point in the channel core. For $Re_\tau = 1000$ the interface resides at $y/\delta = 0.167$, $y^+ = 173$ and the gradient recovers between $0.341 < y/\delta < 0.488$, or $355 < y^+ < 508$. For $Re_\tau = 5200$ the interface is located at $y/\delta = 0.034$, $y^+ = 175$ and the recovery occurs between $0.09 < y/\delta < 0.30$, $470 < y^+ < 1567$.

The variances are plotted separately for both Reynolds numbers in fig. (8). The figures in the left hand side show the total X-LES variances (i.e. $\langle u_i' u_i' \rangle + \tau_{ii}$), while the ones on the right hand side show their constituting resolved and unresolved portions.

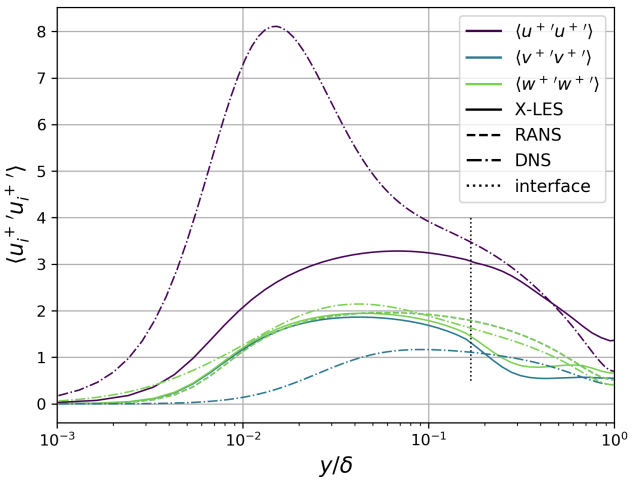

(a) Total variances for $Re_\tau = 1000$

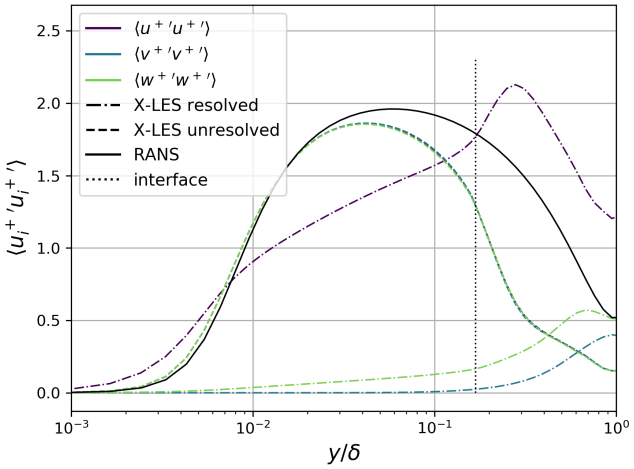

(b) Resolved and unresolved variance contributions for $Re_\tau = 1000$

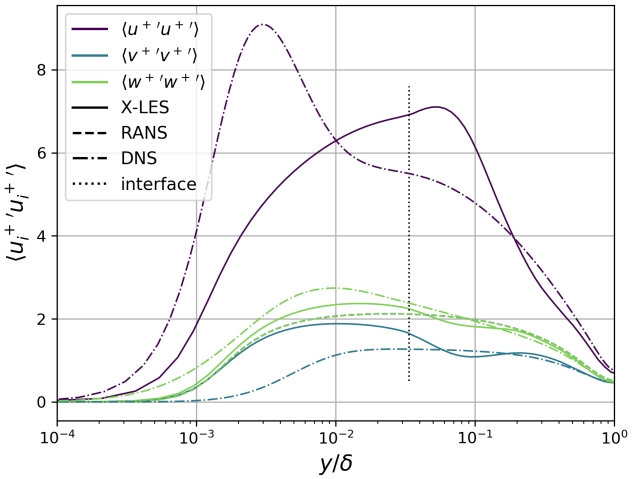

(c) Total variances for $Re_\tau = 5200$

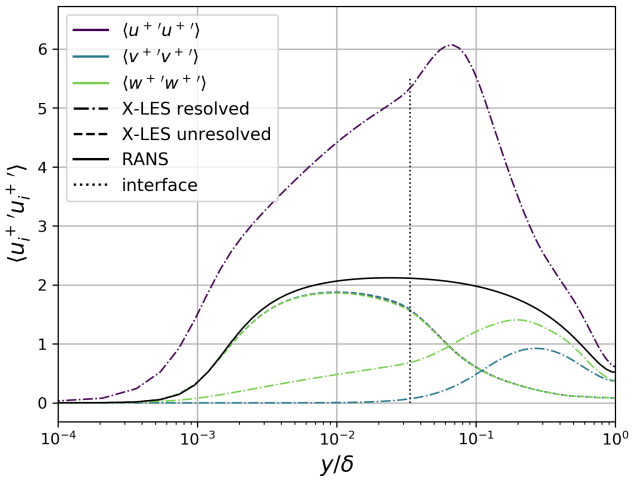

(d) Resolved and unresolved variance contributions for $Re_\tau = 5200$

Figure 8: Turbulent velocity variances and $\langle u'v'\rangle$ covariance of TCF using X-LES and compared to RANS and DNS

For both Reynolds numbers the X-LES and RANS unresolved variances are all approximately equal, and are essentially plots for the isotropic stress dictated by k (as will be seen later in fig. (9) and fig. (15), this is not as simple as assuming the eddy viscosity ν_t is constant, and that therefore integrating rates of strain for the v and w component in the x and z-axis vanish due to periodic boundary conditions. Nevertheless, the anisotropic contributions are small). For the $Re_\tau = 1000$ case, the variances $\langle v'v'\rangle$ and $\langle w'w'\rangle$ initially tend towards the DNS values in the center of the channel, deviate from those trends towards the interface, and within the RANS domain recover to RANS-like values. From the decomposition in fig. (8b) one may see this is due to the resolved components being dissipated, therefore the totals regress towards the same unresolved solution as a pure RANS simulation. A similar type of argument may be applied to the $Re_\tau = 5200$ case, where the initial trends of the $\langle v'v'\rangle$ and $\langle w'w'\rangle$ match the DNS results even better. This is likely because the unresolved components have reduced to an appropriate lower level, as compared to the $Re_\tau = 1000$ case. The better match with DNS results is likely because the core region (as measured in y^+) is much larger when a higher friction Reynolds number Re_τ is attained.

Note that for the $Re_\tau = 5200$ case in fig. (8c), the region where the $\langle v'v' \rangle$ and $\langle w'w' \rangle$ variances drop below the values obtained from DNS occur at the same wall-normal coordinate as where the LLM is present in the velocity profile. When these variances roughly match the DNS prediction in the region $0.20 < y/\delta < 0.30$ the velocity gradient seems to have recovered as well. The same observation is true for the $Re_\tau = 1000$ case, but harder to distinguish due to the relatively smaller core region in which the SGS formulation is applied.

The $\langle u'u' \rangle$ variances are much higher than those for the other two velocity components. Although closer to the DNS results, these are not desirable within the RANS domain as one would expect X-LES to approach a RANS solution near the wall. These high variances are not indicative of properly resolved turbulence, rather of the superstreaks present close to the wall. The instantaneous velocity fields in fig. (9) illustrate the source of the variances.

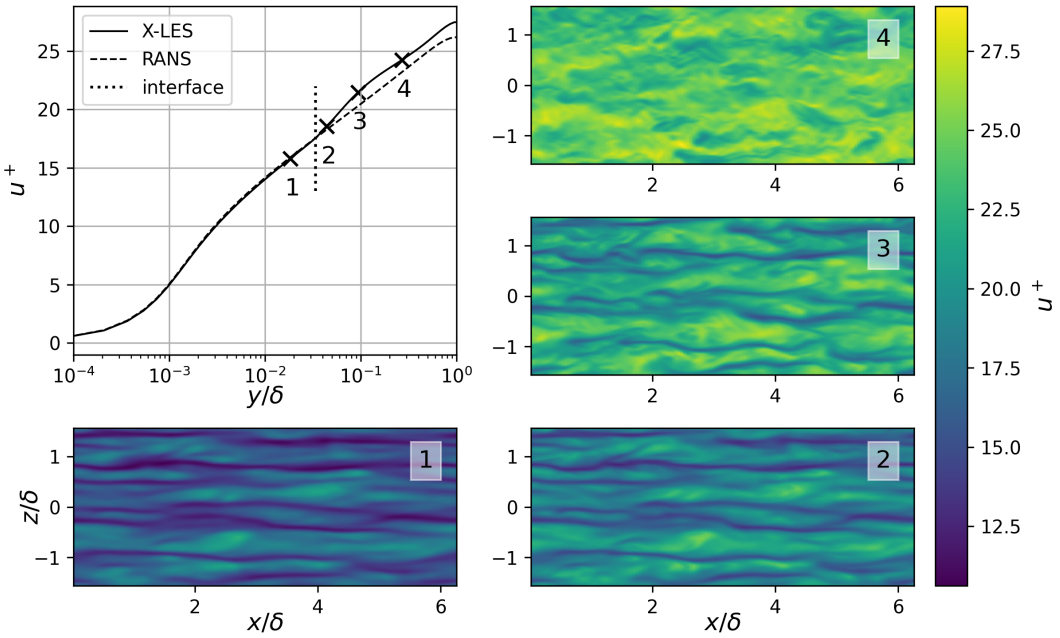

Figure 9: Velocity profile and instantaneous streamwise velocity u^+ visualized in wall-parallel surfaces of TCF using X-LES at $Re_\tau = 5200$

The switch to the LES-formulation occurs at $y/\delta = 0.034$, and the displayed velocity fields are taken from $y/\delta = 0.019, 0.045, 0.095, 0.28$, consecutively. Hence the superstreaks extend rather far into the LES-domain. Fig. (10) shows the explicitly time-averaged velocity field, containing the low and high-speed regions of the superstreaks in a wavelike pattern along the spanwise direction. Each of these superstreaks seems to remain in roughly the same spanwise position. The time-averaged $\langle u'u' \rangle$ field shows that the measured variances are in no small part due to the meandering motion of these superstreaks. It might be that collecting statistics over a significantly larger timespan results in a reduction in the spatial variation of statistics along the x and z-axes.

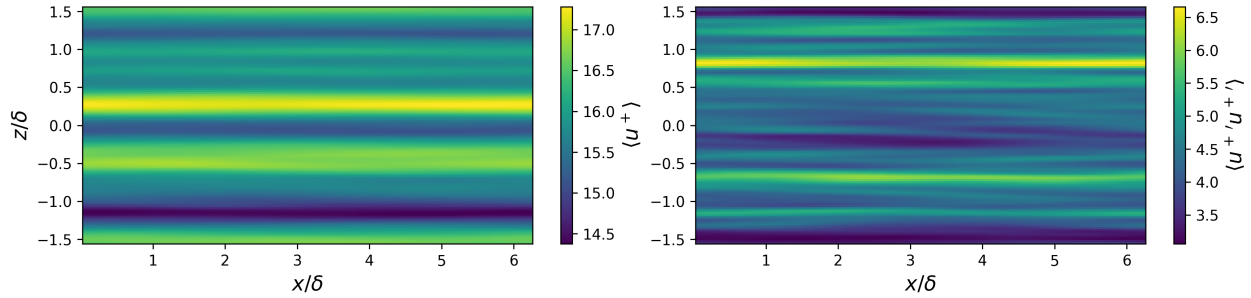

Figure 10: Mean streamwise velocity $\langle u^+ \rangle$ and variance $\langle u'^+ u'^+ \rangle$ at $y/\delta = 0.019$, $y^+ = 100$, near the interface in the RANS-domain

Comparing fig. (9) to fig. (8d), one may conclude that the "hump" at $y/\delta \approx 0.06$ in $\langle u'u' \rangle$ is due to the resolved turbulence developing while the superstreaks start to break up. Especially at $y/\delta \approx 0.10$ one may see that smaller-scale turbulence seems to be developing in the high-velocity regions, while the low-velocity regions are undergoing a large-scale instability.

Given that the mean velocity profile should be governed by eq. (38), the $\langle u'v' \rangle$ covariance (modeled and resolved) should be directly responsible for the LLM. These Reynolds stresses are plotted for both friction Reynolds numbers in fig. (11).

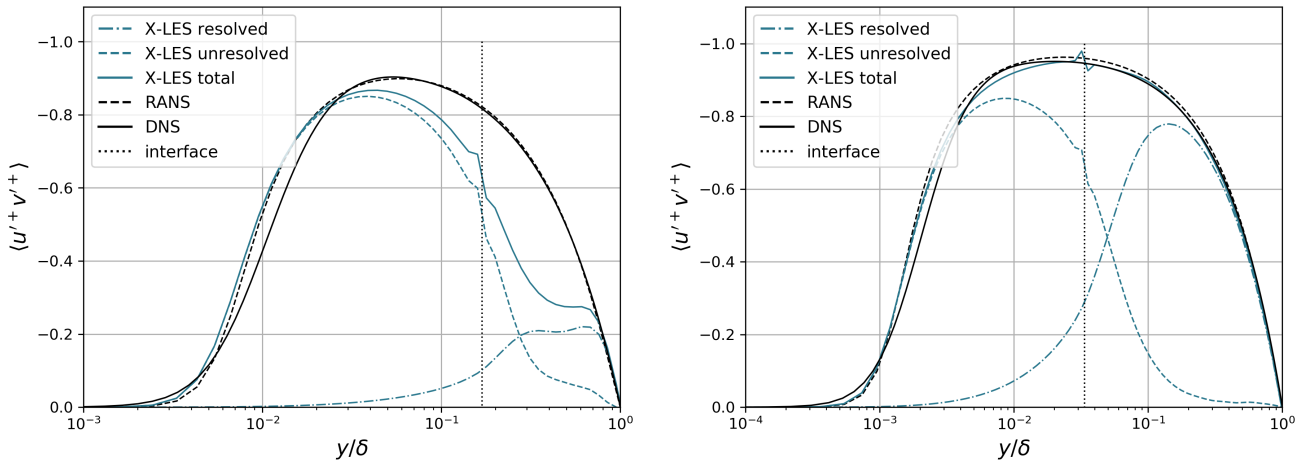

(a) $Re_\tau = 1000$ (b) $Re_\tau = 5200$

Figure 11: Resolved and unresolved turbulent $\langle u'^+ v'^+ \rangle$ stress of TCF using X-LES at $Re_\tau = 5200$ compared to RANS and DNS results.

Both profiles in fig. (11) show a discontinuity in the modeled Reynolds stresses, these will be discussed in section 4.5.3. For the low Reynolds number case fig. (11a) clearly shows that the magnitude of the total covariances are too small, increasing the mean velocity profile gradient, therefore producing a LLM. However, the high Reynolds number case in fig. (11b) shows nearly no error at all, which seems at odds with the governing equation for the mean velocity profile.

Given the superstreaks as shown in fig. (9) and the distributions of the turbulence modeling quantities which will be introduced later in fig. (15), the governing equation require a second look. The starting point is the modeled incompressible momentum equation for the u-velocity component where some turbulence is resolved. Applying temporal averaging (indicated by the ordinary Reynolds averaging operator $\langle \cdot \rangle$) to the equation produces eq. (78). If we now apply spatial averaging over each wall-normal slice (denoted

by $\{\cdot\}_s$), as is done to produce the various graphs in this chapter, then the equation reduces to:

$$\frac{\partial \langle u_i \rangle \langle u \rangle}{\partial x_i} = -\frac{1}{\langle \rho \rangle}\frac{\partial \langle p \rangle}{\partial x} + \frac{\partial 2\langle (\nu + \nu_t)\, S_{i1} \rangle}{\partial x_i} - \frac{\partial \langle u_i^{>} u^{>} \rangle}{\partial x_i}, \tag{78}$$

$$\frac{\partial}{\partial y}\left\{\langle u \rangle \langle v \rangle\right\}_s = -u_\tau^2 + \frac{\partial}{\partial y}\left\{\langle (\nu + \nu_t)\left(\frac{\partial u}{\partial y} + \frac{\partial v}{\partial x}\right)\rangle\right\}_s - \frac{\partial}{\partial y}\left\{\langle u^{>} v^{>} \rangle\right\}_s \ . \tag{79}$$

In the latter equation all derivatives with respect to the x and z-coordinates are removed due to the periodic boundary conditions. Neglecting $\partial v/\partial x$, non-dimensionalizing with respect to the friction velocity u_τ, viscosity ν and channel half-height δ, and performing the integration in y produces eq. (80).

$$\left\{\frac{\partial \langle u^+ \rangle}{\partial y}\right\}_s = Re_\tau \left[\left(1 - \frac{y}{\delta}\right) + \left\{\langle u^+ \rangle \langle v^+ \rangle\right\}_s + \left\{\langle u'^+ v'^+ \rangle\right\}_s\right] - \left\{\langle \nu_t \frac{\partial u^+}{\partial y} \rangle\right\}_s \ . \tag{80}$$

The product of the means is kept separately from the resolved turbulent stress because this term would ordinarily be neglected by assuming $\langle v \rangle = 0$ in each wall-parallel surface. All the terms have been investigated and shown to be important: due to the spatial correlations and non-homogeneous axes $\langle u^+ \rangle \langle v^+ \rangle$ and $\langle \nu_t' \, \partial u'^+ / \partial y \rangle$ may not be neglected, otherwise fig. (11b) shows discrepancies in the covariances.

To show the manifestation of the LLM in fig. (12) the terms on the left- and right-hand side of eq. (80) are plotted for the X-LES simulation, and the terms from eq. (38) are plotted for the DNS. To bring out the LLM the terms are multiplied with y/δ to produce logarithmic derivatives (e.g. $\partial \langle u^+ \rangle / \partial \log(y/\delta)$).

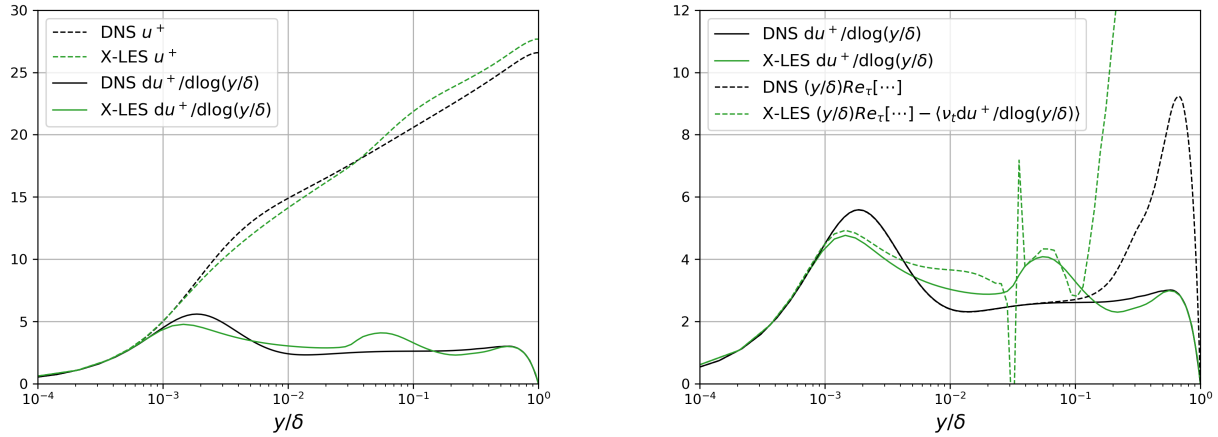

(a) Velocity profiles $\langle u^+ \rangle$ and their derivatives $\partial \langle u^+ \rangle / \partial \log(y/\delta)$

(b) Velocity derivatives and governing terms from eq. (38) and eq. (80)

Figure 12: Terms from the governing equations for the mean velocity profile $\langle u^+ \rangle$ in TCF as produced by X-LES and DNS at $Re_\tau = 5200$.

Close to the wall the right-hand side terms of eq. (80) do not match the velocity profile exactly, this is because well-converged statistics have not been gathered for the eddy-viscosity term, but may also be caused by the sensitivity of the plotted terms to Re_τ in $Re_\tau(1 - y/\delta)$. Above $y/\delta > 0.1$ both the DNS as X-LES data seem not to reproduce the expected velocity profiles.

The discontinuity in the X-LES profile is partially caused by lack of gathered statistics for the eddy visosity term, and partially caused by the fact that a zonal simulation inherently introduces discontinuities in modeled stress at the interface. The discontinuity is likely not the direct cause of the LLM as the LLM is present in non-zonal simulations as well. With the friction Reynolds numbers of the plotted X-LES and DNS profiles nearly equal (as shown in tab. (4)), the conclusion seems to be that the total turbulent stress (including the spatial correlation of $\langle u^+ \rangle \langle v^+ \rangle$) in the X-LES simulation simply does not match

that of DNS. Different from DNS the presence of the superstreaks results in a different physical problem being solved: one where the spatial correlations of mean velocities factor into the evolution of the mean velocity profile. None of the isolated terms in eq. (80) are of comparable magnitude to the discrepancy at $y/\delta \approx 0.06$ in fig. (12).

4.5.2 Effects of Zonal Simulations and the High-Pass Filter

As shown in fig. (11) the unresolved non-diagonal Reynolds stresses display a discontinuity. These errors occur when the X-LES formulation is applied as a zonal method. The reason that these errors are relatively small in the results presented so far is because of the method in which these zonal simulations are set up: an initial non-zonal simulation determines the wall-normal coordinate y where the RANS lengthscale is on average equal to the LES lengthscale, i.e. $l_R = \sqrt{k}/\omega \approx l_L = C_1\Delta$. A subsequent zonal simulation uses this coordinate as interface location to enforce a RANS formulation on one side and an LES formulation on the other side.

Since the grids are generated to adhere to $\Delta_x > \Delta_z > \Delta_y$ and the $\Delta_{\max}$ formulation is used for the filter width, the LES lengthscale is fixed for any given grid in TCF. Resolved turbulence will influence the RANS turbulence modeling such that the modeled turbulent kinetic energy k will fluctuate near the interface. This caues the RANS lengthscale to vary near the predetermined value from the non-zonal simuation.

Suppose that at the interface the lengthscales satisfy $l_R > l_L$ and $l_R - l_L = \Delta_l$. Taking the difference between the Reynolds stresses at the zonal interface between the RANS formulation and the LES formulation and assuming incompressiblity produces

$$\Delta_{\tau_{ij}} = \tau_{ij}^R - \tau_{ij}^L = \rho\left[2\nu_t^R S_{ij} - \frac{2}{3}k\delta_{ij}\right] - \rho\left[2\nu_t^L S_{ij} - \frac{2}{3}k\delta_{ij}\right] = 2\rho\sqrt{k}\left(l_R - l_L\right)S_{ij} = 2\rho\sqrt{k}\Delta_l S_{ij}\ . \quad (81)$$

This shows that, to a first order, a difference in lengthscale Δ_l produces a jump in the Reynolds stresses at the interface proportional to the difference in lengthscale. This analysis disregards the manner in which the entire flow solution responds to such jumps. Applying the same differencing to the production and dissipation terms in the k-equation produces:

$$\Delta_{\mathcal{P}_k} = \rho\sqrt{k}\Delta_l S_{ij}S_{ij}, \quad \Delta_{\epsilon_k} = -\beta_k\rho k^{3/2}\left[\frac{\Delta_l}{l_L\left(l_L + \Delta_l\right)}\right]\ . \quad (82)$$

If $\Delta_l > 0$ then an increase in production and a decrease in dissipation will manifest itself. In the performed simulations $\Delta_l \ll l_L$, such that the increase in production is dominant, except if the rate of strain is already rather small. If Δ_l is large then the jump in τ_{12} causes the velocity gradient to steepen. As long as the jumps in Reynolds stress are reasonably small, then it appears that the simulation results do not suffer too much from the lengthscale difference at the interface.

A similar type of effect occurs whenever the HPF LES formulation is used. Assuming a perfect match of lengthscales ($l_R = l_L \implies \nu_t^R = \nu_t^L$), the difference between Reynolds stresses and production of k at the interface may be written as shown in eq. (83). Hence a jump in Reynolds stress $\Delta_{\tau_{ij}}$ and modeled turbulent kinetic energy production $\Delta_{\mathcal{P}_k}$ occur that are proportional to the mean rate of strain.

$$\Delta_{\tau_{ij}} = 2\rho\nu_t^R S_{ij} - 2\rho\nu_t^L\left(S_{ij} - \langle S_{ij}\rangle\right) = 2\rho\nu_t\langle S_{ij}\rangle, \quad \Delta_{\mathcal{P}_k} = \rho\nu_t\left(S_{ij}\langle S_{ij}\rangle + S'_{ij}\langle S_{ij}\rangle\right)\ . \quad (83)$$

Results from X-LES simulations, with and without HPF, at $Re_\tau = 1000$ are shown in fig. (13) and compared to RANS and DNS results where appropriate.

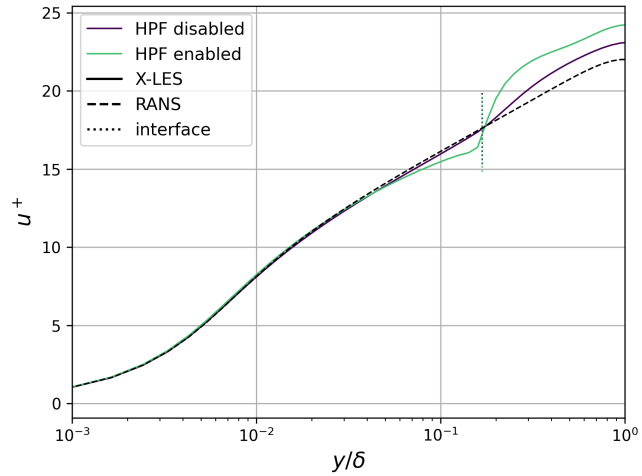

(a) Velocity profiles

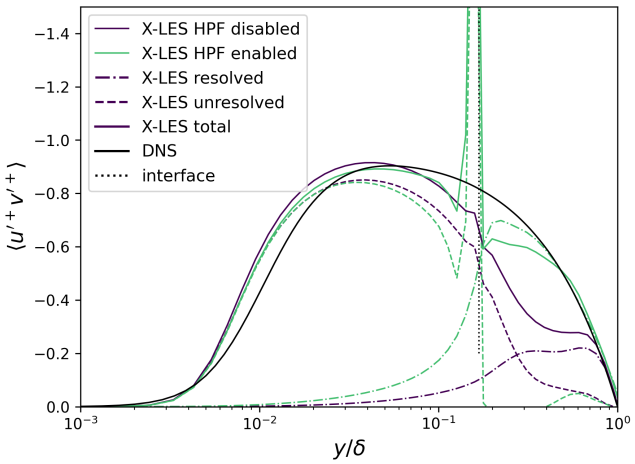

(b) Resolved and unresolved $\langle u'^+ v'^+ \rangle$ contributions

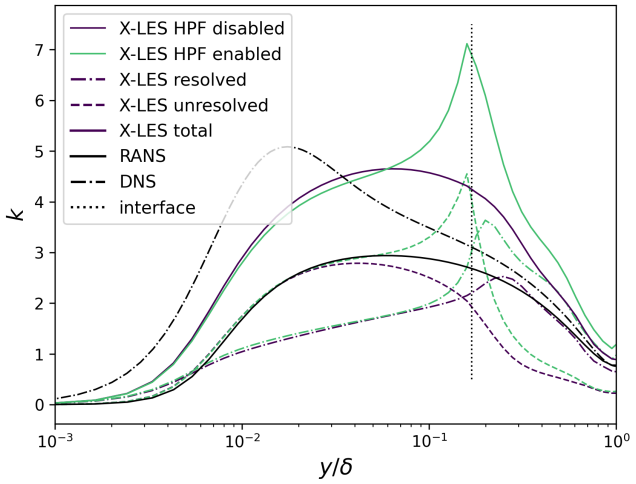

(c) Resolved and unresolved turbulent kinetic energy k contributions

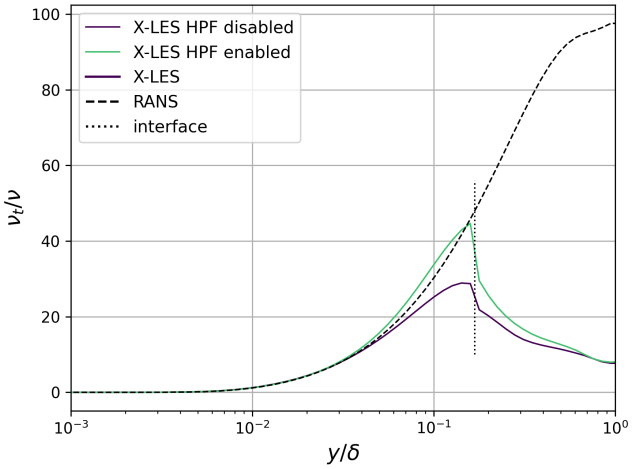

(d) Eddy viscosity ratio

Figure 13: Simulation results of TCF using X-LES with and without applied HPF and compared to RANS and DNS.

Fig. (13b) and (13c) show the manifestation of eq. (83). The jump in $\langle u'^+ v'^+ \rangle$ greatly increases the velocity gradient, as shown in fig. (13a). The combination of the jump in $\mathcal{P}_k$ (being proprtional to the mean rate of strain) and the increase velocity gradient cause a large spike in the profile of the modeled turbulent kinetic energy k to reside at interface. A runaway effect follows where the increased eddy viscosity further increases the mean velocity gradient, therefore increasing production of k. The dissipation ϵ_k is not directly affected by the HPF formulation and prevents an infinite increase in k (ofcourse ω factors into the equation as well, but its increase is smaller than the one in k, as evident from fig. (13d)).

It should be noted that near the center of the channel the resolved $\langle u'^+ v'^+ \rangle$ seem to match RANS and DNS predictions much better when the HPF is applied, even at the relatively low friction Reynolds number $Re_\tau = 1000$. This is not the case for the variances: although not shown here, all resolved variances attain values ≈ 2 times those of DNS in the center of the channel.

The converged solution represents an unphysical flow featuring a large LLM and a large spike in modeled turbulent kinetic energy k. Initial investigations of these solutions showed that the final flow

state depends on the chosen initial conditions, much like the application of a shielding function in (I)DDES causes non-unique solutions [4]. Although the errors introduced by a lengthscale mismatch and the HPF are different in nature, the large lengthscale difference that can arise due to the application of a shielding function might explain the aforementioned non-unique solutions.

4.5.3 Interference with the RANS Turbulence Modeling

As described in section 3.2.2 it has been hypothesized that the hybridization of a RANS and an LES turbulence model will cause excessive stress within the RANS-domain because both resolved turbulent stress and modeled Reynolds stress is acting in this domain while the RANS turbulence model is tuned to produce correct mean flows.

In order to investigate this, the various constitutive terms of the turbulence modeling k-equation are shown in fig. (14) for both friction Reynolds numbers. The figures on the right hand side show the terms near the RANS/LES interface.

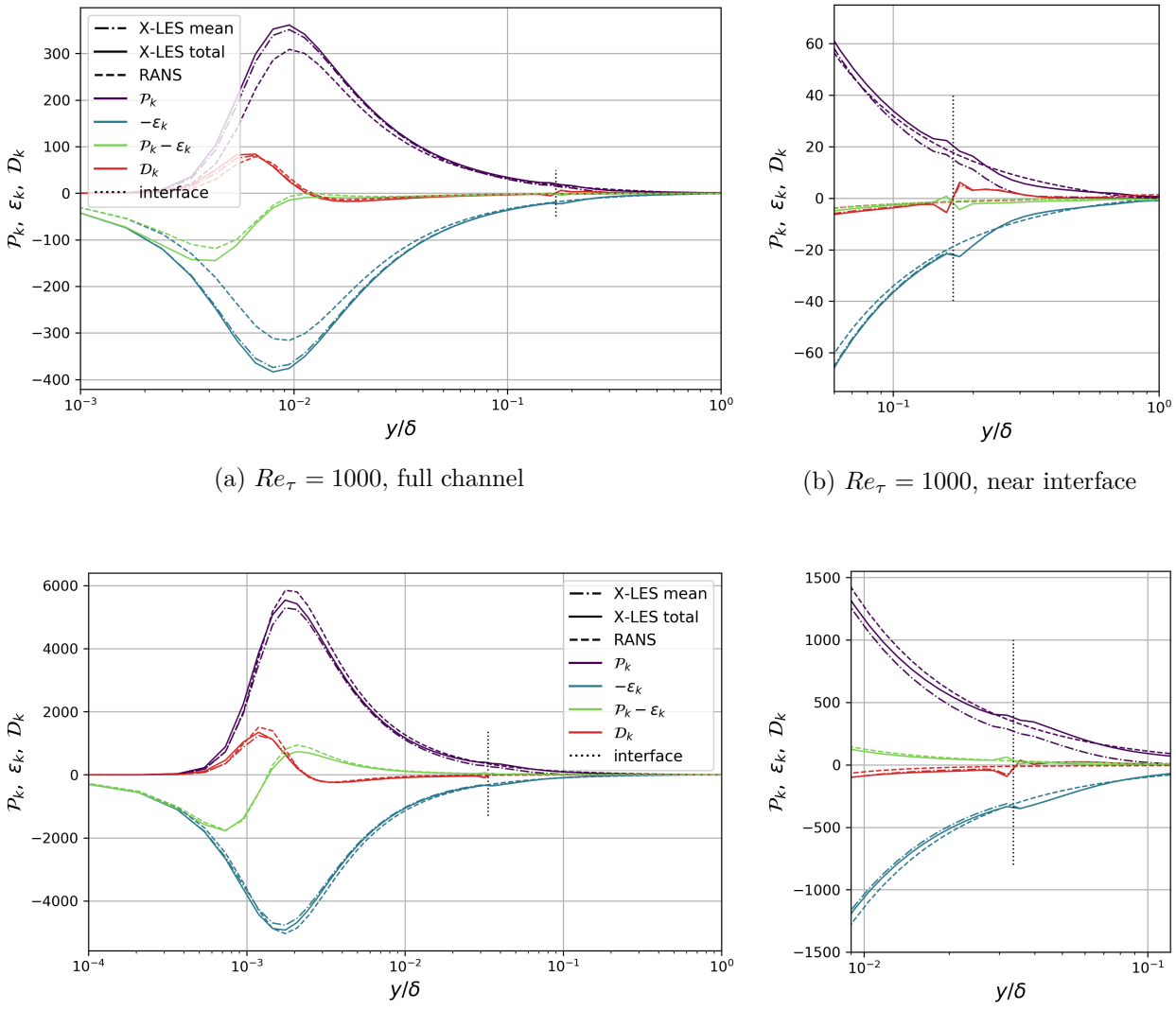

(a) $Re_\tau = 1000$, full channel

(b) $Re_\tau = 1000$, near interface

(c) $Re_\tau = 5200$, full channel

(d) $Re_\tau = 5200$, near interface

Figure 14: Production $\mathcal{P}_k$, dissipation ϵ_k and diffusion $\mathcal{D}_k$ of turbulent kinetic energy k decomposed into contributions from mean and fluctuating terms in a TCF simulation using X-LES compared to RANS results.

Clearly there is a mismatch in production and dissipation of k between the RANS and the X-LES formulation for both friction Reynolds numbers. There are large differences in production and dissipation near the wall, but these amount to relatively small changes in the balance of the two terms. In the regions where difference in the near-wall balance is large the eddy viscosity ν_t is small compared to the molecular viscosity ν. It is hard to arrive at general conclusions because the behaviour of the X-LES profiles compared to the pure RANS profiles is different in the considered friction Reynolds numbers.

Near the interface the discussed errors due to the difference in lengthscale are clearly visible in fig. (14b) and fig. (14d). In both cases the balance between production and dissipation becomes smaller in the LES-domain than in the pure RANS case. Near the interface this is mainly caused by increased dissipation, towards the center of the channel by reduced production. The diffusion term ensures that near the interface turbulent kinetic energy is diffused into the LES-domain. The interference with the RANS modeling is not a physical process, nevertheless desirable as it reduces the eddy viscosity where resolved turbulence is present.

The turbulent fluctuations only represent a small contribution to the total production near the wall. This changes in the LES-domain, where the influence of the mean terms on the total production is negligible. Due to the formulation of dissipation term in the SGS model this term is not decomposed into a mean and a fluctuating contribution, only the mean is shown.

The superstreaks that were mentioned before have a more pernicious character than the averaged turbulence modeling equations show. Fig. (15) shows wall-parallel plots of the turbulence modeling quantities at the same positions as fig. (9) (i.e. $y/\delta = 0.018, 0.045, 0.095, 0.28$. For reference: the interface is located at $y/\delta = 0.033$). To show how these distributions develop throughout the channel the distribution of the turbulence modeling quantities within each wall-parallel surface are treated as statistical quantities and shown in fig. (16). These figures contain the 5%, 25%, 50%, 75%, 95% quantiles and the mean of the X-LES turbulent quantities and compares them to a RANS simulation (where all quantities are the same throughout the wall-parallel surfaces).

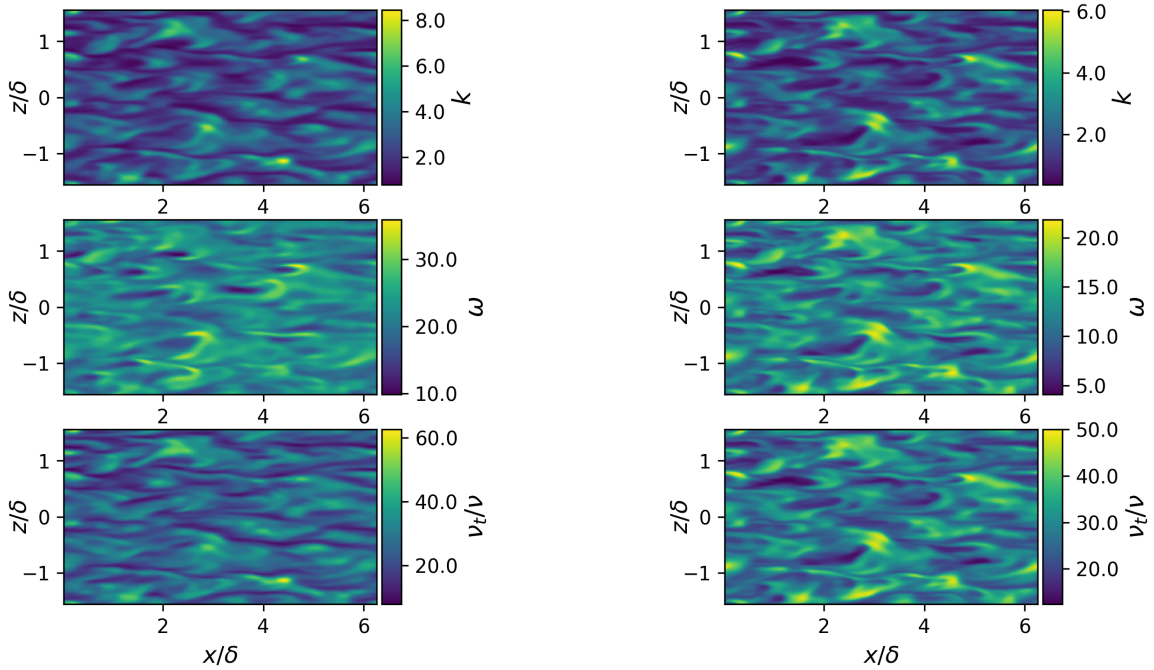

(a) $y/\delta = 0.018$, $y^+ = 95$, in the RANS-domain near the interface

(b) $y/\delta = 0.045$, $y^+ = 232$ in the LES-domain near the interface

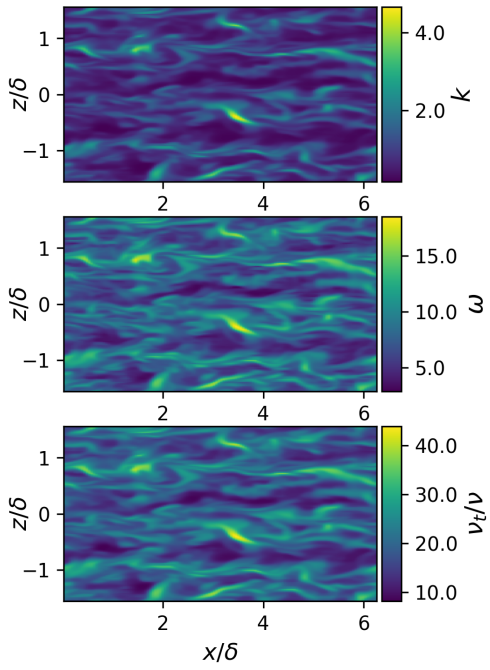

(c) $y/\delta = 0.095$, $y^+ = 495$, in the LES-domain, with noticable LLM

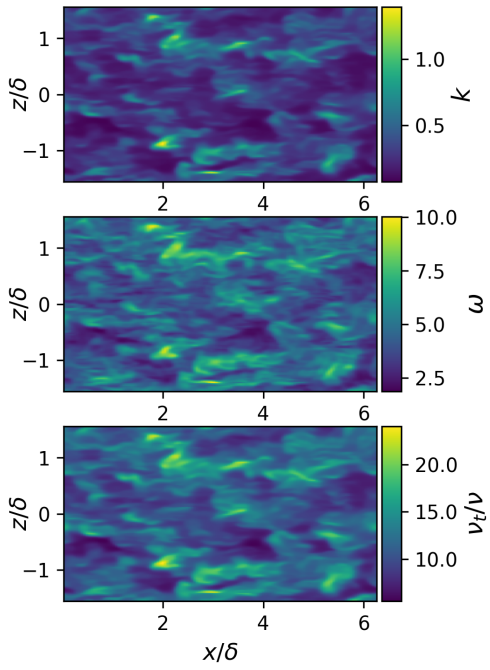

(d) $y/\delta = 0.28$, $y^+ = 1452$, in the LES-domain, with recovered velocity profile

Figure 15: Modeled turbulent kinetic energy k, specific turbulent dissipation ω, and eddy viscosity ν_t visualized on wall-parallel surfaces at the same wall-normal coordinates as in fig. (9).

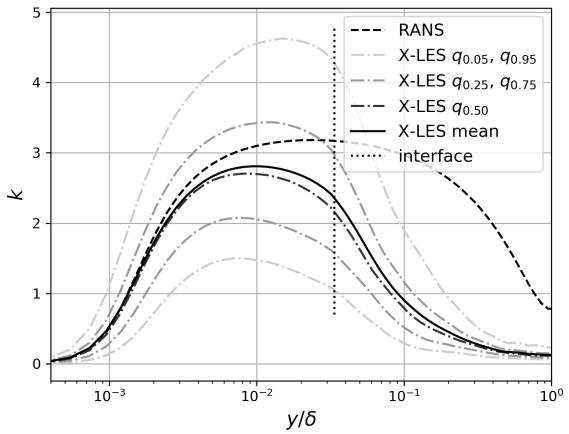

(a) Profiles of turbulent kinetic energy k

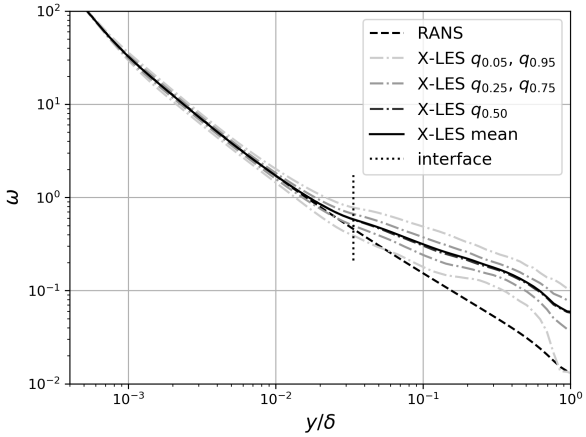

(b) Profiles of specific turbulent dissipation ω

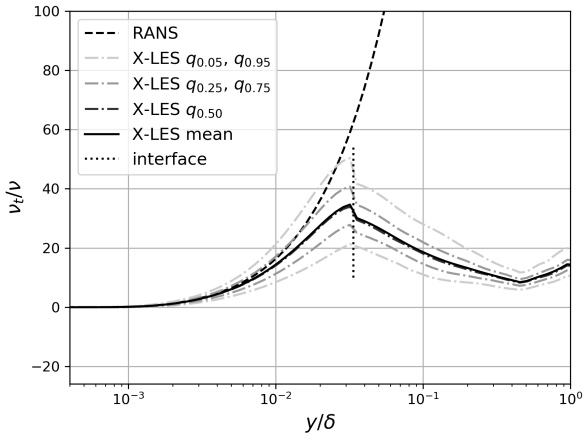

(c) Profiles of eddy viscosity ν_t

Figure 16: Distributions of turbulent kinetic energy k, specific turbulent dissipation ω, and eddy viscosity ν_t obtained from TCF using X-LES at $Re_\tau = 5200$ displayed as 5 quantiles q and the means and compared to the means from a RANS simulation.

Note that the specific turbulent dissipation ω only influences the eddy viscosity ν_t in fig. (15a). fig. (15b) is still representative of the distribution of ω near the interface.

There is a large variation in k near the wall. The spatial distribution of ω in each of the wall-parallel slices is proportional to those in k. The eddy viscosity ν_t varies not nearly as much as k. Since in most of the channel (except when very close to the wall, where relative variation of ω with respect to its mean is very small) the turbulence modeling parameters are similarly distributed, the remaining text will discuss "production and dissipation of eddy viscosity" to simplify the discussion.

Comparing fig. (15) and fig. (9) and remembering the profiles in the turbulence modeling equations one may conclude that the mean production of ν_t is due to the velocity profile $\partial\langle u\rangle/\partial y$. The local spatial variation of these quantities within wall-parallel surfaces is due to the superstreaks: overlaying the freestream velocity distribution onto the distribution of k clearly shows that k is concentrated where $|\partial u/\partial x|$ and $|\partial u/\partial z|$ are large.

Above the interface, the formulation of ν_t suddenly changes and becomes dependent on $C_1\Delta$ instead of ω. The increase in ν_t near the center of the channel in fig. (16c) is due to a badly designed grid, as the wall-normal spacing Δ_y^+ starts to exceed the spacing Δ_x^+ along the mean flow direction. Between fig. (15b) (i.e. slightly above the interface) and fig. (15c), a remarkable change in eddy viscosity distribution takes place: close to the interface ν_t is concentrated near the edges of the superstreaks, while towards the center of the channel ν_t is concentrated in the center of the low-velocity superstreaks. Given the presence of a negative spatial correlation of $\langle u^+\rangle$ and $\langle v^+\rangle$, the flow in the low-velocity superstreaks will get ejected into the center of the channel, carrying the eddy viscosity with it. The concentration of eddy viscosity in these regions towards the center of the channel is clearly hampering the development of longitudinal and spanwise instabilities. That is: fig. (9) shows that while finer-scale turbulence is developing outside the superstreaks, where the eddy viscosity is low, only large-scale instabilities are developing inside of them.

The question of how these superstreaks are formed in the first place remains. This study cannot provide a definitive answer but may provide a hypothesis. From the analysis of DNS of TCF in the Fourier domain, it appears that the turbulent energy spectrum of $\langle u'u'\rangle$ is concentrated along the spanwise wavenumber axis [37]. From roughly $y^+ = 300, y/\delta = 0.058$ towards the wall this energy starts concentrating near somewhat larger wavenumbers, leading to two distinct peaks in concentration of energy. Similarly $\langle v'v'\rangle$ and $\langle w'w'\rangle$ tend to concentrate towards the higher wavenumbers along the spanwise axis as well, but

without the two distinct peaks and more radially distributed in wavenumber space. The hypothesis that is proposed here is that within the LES domain the same kind of transfer starts to take place, but the large peak at higher wavenumbers cannot manifest itself. Larsson et al. [31] analyzed the streamwise and spanwise energy spectra in a DES simulations and showed that this is due to the damping of high wavenumbers, and notes that grid refinement does not remove the presence of the superstreaks. What remains is the low wavenumber concentration of energy at a grid which is relatively coarse. In other words: a spanwise wavelike structure with lengthscales of the same order of magnitude as the domain size.

In a pure RANS simulation (if started with a completely turbulent flow field) of TCF one may safely expect the final converged solution to produce quantities roughly equal along wall-parallel surfaces. A hybrid RANS/LES simulation differs in that the RANS-domain is continuously fed with turbulence persisting in the LES-domain.

The described distribution of eddy viscosity ν_t, extending into the LES-domain, manifests itself once the superstreaks are formed. The regions of low eddy viscosity outside of the superstreaks will ensure that some turbulence will develop, which will advect into the RANS-domain. The regions of high eddy viscosity prevent the proper development of the spanwise and wall-normal fluctuations as shown in fig. (8c), and delays the development of streamwise fluctuations inside the low-speed superstreaks.

4.5.4 Effects of Increased Stochastic Forcing on the Log-Layer Mismatch

As mentioned in section 4.4, the SBS model was recalibrated to a set of coefficients representing a higher forcing intensity. Applying this SBS formulation in an X-LES simulation of TCF provides favourable mean results, as reported by other authors applying stochastic forcing [30, 31]. The grid parameters and obtained Reynolds numbers are shown in tab. (3). The velocity profile, variances and $\langle u'v' \rangle$ covariance are displayed in fig. (18).

Table 3: Grid properties and Reynolds numbers for the TCF runs with retuned SBS model

$Re_{\tau,\text{set}}$	x^+	z^+	y^+_{wall}	y^+_{core}	N_y	N_c	$Re_{\tau,\text{XLES}}$	$Re_{\tau,\text{RANS}}$	$Re_{b,\text{XLES}}$	$Re_{b,\text{RANS}}$	$Re_{b,\text{DNS}}$
1000	200	100	0.49	104.0	96	0	1005.2	1003.5	19770	19780	20000
5200	255	128	1.0	218.7	128	32	5223.7	5218.5	127100	124600	125000

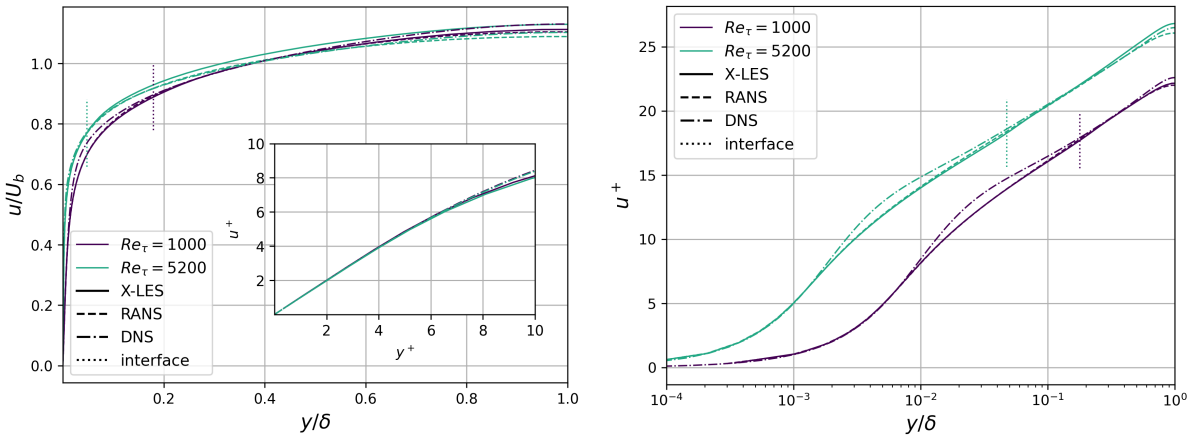

Figure 17: Velocity profile in u^+ of X-LES using the retuned SBS parameters at $Re_\tau = 1000$ and $Re_\tau = 5200$ compared with RANS and DNS.

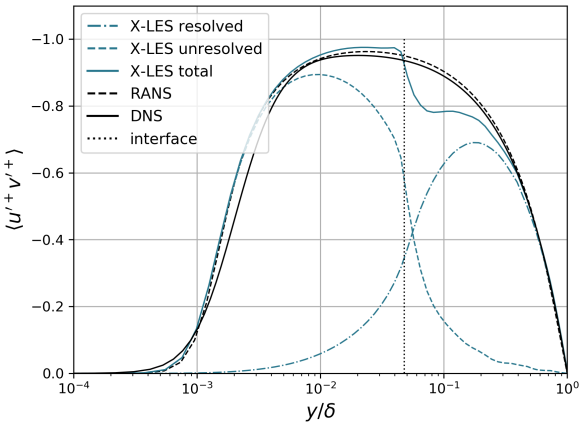

(a) Resolved and modeled $\langle u'v' \rangle$ covariance.

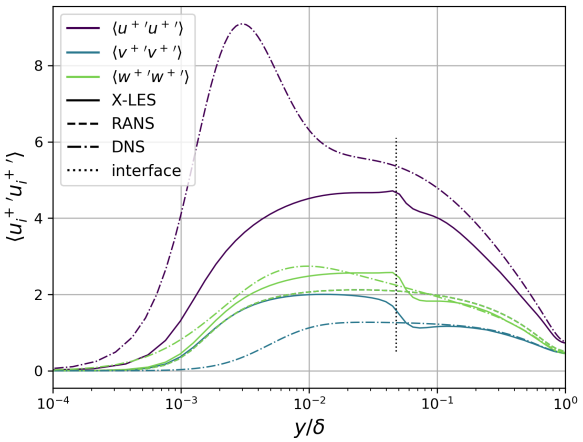

(b) Total variances.

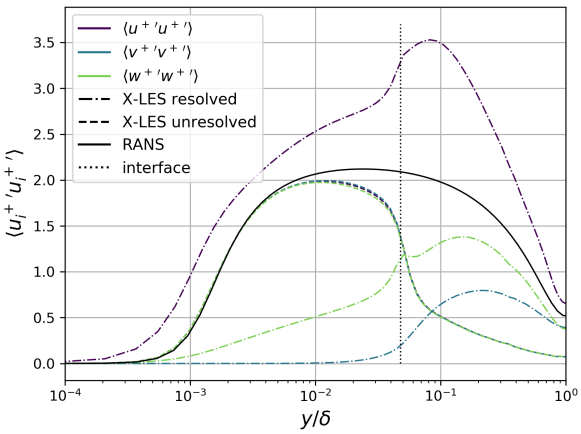

(c) Resolved and unresolved variance contributions.

Figure 18: Turbulent statistics of TCF using X-LES using the retuned SBS parameters at $Re_\tau = 5200$ compared with RANS and DNS.

The velocity profiles in fig. (17) clearly show that the $Re_\tau = 1000$ and $Re_\tau = 5200$ cases approach a pure RANS solution near the wall and the DNS solution near the center of the channel. There is a slight LLM present in both cases, it is unclear whether this is due to errors produced by variations in RANS and LES lengthscale or due to a lack of turbulent stress. The velocity profile of the high Reynolds number case shows a velocity profile that is slightly too steep near the center of the channel, likely caused by the excessive increase in filter width factor C_1. Clearly the $\langle u'v' \rangle$ covariance as shown in fig. (18a) appears to be incorrect. Within the RANS-domain the resolved turbulence is intereferring unfavourably, causing a higher than expected turbulent stress. In the LES-domain there seems to be a clear lack of turbulent stress. It is likely that the stress missing from this graph is the direct influence of the stochastic forcing term on the mean velocity profile. Sadly, these statistics were not obtained in this work.

For the $\langle u'u' \rangle$ variance, there is still a discrepancy compared to DNS, but the large peak caused by the superstreaks has vanished. The sharp spike in $\langle v'v' \rangle$ is caused by the SBS model. It is active only in the LES-domain, so near the interface it is forcing at a high intensity due to the high values of k. The transition from RANS-like to DNS-like $\langle v'v' \rangle$ and $\langle w'w' \rangle$ variances is much more rapid when the SBS model is applied.

The distributions of turbulent quantities are investigated in the same manner as before. The quantiles q and means of turbulence modeling quantities, hence the overall distribution within each wall-parallel surface, is shown in fig. (19).

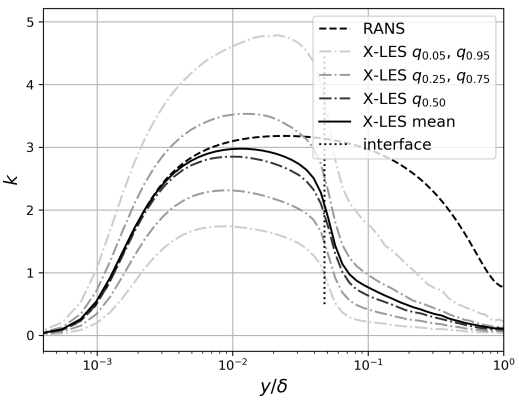

(a) Profiles of turbulent kinetic energy k

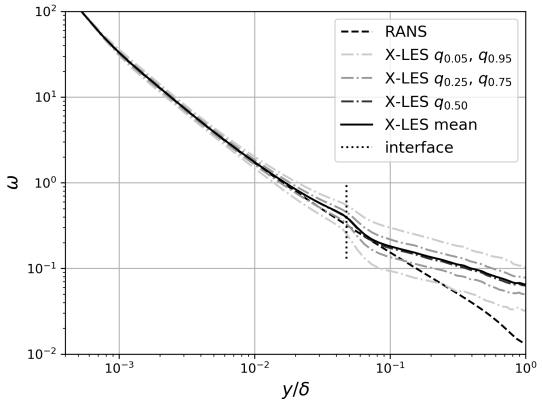

(b) Profiles of specific turbulent dissipation ω

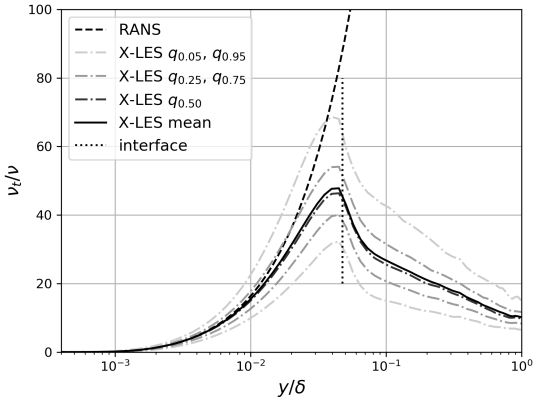

(c) Profiles of eddy viscosity ν_t

Figure 19: Distributions of turbulent kinetic energy k, specific turbulent dissipation ω, and eddy viscosity ν_t obtained from TCF using X-LES and the retuned SBS model at $Re_\tau = 5200$ displayed as 5 quantiles q and the means and compared to the means from a RANS simulation.

There are several main differences. Firstly one may see that the more intense forcing transfers modeled turbulent kinetic energy k into artificial turbulent energy, causing a rapid drop of k within the LES-domain. Towards the center of the channel less forcing is applied, and k is slightly higher than the simulations without SBS model. This causes the eddy viscosity ν_t to remain slightly higher in the central part of the channel than in the no-SBS case. This is expected, as the filter width ratio C_1 is 1.5 times larger than in the previously investigated case.

Another noticable difference is in the specific turbulent dissipation ω. Again: although it doesn't influence the eddy viscosity ν_t in the center of the channel, the behaviour in the LES-domain forms the boundary condition for the behaviour in the RANS-domain, where it does factor into the formulation of eddy viscosity ν_t. The profiles for ω match the RANS formulation much better near the interface than the simulations without SBS.

Surface plots of streamwise velocity u^+ and eddy viscosity ν_t are shown for the wall-normal coordinates $y/\delta = 0.019, 0.072, 0.27$, or $y^+ = 100, 381, 1425$ in fig. (20).

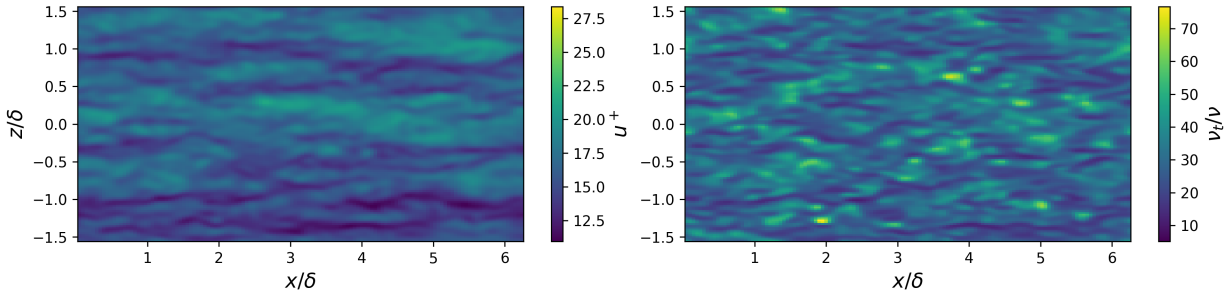

(a) At $y/\delta = 0.019$, $y^+ = 100$, near the interface in the RANS-domain

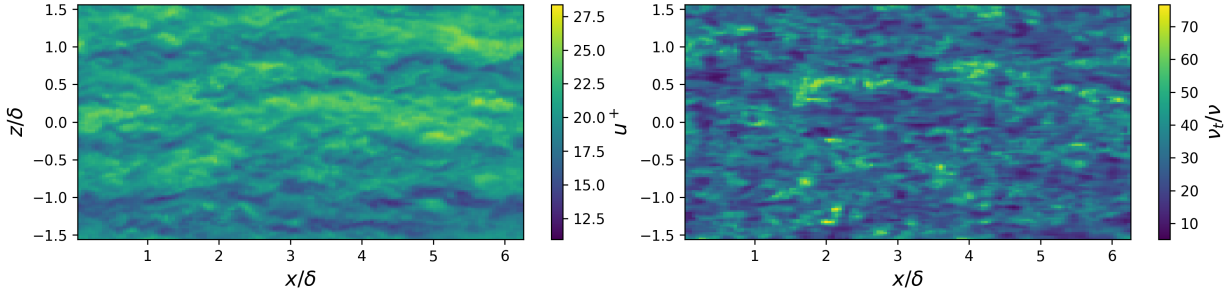

(b) At $y/\delta = 0.072$, $y^+ = 381$, near the interface in the LES-domain

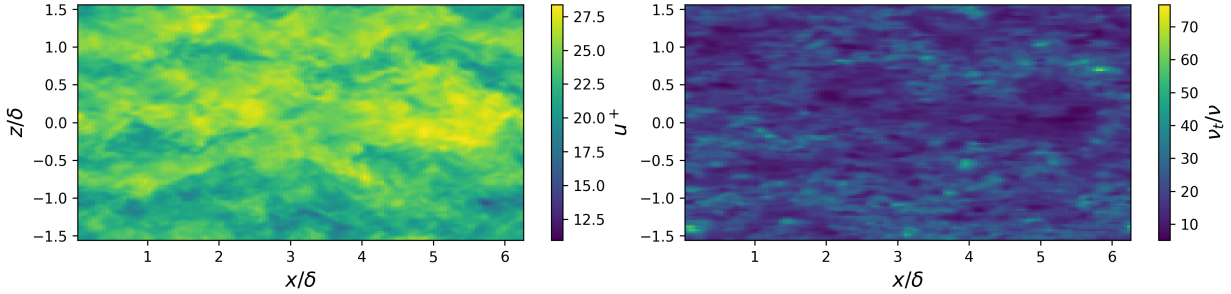

(c) At $y/\delta = 0.27$, $y^+ = 1425$, away from the interface's influence, in the LES-domain

Figure 20: Velocity u^+ and eddy viscosity ν_t visualized in wall-parallel surfaces of TCF using X-LES with the retuned SBS model at $Re_\tau = 5200$.

One may compare the velocity and eddy viscosity from fig. (20a) to the turbulent quantities in fig. (15a) and the velocity profile in fig. (9), all showing the behaviour at $y^+ \approx 100$. The SBS model introduces a lot of high-wavenumber turbulence that is capable of penetrating deep in the RANS-domain. As a result, although the general statistical distribution of eddy viscosity is still roughly the same, it is distributed much more erratically thoughout the wall-parallel plane. The specific turbulent dissipation ω still behaves roughly like before: more spread out than k and arranged in the U-shaped structures as in fig. (15a).

As we move from the RANS-domain into the LES-domain we already find a reasonably turbulent field in fig. (20b). The eddy viscosity ν_t is still being transported into the center of the channel away from the RANS-domain. But because the regions of high eddy viscosity are much smaller, they do not have such a large-scale diffusive effect on the flow as in the case without SBS model.

We may see that although the model behaves very well, it is hard to pinpoint the exact reason for doing so. The superstreaks are broken up, hence the eddy viscosity that is transported into the LES-domain

originates from point-like sources near the interface instead of the streamwise undulating line-like sources. Part of the reason the model behaves better is likely the removal of these large regions in which turbulence is prevented from developing. Judging from the $\langle v'v' \rangle$ and $\langle w'w' \rangle$ variances, for the no-SBS case shown in fig. (8c) and for the SBS case in fig. (18b), this seems the case: the regions in which the mentioned variances drop below the DNS profiles is much smaller.

On the other hand the SBS model is obviously generating artificial turbulence. So it may as well be that the swaths of high eddy viscosity in the LES-domain, as caused indirectly by the superstreaks, have a much smaller effect on the flow as is presumed in this work. In that case the main reason for these favourable results is the dynamics of the Navier-Stokes equations molding the artificially generated turbulence into the desired variances and covariances. The true reason probably lies somewhere inbetween. No method to quantify their relative effects has been persued in this work.

It should be noted that the spatial correlation between the eddy viscosity ν_t and velocity gradient $\partial u^+/\partial y$ seems to have nearly vanished. Furthermore the influence of the spatial correlation of $\langle u^+ \rangle \langle v^+ \rangle$ seems to have dropped to a third of its original value.

5 On RANS/LES Hybridization and the Mean/Fluctuating Decomposition

The governing equations for TCF describe that the LLM is caused by lack of resolved turbulence or a lack of modeled turbulence. Indeed in the LES-domain, near the RANS/LES interface, the eddy viscosity is rather high in all investigated cases, suggesting it plays a role in the lack of total turbulent stress. The investigation of the X-LES method showed that the effects induced by the superstreaks play a role in this high eddy-viscosity: the spatial correlation of $\langle u^+ \rangle$ and $\langle v^+ \rangle$ influences the velocity profile and causes large streamwise ribbons of eddy viscosity to be transported towards the center of the channel.

Although resolved turbulence within the RANS-domain seems undesirable, increased forcing seems to break up the concentrated regions of eddy viscosity spatially correlated with the superstreaks and produces a favourable mean velocity profile. In the ideal case the superstreaks would not form in the first place. This would allow a clearly delineated investigation into development of resolved and modeled turbulent stress and their mutual interaction.

To this end a particular type of hybrid RANS/LES modeling will be investigated in this chapter. The triple decomposition underlying this method will be presented in section 5.1 and used to formulate a particular hybridization in section 5.2. Some preliminary attention to an appropriate RANS turbulence model is given in section 5.3. The implications of explicit time averaging as employed by the model will described in section 5.4, and the potential to hybridize with an LES-governed domain is described in section 5.5.

5.1 Triple Decomposition

In a hybrid RANS/LES simulation one formally applies two types of filters. One obtains a formulation governing the mean flow if Reynolds averaging is applied to the governing equations. Applying spatial filtering results in the governing equations for sum of the mean flow and the resolved turbulence. An idea for formulating a hybrid simulation is to determine the governing equations for the mean flow and the resolved fluctuations separately. To this end a triple decomposition is applied. For any given quantity ϕ the decomposition may be formulated as [22]:

$$\begin{cases} \phi - \langle \phi \rangle & = \phi' \\ \phi - \overline{\phi} & = \phi^< \end{cases} \implies \overline{\phi} - \langle \phi \rangle = \phi' - \phi^< \equiv \phi^> \implies \phi = \langle \phi \rangle + \phi^> + \phi^<, \tag{84}$$

where $\langle \phi \rangle$ is the mean value, $\phi^>$ is the resolved fluctuation, and $\phi^<$ is the unresolved fluctuation. An essential assumption in making the application of Reynolds averaging to this triple decomposition consistent is that $\langle \overline{\phi} \rangle = \langle \phi \rangle$, because this implies that $\langle \langle \phi \rangle + \phi^< \rangle = \langle \phi \rangle$, hence that both $\langle \phi^> \rangle = 0$ and $\langle \phi^< \rangle = 0$.

For compressible flows the decomposition is identically formulated, but using Favre averaging $\{\phi\}$ and Favre filtering $\widetilde{\phi}$. In this case the decomposition and notation is given by:

$$\begin{cases} \phi - \{\phi\} & = \phi'' \\ \phi - \widetilde{\phi} & = \phi^{\ll} \end{cases} \implies \widetilde{\phi} - \{\phi\} = \phi'' - \phi^{\ll} \equiv \phi^{\gg} \implies \phi = \{\phi\} + \phi^{\gg} + \phi^{\ll} \,. \tag{85}$$

This formulation serves as the basis for the presented decomposed turbulence modeling.

5.2 Decomposed Turbulence Modeling

We may now formulate a turbulence model that explicitly accounts for each component of the velocity decomposition. Suppose a compressible simulation where part of the turbulence is resolved. The modeled turbulent stress is denoted by τ_{ij}^M and the modeled turbulent heat flux as q_i^M, leading to the following momentum and energy equations:

$$\frac{\partial \overline{\rho}\widetilde{u_j}}{\partial t} + \frac{\partial \overline{\rho}\widetilde{u_i}\widetilde{u_j}}{\partial x_i} = -\frac{\partial \overline{p}}{\partial x_j} + \frac{\partial \bar{t}_{ij}}{\partial x_i} + \frac{\partial \tau_{ij}^M}{\partial x_i}, \tag{86}$$

$$\frac{\partial}{\partial t}\left[\overline{\rho}\left(E + \frac{1}{2}k_M\right)\right] + \frac{\partial}{\partial x_i}\left[\overline{\rho}\widetilde{u_i}\left(E + \frac{1}{2}k_M\right) + \widetilde{u_i}\overline{p}\right] = \\ = -\frac{\partial}{\partial x_i}\left[\frac{\mu c_p}{Pr_L}\frac{\partial \overline{T}}{\partial x_i} + q_i^M\right] + \frac{\partial}{\partial x_i}\left[\widetilde{u_j}\left(\bar{t}_{ij} + \tau_{ij}^M\right)\right] + \frac{\partial E_{c,i}}{\partial x_i}, \tag{87}$$

where $\bar{t}_{ij}$ is the molecular viscous stress and $E = \widetilde{e} + \widetilde{u}_k\widetilde{u}_k/2 + k_M/2$, in which $\widetilde{e}$ is the internal energy and k_M is the subfilter turbulent kinetic energy as predicted by the turbulence model. The term E_c is a corrective term to the energy equation that will be introduced later. Reynolds averaging is applied to eq. (86) to arrive at the model equation for the mean momentum equation. Applying the identities in eq. (88) (as introduced in the CLES method [16]) results in eq. (89).

$$\langle \overline{\rho}\widetilde{u_j}\rangle = \langle \overline{\rho u_j}\rangle = \langle \rho u_j\rangle = \langle \rho\rangle \{u_j\}, \quad \langle \overline{\rho}\widetilde{u_i}\widetilde{u_j}\rangle = \langle \rho\rangle \{u_i\}\{u_j\} + \langle \overline{\rho}u_i^{\gg}u_j^{\gg}\rangle, \tag{88}$$

$$\frac{\partial \langle \rho\rangle \{u_j\}}{\partial t} + \frac{\partial \langle \rho\rangle \{u_i\}\{u_j\}}{\partial x_i} = -\frac{\partial \langle p\rangle}{\partial x_j} + \frac{\partial \langle t_{ij}\rangle}{\partial x_i} + \frac{\partial \langle \tau_{ij}^M\rangle}{\partial x_i} - \frac{\partial \langle \overline{\rho}u_i^{\gg}u_j^{\gg}\rangle}{\partial x_i}. \tag{89}$$

The first identity in eq. (88) follows from the definition of Favre filtering and the central assumption that $\langle \overline{\phi}\rangle = \langle \phi\rangle$. The second identity follows from the fact that the interaction terms are written as $\langle \overline{\rho}\left(\widetilde{u_i} - \{u_i\}\right)\rangle \{u_j\} = \langle \overline{\rho u_i}\rangle \{u_j\} - \langle \rho\rangle \{u_i\}\{u_j\} = 0$.

Equation 89 is essentially the Reynolds-averaged momentum equation, but with the addition of the resolved turbulent stress $-\tau_{ij}^r = \langle \overline{\rho}u_i^{\gg}u_j^{\gg}\rangle$. Hence to make the mean flow variables behave as if they are governed by a Reynolds stress model τ_{ij}^R, we require:

$$\langle \tau_{ij}^M\rangle + \tau_{ij}^r = \tau_{ij}^R \implies \langle \tau_{ij}^M\rangle = \tau_{ij}^R - \tau_{ij}^r \tag{90}$$

The governing equation for the momentum fluctuations is formed by subtracting the Reynolds average from the model equation in eq. (86). In this compressible formulation the resulting equations feature a lot of extra terms accounting for the density fluctuations, an example of which is:

$$\overline{\rho}\widetilde{u_j} - \langle \overline{\rho}\{u_j\}\rangle = \overline{\rho}u_j^{\gg} + \langle \overline{\rho u_j}\rangle\left(\frac{\overline{\rho}}{\langle \rho\rangle} - 1\right) = \overline{\rho}u_j^{\gg} + \rho^{>}\{u_j\}. \tag{91}$$

Due to these kinds of terms the lengthy momentum equation for fluctuations is omitted. As eq. (86) is essentially already the governing equation for an LES simulation, the model should behave as eq. (92) in order to have the fluctuations evolve according to a SGS turbulence model τ_{ij}^L.

$$\tau_{ij}^M - \langle \tau_{ij}^M\rangle = \tau_{ij}^L - \langle \tau_{ij}^L\rangle. \tag{92}$$

The only possible model that satisfies both eq. (90) and eq. (92) is given by:

$$\tau_{ij}^M = \underbrace{\tau_{ij}^R - \tau_{ij}^r}_{A} + \underbrace{\tau_{ij}^L - \langle \tau_{ij}^L\rangle}_{B}. \tag{93}$$

This is the exact same formulation as given in the CLES and the model-split method [16, 22]. As implied by the requirements, term A was produced by requiring that the mean flow is governed by a Reynolds stress model τ_{ij}^R, and terms B ensures that the fluctuations are governed by a SGS stress model τ_{ij}^L and that the SGS model does not influence the mean flow. If we assume that both $\tau_{ij}^R = -\left(\langle \rho\rangle \{u_iu_j\} - \langle \rho\rangle \{u_i\}\{u_j\}\right)$ and $\tau_{ij}^L = -\left(\overline{\rho}\widetilde{u_iu_j} - \overline{\rho}\widetilde{u_i}\widetilde{u_j}\right)$ are perfect turbulence models (that is: exactly reproducing the effects of

the filtered quantities), then the decomposition in eq. (94) may be applied to produce the same model formulation as in eq. (93), but now by applying the derivation shown in eq. (95).

$$-\langle\tau_{ij}^L\rangle = \langle\overline{\rho}\widetilde{u_i}\widetilde{u_j}\rangle - \langle\overline{\rho}\widetilde{u}_i\widetilde{u}_j\rangle = \langle\rho\rangle\{u_iu_j\} - \Big(\langle\rho\rangle\{u_i\}\{u_j\} + \langle\overline{\rho}u_i^{\gg}u_j^{\gg}\rangle\Big) = -\tau_{ij}^R - \tau_{ij}^r, \tag{94}$$

$$\tau_{ij}^M = \tau_{ij}^L + \langle\tau_{ij}^L\rangle - \langle\tau_{ij}^L\rangle = \tau_{ij}^L + \underbrace{\left(\tau_{ij}^R - \tau_{ij}^r - \langle\tau_{ij}^L\rangle\right)}_{C}. \tag{95}$$

This shows that the term C should be 0 in a simulation with well-resolved turbulence and employing perfect turbulence models. Suppose now that the SGS model τ_{ij}^L does not take changes in filter width into account, and flow is advecting from a region with high filter width into a region with low filter width. In this case the perfect Reynolds stress model τ_{ij}^R still correctly predicts the required level of stress, but the sum of SGS and resolved stress is smaller than the physically correct amount. In this case term C is non-zero and represents the deficit in resolved turbulent stress τ_{ij}^r.

Lastly, if the turbulence models assume their non-perfect formulation, the interpretation becomes that the total stress consists of the SGS stress τ_{ij}^L, which is supplemented by the deficit in stress according to a prediction by a Reynolds stress model τ_{ij}^R.

Applying the same procedure of Reynolds averaging the already-filtered energy equation from eq. (87) produces the following equation:

$$\begin{aligned}
&\frac{\partial}{\partial t}\left[\langle\rho\rangle E_R + \underbrace{\frac{1}{2}\langle\overline{\rho}u_i^{\gg}u_i^{\gg}\rangle + \langle\rho\rangle\frac{1}{2}\{k_M\}}_{A}\right] + \frac{\partial}{\partial x_j}\left[\{u_j\}\left(\langle\rho\rangle E_R + \underbrace{\frac{1}{2}\langle\overline{\rho}u_i^{\gg}u_i^{\gg}\rangle + \langle\rho\rangle\frac{1}{2}\{k_M\}}_{A}\right) + \right.\\
&\qquad\left. + \underbrace{\frac{1}{2}\langle\overline{\rho}u_j^{\gg}k_M\rangle}_{B} + \langle p\rangle\right] = -\frac{\partial}{\partial x_j}\left[\frac{\mu c_p}{Pr_L}\frac{\partial\langle T\rangle}{\partial x_j} + \underbrace{\langle q_j^M\rangle + \langle\overline{\rho}u_j^{\gg}h^{\gg}\rangle}_{C}\right] +\\
&\frac{\partial}{\partial x_j}\left[\underbrace{\langle u_i^{\gg}\overline{\tau_{ij}}\rangle - \frac{1}{2}\langle\overline{\rho}u_j^{\gg}u_i^{\gg}u_i^{\gg}\rangle}_{D}\right] + \frac{\partial}{\partial x_j}\left[\{u_i\}\left(\langle t_{ij}\rangle + \underbrace{\langle\tau_{ij}^M\rangle - \langle\overline{\rho}u_i^{\gg}u_j^{\gg}\rangle}_{E}\right) + \underbrace{\langle u_i^{\gg}\tau_{ij}^M\rangle}_{F}\right] + \frac{\partial\langle E_{c,j}\rangle}{\partial x_j},
\end{aligned} \tag{96}$$

where $E_R = \{e\} + \{u_i\}\{u_i\}/2$ is the total energy in a RANS model. Here we see several similar terms with a similar interpretation as in the momentum equation in eq. (89). The evolution equation for the fluctuating total energy $E^{\gg}$ may be produced by subtracting eq. (96) from eq. (87), but is omitted here for the same reasons as before.

If this equation should evolve the mean total energy E_R as a RANS formulation would, then term A should match the turbulent kinetic energy k_R predicted by a Reynolds stress model. And the fluctuating component of k_M should behave as $\overline{\rho}k_L - \langle\overline{\rho}k_L\rangle$. Although the turbulent kinetic energy of a model is conceptually a subfilter quantity, it is interpreted here as a model quantity consisting of a mean $\{k\}$ and a fluctuating component $k^{\gg}$. This leads to the following formulation:

$$\begin{cases}\langle\rho\rangle\{k_M\} + \frac{1}{2}\langle\overline{\rho}u_i^{\gg}u_i^{\gg}\rangle & = \langle\rho\rangle\{k_R\}\\ \widetilde{\overline{\rho}k_M} - \langle\widetilde{\overline{\rho}k_M}\rangle & = \widetilde{\overline{\rho}k_L} - \langle\widetilde{\overline{\rho}k_L}\rangle\end{cases} \implies \widetilde{\overline{\rho}k_M} = \widetilde{\overline{\rho}k_L} + \left(\langle\rho\rangle\{k_R\} - \frac{1}{2}\langle\overline{\rho}u_i^{\gg}u_i^{\gg}\rangle - \langle\rho\rangle\{k_L\}\right). \tag{97}$$

The interpretation is the same as in the discussion of eq. (95): the Reynolds model's prediction $\langle\rho\rangle\{k_R\}$ is compared to the sum of resolved and subgrid turbulent kinetic energy. If there is a deficit then it is

supplemented. Due to the derivation of the energy equation it comes as no surprise that eq. (97) is the trace of eq. (95).

The same requirement on the turbulent stress as stated in eq. (90) can be found in term E. Term C is the turbulent heat flux equivalent of the Reynolds-stress constraining equations. So defining the resolved heat flux $q_j^r = \langle \overline{\rho} u_j^{\gg} h^{\gg} \rangle$ and combining the requirement from term C with the equivalent requirements for the fluctuating total energy produces the model term

$$\begin{cases} \langle q_j^M \rangle + q_j^r & = q_j^R \\ q_j^M - \langle q_j^M \rangle & = q_j^L - \langle q_j^L \rangle \end{cases} \implies q_j^L + \left(q_j^R - q_j^r - \langle q_j^L \rangle \right) \ . \tag{98}$$

We may continue this line of thinking for all the other terms as well. Due to the nature of the presented decomposition the resolved components are expected in an LES formulation, but should be prevented from acting on the mean flow in the RANS formulation. Term D in eq. (96) contains the resolved molecular diffusion and resolved turbulent transport of turbulent kinetic energy. These are approximated with a diffusion term (i.e. term $\mathcal{D}_k$ in eq. (26)). Hence the equivalent modeled term $\mathcal{D}_k^M$ in terms of the RANS model $\mathcal{D}_k^R$ and SGS model $\mathcal{D}_k^L$ term becomes:

$$\mathcal{D}_k^M = \mathcal{D}_k^L + \left(\mathcal{D}_k^R - \frac{\partial}{\partial x_j} \left[\langle u_i^{\gg} \overline{t_{ij}} \rangle - \frac{1}{2} \langle \overline{\rho} u_j^{\gg} u_i^{\gg} u_i^{\gg} \rangle \right] - \mathcal{D}_k^L \right) \ . \tag{99}$$

The more problematic terms are the terms B, representing the turbulent advection of the fluctuating component of the modeled turbulent kinetic energy k_M, and F, representing the turbulent flux of the modeled stress τ_{ij}^M. Even though one might constrain the various model terms to ensure their mean become RANS-like quantities, their advection is still governed by the turbulent velocity field. Hence to constrain the mean solution of the energy equation one should include a corrective term E_c in the modeled energy equation (i.e. eq. (87)) to account for these terms, which may be formulated as:

$$E_{c,j} = \langle u_i^{\gg} \tau_{ij}^M \rangle - \frac{1}{2} \langle \overline{\rho} u_j^{\gg} k_M \rangle = \langle u_i^{\gg} \tau_{ij}^L \rangle - \frac{1}{2} \langle \overline{\rho} k_L \rangle, \tag{100}$$

where the latter form is constructed using constrained formulations of τ_{ij}^M and k_M as presented in eq. (95) and eq. (97). As the non-averaged terms in the constrained formulations are τ_{ij}^L and k_L, these are the only quantities remaining in the corrective term in eq. (100). Since the corrective term is formulated using mean quantities only, it will not impact the evolution of the fluctuating component of the total energy.

It should be noted that this term is akin to sum of the molecular diffusion flux term and resolved turbulent transport term. In an unmodeled energy equation (i.e. eq. (3)) these terms arise due to the triple-velocity term $u_j u_i u_i$ in the advection term and the molecular diffusion t_{ij} term. Because the modeled energy equation (i.e. eq. (87) includes a τ_{ij}^M and a $\overline{u_j} \widetilde{k}^M$ term, a similar formulation arises.

By constraining the model terms to produce means governed by Reynolds-averaged models, the mean flow is ensured to conform to the one that would be produced by Reynolds-stress models. This explicitly takes care of the double-accounting of stress as the effect of resolved turbulence on the mean flow quantities is removed.

The missing stress, turbulent kinetic energy and heat flux (i.e. the bracketed terms in eq. (95), eq. (97) and eq. (98)) are governed by averaged quantities. Hence the problem of underdeveloped turbulence (i.e. the grey-area problem and perhaps part of the LLM) is not explicitly solved: the presented constraining terms only ensure correct means. Still, the lack of turbulence near the RANS/LES interface is somewhat solved as there is no interface anymore and the LES model is free to govern the development of fluctuations near walls. The resolved quantities are still going to be incorrect when the grid is coarse relative to a well-resolved LES simulation.

The constraining term for the subfilter turbulent kinetic energy $k_R - k_r - \langle k_L \rangle$ (neglecting that the prediction provided by k_R might be incorrect) provides a measure of how much turbulence is expected, which might be factored into the intensity with which a stochastic forcing model excites the flow in order to attain the correct amount of resolved turbulence.

5.3 A Reynolds Stress Model for the Decomposed Formulation

The presented constrained terms all assume that the Reynolds-stress model τ_{ij}^R and heat flux model q_j^R act as averaged quantities and serve as an accurate prediction of the total turbulent stress and heat flux in a simulation. From the analysis of `ensolv` in section 4.5.3 it became apparent that the k-ω equations were influenced by the resolved turbulence, albeit leading to favourable results. To circumvent this problem the Reynolds-stress modeling equations may be formulated in terms of Reynolds- and Favre-averaged quantities. Although the decomposed turbulence modeling is model-agnostic, an example of such an averaged formulation is shown in eq. (101) and eq. (102) for the k-ω turbulence model.

$$\frac{\partial \langle\rho\rangle \{k_R\}}{\partial t} + \frac{\partial \langle\rho\rangle \{u_i\} \{k_R\}}{\partial x_i} = \langle \mathcal{P}_k \rangle - \langle \epsilon_k \rangle + \frac{\partial}{\partial x_i} \left[\langle\rho\rangle \left(\{\nu\} + \sigma_k \{\nu_t\} \right) \frac{\partial \{k_R\}}{\partial x_i} \right], \tag{101}$$

$$\frac{\partial \langle\rho\rangle \{\omega\}}{\partial t} + \frac{\partial \langle\rho\rangle \{u_i\} \{\omega\}}{\partial x_i} = \langle \mathcal{P}_\omega \rangle - \langle \epsilon_\omega \rangle + \sigma_d \frac{\langle\rho\rangle}{\{\omega\}} \max \left[0, \frac{\partial \{k\}}{\partial x_i} \frac{\partial \{\omega\}}{\partial x_i} \right] + \\ + \frac{\partial}{\partial x_i} \left[\langle\rho\rangle \left(\{\nu\} + \sigma_\omega \nu_t \right) \frac{\partial \{\omega\}}{\partial x_i} \right] . \tag{102}$$

The definition of the cross-diffusion term is somewhat questionable as it cannot be formed from the averaging of the ω-equation. However, in a practical simulation $\langle\rho\rangle \{k_R\} = \langle \rho k_R \rangle$ and $\langle\rho\rangle \{\omega\} = \langle \rho\omega \rangle$ would be the modeled quantities. Hence e.g. $\{k_R\}$ can be obtained as $\langle \rho k_R \rangle / \langle\rho\rangle$, where $\langle\rho\rangle$ is indeed explicitly averaged. Then with $\langle \rho\omega \rangle$ acting like an averaged term, eq. (102) should behave just like the pure-RANS turbulence model would.

The molecular viscosity $\langle\mu\rangle = \langle\rho\rangle \{\nu\}$ should be explicitly averaged as well, but as long as the flow is subsonic and no large temperature gradients are imposed on the flow then using it in unaveraged form should suffice. The eddy viscosity ν_t should be explicitly averaged, but again: as long as $\{k_R\}$ and $\{\omega\}$ act as mean terms, then ν_t is implicitly averaged as well.

The production and dissipation terms of the k and ω equation are given by:

$$\langle \mathcal{P}_k \rangle = \langle\rho\rangle \{\nu_t\} \{S_{ij}\} \{S_{ij}\} - \frac{2}{3} \langle\rho\rangle \{k\} \frac{\partial \{u_i\}}{\partial x_i}, \quad \langle \epsilon_k \rangle = \beta_k \langle\rho\rangle \{k\} \{\omega\}, \tag{103}$$

$$\langle \mathcal{P}_\omega \rangle = \alpha_\omega \langle\rho\rangle \{S_{ij}\} \{S_{ij}\} - \frac{2}{3} \langle\rho\rangle \{\omega\} \frac{\partial \{u_i\}}{\partial x_i}, \quad \langle \epsilon_\omega \rangle = \beta_\omega \langle\rho\rangle \{\omega\} \{\omega\} . \tag{104}$$

These equations will produce RANS-like values for $\{k\}$ and $\{\omega\}$ if the mean flow is behaving like it would in a pure RANS simulation. The added complexity is that the averages presented here will have to be explicitly computed. This will cause delays in the mutual interaction of the mean flow and the RANS turbulence modeling equations.

5.4 Implications of Explicit Time Filtering

The presented formulations of the momentum, energy and Reynolds-stress modeling equations all feature Reynolds- and Favre-averaged terms. All of these terms will have to be computed by explicit temporal filtering. This has several implications, both as standalone arguments as for the discussed advantages of the decomposed modeling method.

Although alternate formulations of averages are possible, the initial implementation of this method consists of taking averages at fixed points in space. In general these types of filters are not Galilean invariant. Furthermore, the presented method requires that the flow is statistically stationary. This requirement may be relaxed somewhat by applying the method solely as a wall-modeling method and disabling the corrective terms (containing the explicit averages) away from walls.

The remaining issues are best illustrated with two examples of temporal filtering. The definition of a running time filter and of an exponential time filter are given by:

$$\langle\phi\rangle_t|_{t=T} = \frac{1}{T}\int_0^T \phi\left(t\right)\mathrm{d}t \tag{105}$$

$$\frac{\partial\,\langle\phi\rangle_e|_{t=T}}{\partial t} = \alpha\left[\phi\left(t\right) - \langle\phi\rangle_e|_{t=T}\right] \implies \langle\phi\rangle_e\left(T\right) = \int_0^T \alpha\left[\phi\left(t\right) - \langle\phi\rangle_e|_{t=T}\right]\mathrm{d}t \tag{106}$$

With any kind of explicit time filter $\langle\cdot\rangle$, the (co)variances are computed as:

$$\langle u^{\gg} v^{\gg}\rangle = \langle\left(\widetilde{u} - \{u\}\right)\left(\widetilde{v} - \{v\}\right)\rangle = \langle\widetilde{u}\widetilde{v}\rangle - \{u\}\,\{v\} \tag{107}$$

The statement that the constraining terms only affect the mean flow and do not influence the turbulent fluctuations is only true if the time averages are relatively converged and the filters are good low-pass filters.

In practice this is not the case. The running time filter has a cut-off frequency that recedes from an infinite value to an infinitesimally small value as time progresses. During the start-up period of a simulation the explicitly averaged resolved turbulence and averaged SGS stress is negligible, causing the model to act with the full dissipation of the sum of instantaneous SGS stress and instantaneous Reynolds stress. As the averaging operator initially has a large cutoff frequency these terms will act upon the turbulent fluctuations. As a result any turbulence initially present in the simulation is likely rapidly damped. As long as the grid is fine enough then turbulence may develop freely at a later point in time. If the running time averaging filter measures a lack of turbulence over a large span of time then it will take an even longer amount of time to obtain correct velocity statistics. In the intermediate period there will be too much modeled turbulent stress acting upon the mean flow, which will influence its development.

Some of these issues may be circumvented by using the exponential filter defined in eq. (106), as is done by other authors [20, 22]. Such a filter may have an arbitrarily small cutoff frequency, but initial values have a large effect on the evolution of the measured means. If the cut-off frequency is too large, then the mean terms in the modeled stress act upon the turbulent fluctuations to some degree and the computed statistics might be incorrect. If the cut-off frequency is very low then convergence takes a long amount of time.

From the analysis of the X-LES solver in TCF it became apparent that the simulation should run for approximately $TU_b/\delta \approx 240$ until the resolved Reynolds stress was accurately computed using the running time filter. In the constrained formulation, assuming all other terms are correct, it will take this amount of time before the formulation converges to its intended values.

5.5 Hybridization with an LES Model

The method presented so far will not be able to accurately compute any kind of inherently oscillating flows (e.g. von Kármán vortex streets, large regions of separated flow or oscillating shear layers). This is because the application of explicit time averaging assumes statistically stationary flows and Reynolds-stress models are known to fail in flows exhibiting large regions of separation. It is a primary goal of hybrid RANS/LES methods to accurately compute these separated regions using an LES formulation, and to restrict the RANS formulation to near-wall regions.

For this reason it seems desirable to, like hybrid RANS/LES models, transition to a pure LES formulation at some point away from the wall. We assume there is an interface at some position in the flow where the constrained formulation is applied on one side and a SGS model on the other side. Then to ensure a smooth transition between the two formulations one requires:

$$\Delta_{\tau_{ij}} = \left[\tau_{ij}^L + \left(\tau_{ij}^R - \tau_{ij}^r - \langle\tau_{ij}^L\rangle\right)\right] - \tau_{ij}^L = \tau_{ij}^R - \tau_{ij}^r - \langle\tau_{ij}^L\rangle \to 0 \ . \tag{108}$$

This implies that the flow should be well-resolved according to the prediction made by the Reynolds stress model. This formulation implicitly formulates 6 separate interface locations, not mentioning the additional conditions for the turbulent heat flux and turbulent kinetic energy equations. Note that this requirement only applies to the mean flow: due to the formulation of the constrained model the governing equations for the turbulent fluctuations will always smoothly transition between formulations, independent of the interface location.

Since no simulation with such an interface formulation is performed by this author, definitive statements about suitable switching conditions cannot be made. That said, and restricting the discussion to incompressible flows, it seems like a desirable property to have a single scalar quantity governing the transition between model formulations.

In case the switching condition is formulated solely on the basis of the constraining terms, then the constraining condition on the turbulent kinetic energy might serve as a guide (with potentially a scaling factor for the turbulent kinetic energy k_R from the Reynolds stress model):

$$\tau_{ij}^M = \begin{cases} \tau_{ij}^L - \left(\tau_{ij}^R - \tau_{ij}^r - \langle\tau_{ij}^L\rangle\right) & \text{if } \langle\rho\rangle\{k_R\} - \frac{1}{2}\langle\overline{\rho}u_i^{\gg}u_i^{\gg}\rangle - \langle\rho\rangle\{k_L\} \geq 0 \\ \tau_{ij}^L & \text{otherwise} \end{cases} \tag{109}$$

Alternatively, if an empirical blending function f_b (e.g. the shielding function in the DDES method [14] or the blending function in the two-velocity method [21]) is used, then it is best applied to the mean term in the model formulation:

$$\tau_{ij}^M = \tau_{ij}^L + f_b\left(\tau_{ij}^R - \tau_{ij}^r - \langle\tau_{ij}^L\rangle\right) \ . \tag{110}$$

Such a formulation will ensure that the evolution of the turbulent fluctuations are not impacted by the blending, only the mean quantities are. If the blending function is formulated in terms of flow variables, one should be careful to only use explicitly averaged quantities in order to prevent the fluctuations in the blending function causing the constraining term to have an effect on the evolution of fluctuating quantities.

6 Lessons Learned from a Decomposed Modeling Formulation

A particular form of the presented decomposed modeling formulation has been investigated. Note that these only represent preliminary results. The bulk of the work on this method was performed during the last stages of the execution of this thesis. During this period several changes had to be made that deviated from the originally intended formulation (e.g. the introduction of van Driest-like damping the SGS modeling equation to make sure that the simulation was numerically stable), such that it is hard to pin down the exact reasons for the obtained simulation results.

6.1 Governing Equations

A model is formulated based on the decomposition method in chapter 5. To attain a one-parameter blending function eq. (97) is used as the constraining term, much like the model-split method does [22]. The corrective term in each of the constrained definitions of Reynolds stress, turbulent kinetic energy and heat flux depends on mean quantities. The assumption is made that each of these constraining terms is equal to a scaled RANS term, as shown in eq. (111). In eq. (112) the assumption for the turbulent kinetic energy is used to formulate the blending parameter for k, which is of similar form as the model-split method.

$$\tau_{ij}^R - \tau_{ij}^r - \langle \tau_{ij}^L \rangle \approx f_b \tau_{ij}^R, \quad k_R - k_r - \langle k_L \rangle = f_b k_R, \quad q_{j,R} - q_{j,r} - \langle q_{j,R} \rangle \approx f_b q_{j,R}, \tag{111}$$

$$f_b = \frac{k_R - k_r - \langle k_L \rangle}{k_R} = 1 - \frac{\langle \overline{\rho} u_i^{\gg} u_i^{\gg} \rangle + k_L}{k_R}, \tag{112}$$

where the k_R term in the denominator is limited by a small positive lower bound. The corrective term E_c in the energy equation, as described in eq. (96), is neglected. The presented model then assumes that the Reynolds stress and the diffusion term from the k-equation scale with their respective turbulent kinetic energies. The turbulent heat flux term is likely incorrect. However, as the performed simulations are practically incompressible, the impact of this term should be small.

The particular form of the blending term f_b, suggests that the corrective term may be switched off if $f_b < 0$. In this case the modeling reverts to an LES formulation. Hence the blending factor f_b is defined as:

$$f_b = \max\left[0, 1 - \left(\langle \overline{\rho} u_i^{\gg} u_i^{\gg} \rangle + k_L\right) / k_R\right] \ . \tag{113}$$

The model is implemented within the existing code of `ensolv`. Without any modifications to the SGS k-equation unidentified numerical issues near the wall caused the model to fail. A solution was to implement a type of van Driest-like damping to the filter width Δ as $D\Delta$. The model by Balaras shown in eq. (114) was adapted to function within the k-equation (it is by no means implied that this is a correct modeling assumption) [38]. By assuming that the production term $\mathcal{P}_k$ and the dissipation term ϵ_k in eq. (53) are equal, the eddy viscosity must be equal to eq. (115). Then the damping term D may be, by comparison, formulated as shown in eq. (116). The friction Reynolds number Re_τ used to determine y^+ is set in ad-hoc fashion to the preconfigured friction Reynolds number that determines the driving body force.

$$\nu_t = (\kappa y)\left(1 - \exp\left[-\left(\frac{y^+}{A^+}\right)^3\right]\right)\sqrt{\widehat{S}_{ij}\widehat{S}_{ij}} \tag{114}$$

$$\nu_t = C_1^2 \sqrt{\frac{1}{\beta_k}} (D\Delta)^2 \sqrt{\widehat{S}_{ij}\widehat{S}_{ij}} \tag{115}$$

$$D = \min\left[1, \frac{\kappa y}{C_1 \Delta} \beta_k^{1/4} \sqrt{1 - \exp\left[-\left(\frac{y^+}{A^+}\right)^3\right]}\right] \tag{116}$$

Where κ is the von Kármán constant and $A^+ = 26$ is the van Driest damping parameter.

Summarizing, the fluid modeling equations are defined in eq. (86) and eq. (87). In these equations the corrective term E_c is neglected, and the turbulent stress model τ_{ij}^M and turbulent heat flux q_i^M are defined as shown in eq. (117). Where the blending factor f_b is defined in eq. (113). The Reynolds stress term τ_{ij}^R is modeled by a k-ω model as defined in eq. (101) and eq. (102). The SGS stress term is modeled by a k-equation model as defined in eq. (53), where the lengthscale Δ is redefined as $D\Delta$, with the damping term D given by eq. (116).

$$\tau_{ij}^M = \tau_{ij}^L + f_b\tau_{ij}^R, \quad q_i^M = q_i^L + f_b q_i^R, \quad k_M = k_L + f_b k_R \tag{117}$$

Harking back to the introduction of the hybrid models in section 3.1, the model is very similar to the isotropic/anisotropic decomposition of the two-velocity and model-split method, while incorporating terms from the CLES method in order to formulate the constraining terms.

6.2 Explicit Time Filtering

Initial tests with the method failed when using a running time average to compute the explicitly averaged terms. As an ad-hoc solution the exponentially filtered method defined in eq. (106) was used. In order to interpet the scaling term α it is redefined in terms of the cutoff frequency ω_c. Applying the Fourier transform $\mathcal{F}[\cdot]$ to the filter equation and applying the cutoff frequency criterion results in eq. (118).

$$i\omega\mathcal{F}[\langle\phi\rangle] = \alpha\left(\mathcal{F}[\phi] - \mathcal{F}[\langle\phi\rangle]\right) \implies |H(\omega)|^2 = \left|\frac{\mathcal{F}[\langle\phi\rangle]}{\mathcal{F}[\phi]}\right|^2 = \frac{\alpha^2}{\alpha^2+\omega_c^2} = \frac{1}{2} \implies \alpha = \omega_c \tag{118}$$

Which is rewritten in terms of a cutoff timescale as $T_c = 2\pi/\alpha$, or in non-dimensional terms as $T_c' = 2\pi\delta/(\alpha U_b)$. In a range of tests T_c' was allowed to vary between 6 and 36 in steps of 6 (with the length of the channel set to 2π, each step of 6 corresponds roughly to one complete flow-through of the periodic channel's length at the bulk velocity). At the lower range of $T_c' = 6, 12$ the turbulence was clearly affected by the constraining term $f_b\tau_{ij}^R$. This is because both the formulation of f_b as the evolution of $\nu_t^R = k/\omega$ depend on the explicitly averaged terms.

The time evolution of the explicitly averaged terms is implemented as forward Euler integration at the end of all subiterations of a single implicit Runge-Kutte timestep. To this end the scaling term α is modified to take the discrete timestep into account.

6.3 Preliminary Results on Turbulent Channel Flow

The results obtained from the proposed method where the SGS model is not high-pass filtered are inaccurate due to a software bug, hence only the results using the HPF SGS model are presented. To show the variability of the method results are shown for a cutoff timescale of $T_c' = 24, 30, 36$. The results are collected for a rather large time $TU_b/\delta \approx 1500$ to ensure that the results were somewhat converged. Even at this timespan (the analysis of the X-LES method used a timespan of $TU_b/\delta \approx 240$ to ensure that the mean flow was converged, followed by a similar timespan to collect the turbulent statistics) there is reason to believe that the $T_c' = 30$ and $T_c' = 36$ cases are still unconverged.

For these simulations the obtained velocity profiles are shown in fig. (21), and the turbulent kinetic energy k and u,v covariances are shown in fig. (22). To prevent confusion, the modeled Reynolds stress in the hybrid model will be called the RANS-portion, and the results from a RANS-only simulation will be called pure RANS.

Table 4: Grid properties for the TCF simulations with decomposed hybrid model

$Re_{\tau,\text{set}}$	T_c'	x^+	z^+	y^+_{wall}	y^+_{core}	N_y	N_c	$Re_{\tau,\text{sim}}$	$Re_{b,\text{sim}}$
1000	24	200	100	0.77	42.0	96	32	991.0	21840
1000	30	200	100	0.77	42.0	96	32	1008.9	22120
1000	36	200	100	0.77	42.0	96	32	994.3	23360

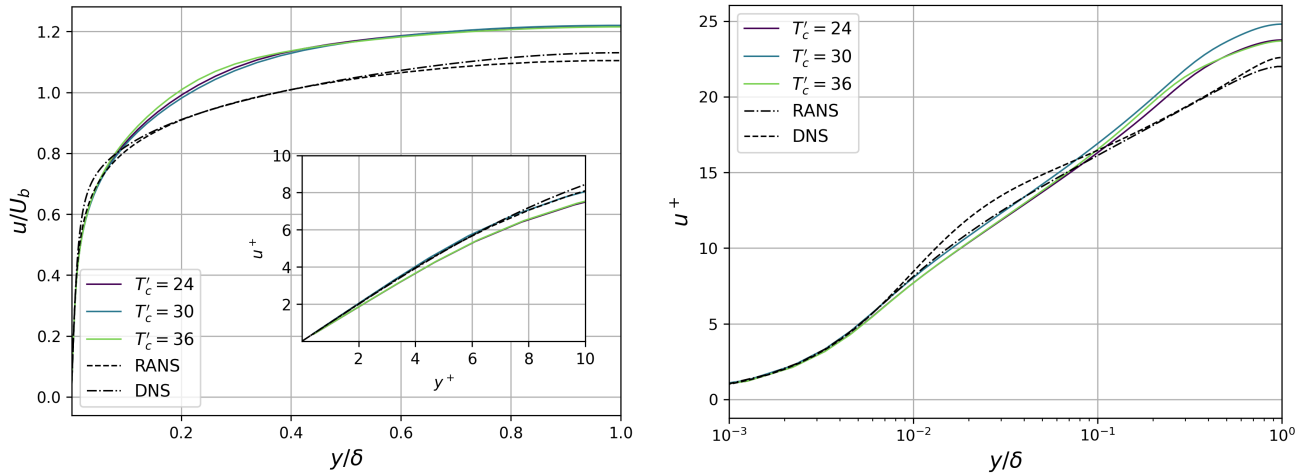

Figure 21: Velocity profiles of TCF using the proposed hybrid method at different cutoff timespans T_c' compared to RANS and DNS results at $Re_\tau = 1000$.

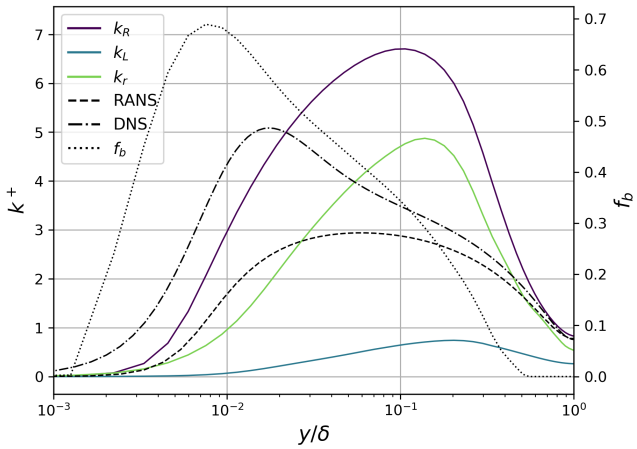

(a) Turbulent kinetic energy k at $T_c' = 24$

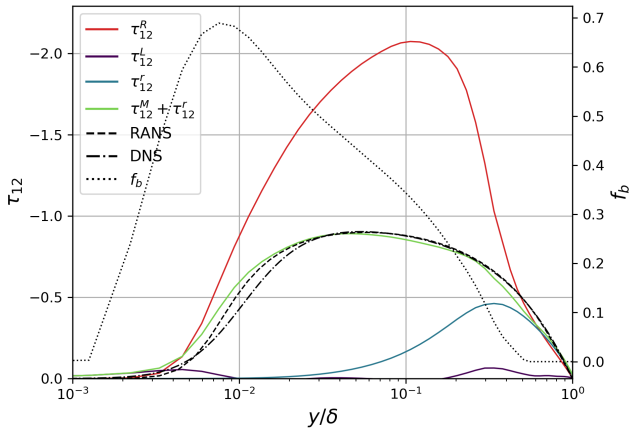

(b) Resolved and subfilter stress τ_{12} at $T_c' = 24$

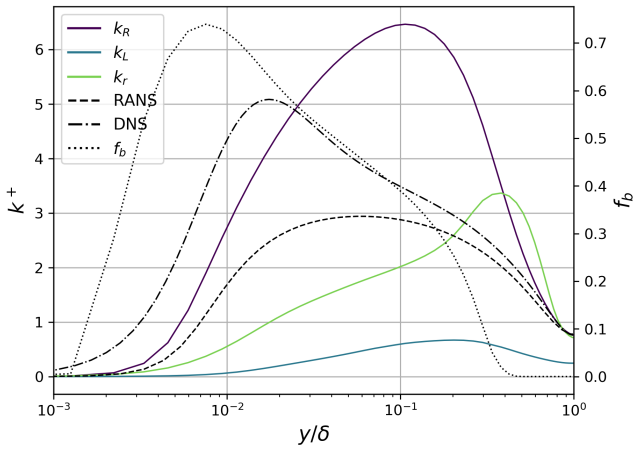

(c) Turbulent kinetic energy k at $T_c' = 30$

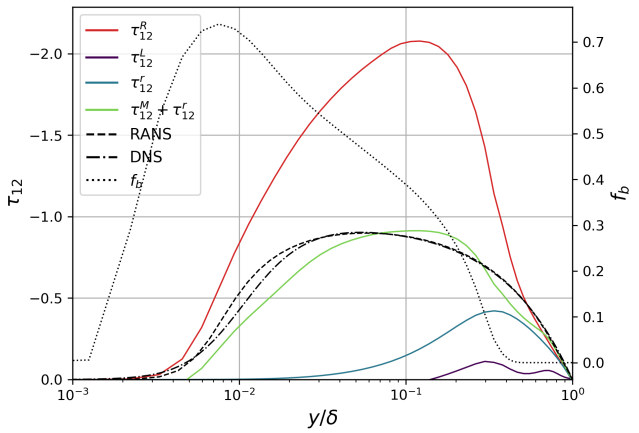

(d) Resolved and subfilter stress τ_{12} at $T_c' = 30$

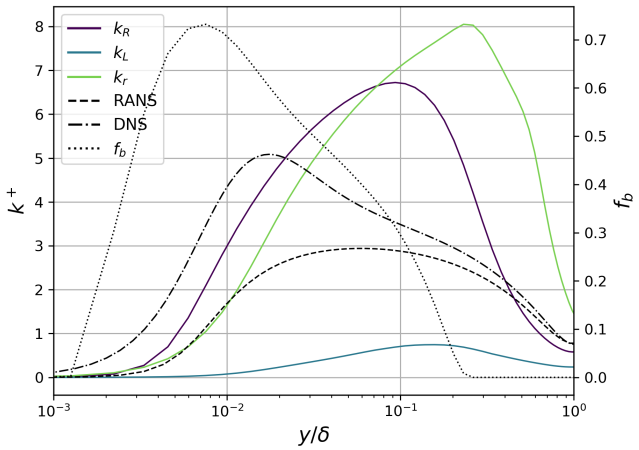

(e) Turbulent kinetic energy k at $T_c' = 36$

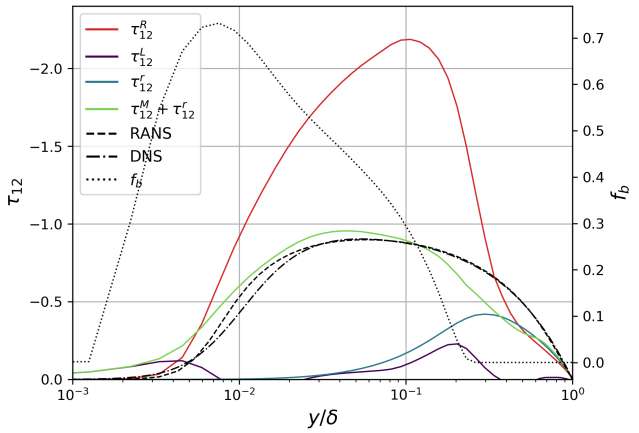

(f) Resolved and subfilter stress τ_{12} at $T_c' = 36$

Figure 22: Turbulent kinetic energy k and subfilter stress τ_{12}, decomposed into modeled and resolved contributions, of TCF using the proposed hybrid method compared to RANS and DNS at $Re_\tau = 1000$.

Looking at the velocity profiles in fig. (21) there is a large overestimation of the velocity in the center of the channel where the blending f_b reduces to 0, while to some degree the velocity profiles match the RANS velocity profile near the wall rather well.

The decomposition of the turbulent kinetic energy and covariances show what is going wrong. The resolved turbulent kinetic energy k_r in the hybrid model is very large, as may be seen in the subfigures on the left hand side of fig. (22). This is to some degree due to the presence of superstreaks in the hybrid model's solution. However the flow is also wildly oscillating in its streamwise velocity component. This causes the blending factor f_b to be much lower than it should be if indeed $\tau_{12}^r \propto k_r$.

The presence of the superstreaks is somewhat unexpected. Their structure and maximum- to minimum velocity ratios are similar to the results obtained from the X-LES method. Different from the X-LES method the variation of eddy viscosity within wall-parallel surfaces is much smaller.

The turbulent kinetic energy k_R of the RANS-portion of the hybrid model is also much larger than it should be. The reason is that the constraining term is applied in the momentum equation as $f_b \tau_{ij}^R$. The constraining term is the dominant term close to the wall (i.e. $y/\delta < 0.03$) and determines the shape of the velocity profile in this region. As a response to the fact that the resolved turbulent kinetic energy k_r does not correspond to a proportional amount of resolved turbulent stress τ_{12}^r the turbulent kinetic energy

of the RANS-portion of the model increases such that the correct velocity profile is attained close to the wall. This is especially well visible in fig. (22b). Where at $y/\delta < 0.1$ the RANS-portion τ_{12}^R is dominant and seems to scale inversely to f_b, causing the total turbulent stress $\tau_{12}^M + \tau_{ij}^r$ to approach the RANS and DNS solutions.

There is also the issue of the blending function f_b going to 0 as the wall is approached. The formulation of the blending function f_b depends on the resolved and both of the unresolved turbulent kinetic energies. They all approach 0 near the wall at different rates (but k_R at a slightly slower rate) such that the blending function tends to approach 0 near the wall as well. Both because of this reason, and because the SGS-portion of the hybrid model is interfering with the stresses near the wall, the viscous sublayer should be protected in one way or the other.

7 Conclusions

The X-LES solver has been analyzed by comparing TCF simulations to DNS and RANS results. Both in its zonal and non-zonal configuration the solver performs reasonably well, as long as most of the center of the channel is governed by the LES-formulation. Especially at the higher Reynolds number the turbulent statistics match those of DNS in the center of the channel and match those of RANS near the wall.

The X-LES method is not exempt from the problematic formation of superstreaks and the ocurrence of the LLM. Without the SBS model or the HPF the log-layer mismatch is present due to, arguably, a lack of resolved turbulence or a lack of modeled turbulence. A part of the problem lies in the presence of the superstreaks. These structures extend from some distance above the wall in the RANS-domain to well into the LES-domain. In the RANS-domain there is localized production of eddy viscosity spatially correlated with the edges of the superstreaks. This eddy-viscosity gets ejected, originating from the low-speed superstreaks, into the LES-domain above the interface through transport with the flow. The reason for the ejection is a relatively strong negative spatial correlation between $\langle u^+ \rangle$ and $\langle v^+ \rangle$. Within the LES-domain the regions of high eddy viscosity seem to prevent the proper development of small-scale turbulence.

The SBS model, at its originally tuned parameter values, did not seem to significantly reduce the LLM or the superstreaks. Enabling it did cause a more rapid development of resolved turbulence within the simulation. The SBS model was retuned, causing it to be active at different spatial and temporal scales, but also to force the flow at a higher intensity (as measured by the amount of dissipation that was needed to obtain proper $-5/3$ Kolmogorov spectra in HIT simulations matching experiments). With this retuned model, the superstreaks are broken up and the log-layer mismatch is nearly gone. It remains unclear how much the direct stimulation of turbulence and the prevention of superstreak formation factors into producing this agreeable result. Note that, whereas previously the interference with the k-ω turbulence model resulted in a correct total turbulent stress, now the increased forcing causes a velocity profile that deviates somewhat from the pure RANS results.

With regards to the zonal interface it seems unwise to apply the method in a zonal fashion in regions where high velocity gradients are present (i.e. near walls), unless it is placed in roughly the same position as it would be in a non-zonal simulation. The jump in lengthscale incurred by zonal simulations produces discontinuities in the Reynolds stresses and the turbulence modeling terms. If the errors are large enough then the flow will be severly impacted, causing problems such as unphysically large changes in velocity gradients (in the context of TCF) or large changes in net production/dissipation of turbulent kinetic energy.

A similar type of problem was found in the application of the HPF, where the errors were proportional to the rate of strain near the interface. Hence like the zonal/non-zonal conclusions, the HPF should only be applied in a domain as long as all its bounding interfaces do not experience high velocity gradients.

An attempt was made to develop a consistent framework for hybrid turbulence modeling. This method uses explicit time filtering to formulate the evolution of the mean and the fluctuating parts of the flow separately. In practice the cut-off frequency of the explicit time filter needs to be very low to ensure that the component of the model that is responsible for the mean quantities does not interfere with the modeling of the fluctuating quantities. However, such a low cut-off frequency is in conflict with the desire to have a simulation methodology that converges rapidly. As the goal of the method is to produce an efficient hybrid RANS/LES method that is industrially applicable, it seems that the application of the explicitly filtered quantities should be used more sparingly then employed in this thesis.

That being said it is an interesting approach to performing hybrid RANS/LES methods, where there is no longer a region where turbulence is excessively damped and a region where the turbulence is allowed to develop freely. Rather, both formulations can exist simultaneously. Currently, the method suffers

from insufficient damping of turbulent fluctuations near the wall due to the SGS model. This causes the formulation of the blending function f_b to be incorrect. In turn, by coupling between the momentum equation and the RANS turbulence modeling equations, the RANS turbulent kinetic energy k_R becomes much larger than it should be.

8 Recommendations

The SBS model with retuned model parameters caused a smoother transition between RANS and LES formulations in the X-LES model, with an accompanied reduction in the LLM. Although some effort has been expended into an appropriate combination of parameters, it is unclear how much each of these parameters (the spatial correlation, temporal correlation and forcing intensity) contributed to the results.

Further research should concentrate on the solution surface to the minimization problem defined in section 4.4. Once this is determined the effectiveness of the SBS model to reduce the LLM may be futher investigated. It seems logical that at too low an intensity the SBS model does not influence the simulation results at all, while at a very high intensity the accuracy of the X-LES model might suffer. There must be some subset of the aformentioned solution surface that reduces the LLM while minimally interfering with the simulation results.

Although not investigated in this thesis, X-LES seems to suffer from spurious switching between the RANS and LES formulations in the center of the channel. It would seem unwise to modify the terms in the SGS model's k-equation. But as the ω-equation is only solved in the LES-domain in order to provide boundary conditions for the equation in the RANS-domain, it may be possible to force the ω-equation to act more like it would in a RANS simulation. With a lower value for ω this would increase the RANS lengthscale, therefore possibly preventing the spurious switching of the model.

There are a variety of issues with the presented decomposed hybrid modeling. Its performance and convergence requires an explicit time filter with a low and sharp cutoff. It would be interesting to implement several different types of time filters to see how well they can filter out high-frequency motions from the flow and how long it takes for them to produce correct flow statistics.

The decomposed formulation itself should be investigated without the additional modeling assumptions presented in this work. This would reproduce the CLES model, but with some additional constraints. Furthermore, the effect of removing several corrective terms (e.g. the correction term E_c in the energy equation, or explicitly averaged terms in the k-ω equations) should be investigated. Perhaps the delayed interaction between the turbulence modeling equations and mean flow equations can be reduced by, like in the derivations of the momentum and energy equations in eq. (89) and eq. (96), subtracting resolved turbulent statistics from the various terms in the k-ω equations. This in contrast to the current use of explicitly averaged means in eq. (101) and eq. (102).

Some effort should be expended in finding ways to increase the damping of resolved turbulence near the wall. Given the effects of the implicit time filter on the resolved fluctuations, an interesting approach might be to reduce the timespan over which the averaging occurs near the wall.

Lastly the possiblity to use single-parameter blending functions should be investigated in a more fundamental manner. This should be preferentially done by investigating results from simulations using the implicit switching conditions in eq. (108).

Like many other hybrid RANS/LES methods, the X-LES and proposed hybrid method seem to suffer from superstreaks to some degree. Since these structures seem resistent to different turbulence modeling methods, interface location and matching conditions [31], it would be interesting to see if they arise due to some kind of pseudo-physical process. Comparing the Reynolds stress tensor equation terms of a high Reynolds number TCF simulation to DNS data [37] might provide some insight into which process is responsible for the superstreaks.

It is clear that the superstreaks produce a rather distinct spatial distribution in the velocity field and the turbulence modeling fields. Alternative methods to remove these structures or their secondary effects should be investigated. This would hopefully allow quantifying to which degree they are indirectly responsible for the lack of resolved stress in the LES-domain.

References

[1] P. Spalart, "RANS Modelling into a Second Century," *International Journal of Computational Fluid Dynamics*, vol. 23, no. 4, pp. 291–293, 2009.

[2] U. Piomelli, "Wall layer models for LES," (Reno, Nevada), American Institute of Aeronautics and Astronautics, Jan. 2008.

[3] J. Fröhlich and D. von Terzi, "Hybrid LES/RANS Methods for the Simulation of Turbulent Flows," *Progress in Aerospace Sciences*, vol. 44, pp. 349–377, 2008.

[4] P. Spalart, "Detached-Eddy Simulation," *Annu. Rev. Fluid Mech.*, vol. 41, pp. 181–202, 2009.

[5] N. Niktin, F. Nicoud, B. Washistho, K. Squires, and P. Spalart, "An Approach to Wall Modeling in Large-Eddy Simulations," *Physics of Fluids*, vol. 12, no. 7, 2000.

[6] J. Kok, H. Dol, B. Oskam, and H. van der Ven, "Extra-Large Eddy Simulation of Massively Separated Flows," (Reno, Nevada), American Institute of Aeronautics and Astronautics, Jan. 2004.

[7] J. Kok, "A Stochastic Backscatter Model for Grey-Area Mitigation in Detached Eddy Simulations," *NLR Technical Report NLR-TP-2016-233*, 2017.

[8] F. White, *Viscous Fluid Flow*. 2 Penn Plaza, New York, NY 10121: McGraw-Hill Education, 3rd ed., 2006.

[9] S. Pope, *Turbulent Flows*. Cornell University, New York: Cambridge University Press, 2000.

[10] D. Wilcox, *Turbulence Modeling for CFD*. La Canada, California: DCW Industries, Inc., 1993.

[11] F. Nieuwstadt, B. Boersma, and J. Westerweel, *Turbulence - Introduction to Theory and Applications of Turbulent Flows*. Delft University of Technology, Delft: Springer Nature.

[12] J. Kok, "Resolving the dependence on free-stream values for the k-omega turbulence model," *NLR Technical Report NLR-TP-1995-295*, 1995.

[13] P. Spalart, W.-H. Jou, M. K. Strelets, and S. Allmaras, "Comments on the Feasibility of LES for Wings, and on a Hybrid RANS/LES Approach," *Advances in DNS/LES*, pp. 137–147, 1997. Columbus, OH: Greyden Press.

[14] P. Spalart, S. Deck, M. Shur, K. Squires, M. K. Strelets, and A. Travin, "A New Version of Detached-Eddy Simulation, Resistant to Ambiguous Grid Densities," *Theoretical Computational Fluid Dynamics*, vol. 20, pp. 181–195, 2006.

[15] M. Shur, P. Spalart, M. K. Strelets, and A. Travin, "An Enhanced Version of DES with Rapid Transition from RANS to LES in Separated Flows," *Flow Turbulence and Combustion*, vol. 95, no. 4, pp. 709–737, 2015.

[16] S. Chen, S. Yipeng, X. Zuoli, W. Xia, and J. Wang, "Constrained Large Eddy Simulation of Wall-Bounded Turbulent Flows," *Notes on Numerical Fluid Mechanics and Multidisciplinary Design*, no. 117, 2012.

[17] Z. Xia, Z. Xiao, Y. Shi, and S. Chen, "Constrained Large-Eddy Simulations for Aerodynamics," *Notes on Numerical Fluid Mechanics and Multidisciplinary Design*, vol. 130, pp. 105–115, 2014.

[18] J. Uribe, N. Jarrin, R. Prosser, and D. Laurence, "Development of a Two-Velocities Hybrid RANS-LES Model and its Application to a Trailing Edge Flow," *Flow Turbulence and Combustion*, vol. 85, pp. 181–197, 2010.

[19] J. Baggett, "On the feasibility of merging LES with RANS for near-wall region of attached turbulent flows," *Center for Turbulent Research: Annual Research Briefs*, pp. 267–277, 1998.

[20] H. Xiao and P. Jenny, "A consistent dual-mesh framework for hybrid LES/RANS modeling," *Journal of Computational Physics*, no. 231, pp. 1848–1865, 2012.

[21] P. Nguyen, J. Uribe, I. Afgan, and D. Laurence, "A seamless hybrid RANS/LES model with Dynamic Reynolds-Stress Correction for high Reynolds number flows on coarse grids," (Montpellier, France), Sept. 2018.

[22] S. Haering, T. Oliver, and R. Moser, "Towards a Predictive Hybrid RANS/LES Framework," (San Diego, California), American Institute of Aeronautics and Astronautics, Jan. 2019.

[23] M. Fuchs and C. Mockett, "Go4Hybrid: Grey Area Mitigation for Hybrid RANS-LES Methods - Direct Comparison of Non-Zonal Methods," *Notes on Numerical Fluid Mechanics and Multidisciplinary Design*, vol. 134, pp. 209–233, 2018.

[24] N. Jarrin, R. Prosser, J.-C. Uribe, S. Benhamadouche, and D. Laurence, "Reconstruction of turbulent fluctuations for hybrid RANS/LES simulations using a Synthetic-Eddy Method," *International Journal of Heat and Fluid Flow*, vol. 30, pp. 435–442, 2009.

[25] S. Deck, P. Weiss, and N. Renard, "A rapid and low noise switch from RANS to WMLES on curvilinear grids with compresible flow solvers," *Journal of Computational Physics*, vol. 363, pp. 231–255, 2018.

[26] S. Deck, "Recent improvements in the Zonal Detached Eddy Simulation (ZDES) formulation," *Theoretical Computational Fluid Dynamics*, vol. 26, pp. 1–28, 2011.

[27] S. Bose and G. Park, "Wall-Modeled Large-Eddy Simulation for Complex Turbulent Flows," *Annual Review of Fluid Mechanics*, vol. 50, pp. 535–561, 2018.

[28] G. Medic, G. Daeninck, J. Templeton, and G. Kalitzin, "A framework for near-wall RANS/LES coupling," *Center for Turbulence Research: Annual Research Briefs*, pp. 169–182, 2005.

[29] U. Piomelli, E. Balaras, H. Pasinato, K. Squires, and P. Spalart, "The inner-outer layer interface in large-eddy simulations with wall-layer models," *Heat and Fluid Flow*, vol. 24, pp. 538–550, 2003.

[30] A. Keating and U. Piomelli, "A dynamic stochastic forcing method as a wall-layer model for large-eddy simulation," *Journal of Turbulence*, vol. 7, no. 12, 2006.

[31] J. Larsson, F. Lien, and E. Yee, "The artificial buffer layer and th effects of forcing in hybrid LES/RANS," *International Journal of Heat and Fluid Flow*, no. 28, pp. 1443–1459, 2007.

[32] F. Hamba, "Log-layer mismatch and commutation error in hybrid RANS/LES simulation of channel flow," *International Journal of Heat and Fluid Flow*, vol. 30, pp. 20–31, 2009.

[33] F. Hamba, "A Hybrid RANS/LES Simulation of Turbulent Channel Flow," *Theoretical and Computational Fluid Dynamics*, vol. 16, pp. 387–403, 2003.

[34] W. Rozema, *Low-Dissipation Methods and Models for the Simulation of Turbulent Subsonic Flow: Theory and Applications*. PhD thesis, University of Groningen, Groningen, 2015.

[35] G. Comte-Bellot and S. Corrsin, "Simple Eulerian time correlation of full- and narrow-band velocity signals in grid-generated, 'isotropic' turbulence," *Journal of Fluid Mechanics*, vol. 2, no. 48, pp. 273–337, 1970.

[36] M. Lee and R. Moser, "Direct Numerical Simulation of Turbulence Channel Flow up to $Re_\tau \approx 5200$," *Journal of Fluid Mechanics*, vol. 774, pp. 395–415, 2015.

[37] M. Lee and R. Moser, "Spectral analysis of the budget equation in turbulent channel flow at high Reynolds number," *Journal of Fluid Mechanics*, no. 860, pp. 886–938, 2019.

[38] E. Balaras and C. Benocci, "Subgrid Scale Models in Finite Difference Simulations of Complex Wall Bounded Flows," in *Agard Conference Proceedings 551*, (Chania, Crete, Greece), Apr. 1994.